VOL. 2 No. 5
OCTOBER 1960

NAL OF THE

LESS-COMMON METALS

UNIVERSITY OF HAWAII
LIBRARY
FEB 6 '61

AN INTERNATIONAL JOURNAL ON
THEIR CHEMISTRY AND METALLURGY

HBERTSON (Nottingham)
OTHER (Manchester)

L ADVISORY BOARD:
(Paris)
COOK (Birmingham)
LY (Brussels)
GHEUZIAN (Ottawa)
CHER (Harwell)
SER (Columbus, Ohio)
N (Frankfurt a.M.)
LI (Genoa)
M (Münster)
LL (Corvallis, Ore.)
Y (Harwell)
NY (Vienna)
EON (Toronto)
LL (Wembley)
TON (Hyattsville, Md.)
ARKEL (Leyden)
NER (Melbourne)
MA (Menlo Park, Calif.)

ELSEVIER

GENERAL INFORMATION

Types of contributions

(a) Original research work not previously published in other periodicals.
(b) Reviews on recent developments in various fields.
(c) Short communications.
(d) Bibliographical notes and book reviews.

Languages

Papers will be published in English, French or German.

Submission of papers

Papers should be sent to one of the following Editors:

Professor J. W. CUTHBERTSON (*Metallurgy*), Department of Metallurgy, The University, University Park, Nottingham, England.
Professor F. FAIRBROTHER (*Chemistry*), The University of Manchester, Department of Chemistry, Manchester 13, England.

Authors should preferably submit two copies in double-spaced typing on pages of uniform size. Legends for figures should be typed on a separate page. The figures should be in a form suitable for reproduction, drawn in Indian ink on drawing paper or tracing paper, with lettering etc. in thin pencil. The sheets of drawing or tracing paper should preferably be of the same dimensions as those on which the article is typed. Photographs should be submitted as clear black and white prints on glossy paper.
All references should be given at the end of the paper. They should be numbered and the numbers should appear in the text at the appropriate places.
A summary of 50 to 200 words should be included. Authors of papers in French or German are encouraged to supply also a translation of the summary in English.

Reprints

Twenty-five reprints will be supplied free of charge. Additional reprints can be ordered at quoted prices. They must be ordered on order forms which are sent together with the proofs.

Publication

The *Journal of the Less-Common Metals* will have six issues to the volume, approx. 500 pages per volume.
Subscription price: £ 5.7.6 or Dfl. 57.— per volume (post free).
For advertising rates apply to the publishers.

Subscriptions

Subscriptions should be sent to:

ELSEVIER PUBLISHING COMPANY, Spuistraat 110-112, Amsterdam-C., The Netherlands.

A SOLUBILITY FACTOR SERIES FOR SOLID METALS*

Y. L. YAO

Physical Metallurgy Division, Mines Branch, Department of Mines and Technical Surveys, Ottawa (Canada)

(Received May 7th, 1960)

SUMMARY

A solubility factor series is proposed on an empirical basis. Some regularities in the continuous series of solid solutions, intermediate phases and simple phase diagrams are observed which could be explained on the basis of the interplay among solubility factor, atomic size factor and crystal structure factor.

INTRODUCTION

Crystal structure, atomic size and chemical activity are the three main characteristics governing alloying behaviour in binary alloys. Of these properties, structure and size have been determined for all elements, but electrochemical energies have not been established. The practical applicability of the semi-empirical electronegativity scales proposed by PAULING, HAISSINSKY AND GORDY is not obvious and the standard electrode potentials derived from measurements in aqueous solutions cannot be used for metallic solid solutions and intermediate phases without modification. This paper presents and discusses the results of an empirical attempt to tabulate the metals in the order of their decreasing solubility factor values. They are not developed from any foundation of fundamental theory; however, it appears that, in combination with other factors, they could have some predicative value in continuous series of solid solutions and they could explain some regularities in intermediate phases and simple phase diagrams.

DERIVATION OF SOLUBILITY FACTOR VALUES

The method by which the solubility factor values are derived was based on the premise that, for those pairs of metals which do not form continuous series of solid solutions (hereafter abbreviated as *css*), the atomic terminal solution of the metal with the larger solubility factor value (hereafter designated by *S*) tends to be smaller than that of the other metal. An extensive survey of all terminal solutions for which information could be found in HANSEN's compilation[2] yielded a series from Na to Th shown in the first column of Table I. Out of about 235 systems in which both solubility limits were determined, 7 exceptions were found and listed elsewhere[3]. A search of the literature since the middle of 1958 shows that about 25 more systems are available for test. The Ni–Ru (unpublished investigation quoted in ref. 4) and Ag–Ti[5] systems constitute additional exceptions.

* Published by permission of the Director, Mines Branch, Department of Mines and Technical Surveys, Ottawa, Canada.

TABLE I

SOLUBILITY FACTOR VALUES AND ATOMIC SIZES[1] OF COMMON METALS

Metal	*Solubility factor value*	*Goldschmidt radius for c. n. 12 in KX units*	*Metal*	*Solubility factor value*	*Goldschmidt radius for c. n. 12 in KX units*
Cs	0.92	2.74	Cr	—0.11	1.28
Rb	0.88	2.53	Re	—0.14	1.37
K	0.84	2.36	W	—0.17	1.41
Na	0.80	1.92	Mo	—0.20	1.40
Zn	0.76	1.37	Cu	—0.23	1.28
Cd	0.72	1.52	V	—0.26	1.36
Ga	0.68	1.39	Ta	—0.29	1.46
Bi	0.64	1.82	Fe	—0.32	1.27
Ge	0.60	1.39	Ru	—0.35	1.32
Sb	0.56	1.61	Nb	—0.38	1.47
As	0.52	1.48	Co	—0.41	1.26
Hg	0.48	1.55	Ti	—0.44	1.45
Sn	0.44	1.58	Hf	—0.47	1.58
Si	0.40	1.34	Ni	—0.50	1.24
Mg	0.36	1.60	Os	—0.53	1.34
Li	0.32	1.57	Zr	—0.56	1.60
Ba	0.28	2.25	Ir	—0.59	1.35
In	0.24	1.57	Pt	—0.62	1.38
Sr	0.20	2.16	Au	—0.65	1.44
Tl	0.16	1.71	U	—0.68	1.54
Pb	0.12	1.75	Rh	—0.71	1.34
Al	0.08	1.43	Ce	—0.74	1.83
Ca	0.04	1.97	Pd	—0.77	1.37
Be	—0.05	1.13	Ag	—0.80	1.44
Mn	—0.08	1.31	Th	—0.83	1.80

It is seen that the transition metals, in which Be, Cu, Au and Ag are included, are lower in the series. Arbitrarily the S of Zn is assumed to be 0.76 and a sequence of positive numbers in 0.04 steps are assigned to the other non-transition metals; similarly the S of Ag is assumed to be —0.80 and a sequence of negative numbers in 0.03 steps are assigned to the other transition metals. These numbers related to the serial numbers in the series are tabulated in the second column of Table I.

SOLUBILITY-FACTOR EFFECT AND SIZE-FACTOR EFFECT

If ΔS of two metals is greater than 0.30, the ratio of the two terminal solubilities is usually greater than 2. For example, the maximum solid solubility of Zn in Mn, Cu, Fe, Co, Ni, Pt, Au, Pd or Ag is at least 18 at.%, but the reciprocal solubility in Zn is at most 5%. Similarly, the solubility of Al in Cu, V, Fe, Ni, Ti, Zr, Au, U or Pd is at least 6%, but the reciprocal solubility in Al is at most 2.5%. The severe restriction on the terminal solution of the metal with larger S is associated with the formation of an intermediate phase. It is expected that the intermediate phase formed due to large ΔS of the components will be richer in the metal with larger S.

If, in addition to large ΔS, there is considerable difference in atomic sizes of these two metals, both terminal solutions will be severely restricted, although the termina

solution of the metal with larger S is still relatively smaller. A so-called "size-factor compound" may be formed to relieve the strain caused by the accommodation of two kinds of atoms of different sizes. It is usually assumed that only strain of importance is produced when larger atoms are accommodated among smaller ones[6]. Thus it is expected that the intermediate phase formed due to the large size ratio of the components will be richer in the metal of smaller size.

What has been said refers to the extreme cases, but it is clear that two typical kinds of intermediate phases could be recognized. Throughout this paper, the terms "compound" and "intermediate phase" are used synonymously, but "size-factor compound" refers to an intermediate phase in which the size-factor effect is predominant and "solubility-factor compound" to that with the predominant solubility-factor effect. The interplay of these two effects also reveals itself in *css* and in eutectiferrous and peritectiferrous phase diagrams.

Before discussing these, however, it is necessary to establish a common unit of the solubility-factor energy effect with the strain energy effect imposed by atomic size factors. The following expressions are assumed to represent the solubility-factor and size-factor effect respectively:

$$(1)\quad F(S - S')$$

$$(2)\quad 2/3\ GV\ [(D/D')^3 - 1]^2$$

In the first expression, F is a constant equal to 23,060 cal, and $S - S'$ the difference of solubility-factor values, S being algebraically larger than S'.

In the second expression, which represents strain energy[7], G is the shear modulus, V is the molar volume of the solvent metal and D/D' is the ratio of Goldschmidt diameters for coordination number 12, D being larger than D'. The value of GV does not vary much from metal to metal and may be taken as 60,000 cal.

CONTINUOUS SERIES OF SOLID SOLUTIONS

Alloys of transition metals

In order to utilize the information contained in Table I and the formulae shown above, the obvious procedure was to look for some regularities among crystal structure, S and Goldschmidt diameters. The *css* of transition metals, excluding rare earths, were chosen for study first. Since only metals of the same crystal structure can forms *css*, the transition metals were separated into their three crystal groups and binary combinations of each group were studied separately. The groups* are shown as follows:

(1) body-centered cubic, Cr, Fe, Hf, Mo, Nb, Ta, Th, Ti, U, V, W, Zr;

(2) face-centered cubic, Ag, Au, Co, Cu, Fe, Ir, Mn, Ni, Pd, Pt, Rh;

(3) hexagonal, Co, Hf, Os, Re, Ru, Ti, Zr.

Careful study of these systems disclosed that the conditions postulated below fairly accurately reveal the relationships governed by sizes and S in these systems:

* Though Cr may possess an *f.c.c.* form, it is not included in the components of the *f.c.c.* solutions. That Cr and Cu, having the same atomic diameter and differing in S by 0.12, do not form a *css* shows that the *f.c.c.*-forming tendency of Cr is weak. Similarly Mn is not included in the components of the *b.c.c.* solutions. That Mn and Cr, with $D/D' = 1.02$ and $\Delta S = 0.03$, do not form a *css*, indicates that the b.*c.c.*-forming tendency of Mn is weak. Also, Th is not included in those of the *f.c.c.* solutions because its atomic diameter is much larger than that of the other *f.c.c.* metals.

(*a*) *Solubility-factor effect* > *size-factor effect*

Condition I, $\Delta S < 0.30$, stable *css* persist at all temperatures;
Condition II, $0.48 > \Delta S > 0.30$, *css* are formed but ordered at low temperatures;
Condition III, $\Delta S > 0.48$, *css* are not formed;

(*b*) *Solubility-factor effect* < *size-factor effect*

Condition IV, $D/D' < 1.123$, *css* are formed but segregated or decomposed at low temperatures;
Condition V, $1.152 > D/D' > 1.123$, *css* are not formed;
Condition VI, $D/D' > 1.152$, *css* are not formed.
The two effects counterbalance each other for the pairs of values of $\Delta S = 0.30$ and $D/D' = 1.123$ or for the pair of 0.48 and 1.152.

TABLE II

BODY-CENTERED CUBIC CONTINUOUS SOLID SOLUTIONS IN TRANSITION METALS[2]

Components: Cr, Fe, Hf, Mo, Nb, Ta, Th, Ti, U, V, W, Zr

Pair			*Condition*	*Predicted*	*Observed*	*Total no. of pairs*
Cr–V*	Hf–Ta*	Hf–Zr	I	*css stable*	*css stable*	17
Mo–Nb	Mo–Ta	Mo–Ti				
Mo–V	Mo–W	Nb–Ta				
Nb–Ti	Nb–V	Nb–W				
Ta–Ti	Ta–W	Ta–Zr**				
Ti–V	V–W**					
Cr–W	Fe–V(i)	Hf–Nb**	IV	*css* seg. or decomp.	*css* seg. or decomp.	6
Nb–Zr	Ta–V**	Th–Zr				
Cr–Hf?	Cr–Nb	Cr–Ta		no *css*	no *css*	30
Cr–Th	Cr–U	Cr–Zr				
Fe–Hf?	Fe–Nb	Fe–Ta				
Fe–Th	Fe–Ti	Fe–U				
Fe–Zr	Hf–Mo?	Hf–Th[8]	III,			
Hf–V?	Hf–W?	Mo–Th	V			
Mo–U	Mo–Zr	Nb–Th	or			
Ta–Th	Th–Ti	Th–U	VI			
Th–V	Th–W	U–V				
U–W	V–Zr	W–Zr				
Cr–Fe(i)	Hf–U[9]	Ti–U(i)	I	*css* stable	*css* seg. or decomp.	4
U–Zr(i)						
Nb–U			II	*css* ordered	*css* seg.	1
Cr–Mo	Hf–Ti*	Ti–Zr	IV	*css* seg. or decomp.	*css* stable	3
Ti–W			I	*css* stable	no *css*	1
Ta–U			II	*css* ordered	no *css*	1
Fe–Mo	Fe–W		IV	*css* seg. or decomp.	no *css*	2
Cr–Ti(i)			V	no *css*	*css* decomp.	1
						66

(i) intermediate phase.
* observation not confirmed.
** limited information.
? information not available.

TABLE III

FACE-CENTERED CUBIC CONTINUOUS SOLID SOLUTIONS IN TRANSITION METALS[2]

Components: Ag, Au, Co, Cu, Fe, Ir, Mn, Ni, Pd, Pt, Rh

Pair			*Condition*	*Predicted*	*Observed*	*Total no. of pairs*
Ag–Au Au–Pd Cu–Mn Fe–Mn	Ag–Ir? Co–Ir Cu–Ni Ni–Pd**	Ag–Pd Co–Rh Fe–Ir** Ni–Rh?	I	*css* stable	*css* stable	12
Au–Cu Cu–Pt Fe–Rh**	Co–Mn* Fe–Pd Mn–Ni	Cu–Ir? Fe–Pt	II	*css* ordered	*css* ordered	8
Au–Pt Ir–Pt	Au–Rh**	Ir–Ni?	IV	*css* seg.	*css* seg.	4
Ag–Co Ag–Ni Au–Mn Mn–Pd	Ag–Cu Au–Co Cu–Rh Mn–Pt	Ag–Mn Au–Fe Ir–Mn Mn–Rh	III, V or VI	no *css*	no *css*	12
Co–Fe Fe–Ni	Co–Ni	Co–Pt	I	*css* stable	*css* ordered	4
Ir–Pd Pd–Rh	Ir–Rh* Pt–Rh*	Pd–Pt*	I	*css* stable	*css* seg[4]	5
Co–Pd			II	*css* ordered	*css* stable	1
Ni–Pt			IV	*css* seg.	*css* ordered	1
Ag–Pt	Co–Cu	Cu–Fe	I	*css* stable	no *css*	3
Ag–Fe			II	*css* ordered	no *css*	1
Ag–Rh	Au–Ir		IV	*css* seg.	no *css*	2
Cu–Pd			III	no *css*	*css* ordered	1
Au–Ni			VI	no *css*	*css* seg.	1
						55

observation not confirmed.
* limited information.
information not available.

TABLE IV

HEXAGONAL CONTINUOUS SOLID SOLUTIONS IN TRANSITION METALS[2]

Components: Co, Hf, Os, Re, Ru, Ti, Zr

Pair			*Condition*	*Predicted*	*Observed*	*Total no. of pairs*
Co–Os Hf–Zr	Co–Re Os–Ru?	Co–Ru Re–Ru?	I	*css* stable	*css* stable	6
Re–Ti?			II	*css* ordered	—	1
Os–Ti(i)	Ru–Ti(i)		IV	*css* seg. or decomp.	—	2
Co–Hf? Hf–Os? Os–Zr?	Co–Ti Hf–Re? Re–Zr?	Co–Zr Hf–Ru? Ru–Zr?	V or VI	no *css*	no *css*	9
Os–Re**			II	*css* ordered	*css* stable	1
Hf–Ti*	Ti–Zr		IV	*css* seg. or decomp.	*css* stable	2
						21

(i) intermediate phase.
observation not confirmed.
* limited information.
information not available.

The predictions for the *b.c.c.*, the *f.c.c.* and the hexagonal *css* in transition metals are listed in Tables II, III and IV respectively. It is noticed that, in Tables II and IV, a stable *css* is predicted in Hf–Zr system and a *css* is predicted to decompose or segregate at low temperatures in Hf–Ti and Ti–Zr systems. Actually, two sets of *css* are observed in these three systems.

With respect to *css* with rare earths as one component, Th is probably the only transition metal possessing large enough atomic diameter to be the other component. So far *css* of Ce–Th, La–Th[2] and Y–Th[10] alloys are known. Evidently more *css* of this kind will be found. Furthermore, *css* of Ce–La[2] and Ce–Y[11] alloys are known at present. It is expected that more *css* will be found among the rare earths, but probably they will be segregated at low temperatures.

Alloys of non-transition metals

In contrast to transition metals, non-transition metals have a relatively large number of crystal structures. The *css* in most combinations of non-transition metals are ruled out by the structure factor alone. On the basis of the conditions stated above, *css* are expected to form in the following alloys: As–Sb (segregated at low temperatures), Ba–Sr, Ca–Sr, Cd–Mg (ordered at low temperatures), Cs–Rb (segregated at low temperatures), Ge–Si, K–Rb (segregated at low temperatures), Mg–Tl.

Only in As–Sb alloys is there evidence to indicate that a solid miscibility gap might exist. The existence of a *css* in Ba–Ca, Bi–Sb or Cs–K alloys cannot be predicted. A *css* is not formed in Mg–Tl alloys.

INTERMEDIATE PHASES IN TRANSITION METALS

The discussions which follow are limited to several important structural types of binary intermediate phases. Those phases formed entirely from non-transition metals are excluded. An attempt is made in each type to ascertain (1) whether the intermediate phase is a solubility-factor or a size-factor compound, (2) whether its components can be rationalized according to sizes or S if its composition is not equiatomic, (3) whether its components are decreased or increased in size, as compared with Goldschmidt diameters, and (4) what is the effect of crystal structure of the components, if there is any. Undoubtedly many more intermediate phases in each type will be found in future and the statements below may need modifications.

Sigma phases

The 34 known sigma phases are listed in Table V. Except in Co–Mo, Cr–Re, Fe–Mo and Fe–V alloys (condition IV), the sigma phases are solubility-factor compounds (condition I or II). It is noted that no sigma phases composed entirely of non-transition have been reported. For those composed entirely of transition metals, the composition is richer in the metal with larger S and the trend for the composition to be increasingly richer with the increasing ΔS of the components is unmistakable. However, in Al–Nb alloys, the lone representative with one non-transition metal component, the composition is richer in the metal with smaller S. Furthermore, all sigma phases may be considered as being composed of the two components having different crystal structures.

According to STUEWE[14], the lattice parameter "c" of the sigma phases may be interpreted as an overall contraction of the atoms along the direction of the c-axis. As to

TABLE V

SIGMA PHASES[2,12,13]

The atomic % listed refer to the approximate composition of sigma phases. If the composition range is wide, the average of the upper and lower homogeneity range is taken as the representative composition. The numbers in parentheses are solubility factor values and the letters in parentheses refer to crystal structure. The asterisks indicate the presence of Cr_3O-type in the same system.

	At.% element present						
	Cr (−0.11) (*b*)	*Re* (−0.14) (*h*)	*W* (−0.17) (*b*)	*Mo* (−0.20) (*b*)	*V* (−0.26) (*b*)	*Ta* (−0.29) (*b*)	*Nb* (−0.38) (*b*)
Al (0.08) (f)							67*
Mn (—0.08) (f)	23			36	19	50	40
Re (—0.14) (h)	37		48	38			
Fe (—0.32) (f)	47	40		46	47		
Ru (—0.35) (h)	67*		60	63			
Co (—0.41) (f)	61			60	56*		
Ni (—0.50) (f)					62*		
Os (—0.53) (h)	60*		63*	65*		63	60*
Ir (—0.59) (f)			70	70*	*	75	65*
Pt (—0.62) (f)	*				*	75	63*
Rh (—0.71) (f)	*				*	60	60*
Pd (—0.77) (f)							60

the atoms in the planes perpendicular to the *c*-axis, there is clear indication of a slight expansion in Fe–Cr alloys. From the linear relationship represented in Fig. 2 of his paper, the slight expansion may also occur in the other alloys.

Cr_3O-type compounds

The 43 known Cr_3O-type (formerly called β W-type) compounds listed in Table VI are solubility-factor compounds (condition I, II or III). Except that the Cr_3O-type has a narrow range of homogeneity, the remarks on composition of the sigma phase and crystal structure of their components are also true for the Cr_3O-type. As it is seen from the asterisks marked in Table V, both sigma phases and Cr_3O-type exist in quite a large number of systems.

TABLE VI

Cr_3O-TYPE COMPOUNDS[2,15,16]

Composed entirely of transition metals							
$AuNb_3$	$AuTi_3$	AuV_3	CoV_3	Cr_3Ir?	Cr_3Os	Cr_3Pt	Cr_3Rh
Cr_3Ru	$IrMo_3$	$IrNb_3$	$IrTi_3$	IrV_3	Mo_3Os	Nb_3Pt	Nb_3Os
Nb_3Rh	NiV_3	OsW_3	$PtTi_3$	PtV_3	RhV_3		
Composed of one transition metal and one non-transition metal							
$AlMo_3$	$AlNb_3$	AsV_3	Cr_3Ga	Cr_3Ge	Cr_3Si	$GaMo_3$	$GaNb_3$
GaV_3	$GeMo_3$	$GeNb_3$	GeV_3	$HgTi_3$	$HgZr_3$	Mo_3Si	Nb_3Sb
Nb_3Sn	SbV_3	SiV_3	$SnTa_3$	SnV_3			

(?) information not confirmed.

According to LAVES[1], the lattice parameter of these compounds may be interpreted as that, in the general formula A_3B, A decreases in size and B increases slightly.

Laves phases

The Laves phases crystallize in three MgX_2-types: $MgZn_2$-, $MgCu_2$- and $MgNi_2$-type. Neglecting the $MgNi_2$-type, which is small in number, the known representatives of the other two types are listed in Table VII.

TABLE VII

LAVES PHASES[2,8,17,18]

(*a*) *$MgZn_2$-type*

f.c.c. + b.c.c.:
Mn_2Th

hexa. + hexa.:
Be_2Re, $CaCd_2$, $CaLi_2$, $CaMg_2$, $ErRu_2$, $GdOs_2$, $CdRu_2$, $HfOs_2$, $HfRe_2$, $LuOs_2$, $LuRu_2$, Mg_2Sr, $MgZn_2$, $NdOs_2$, Os_2Pr, Os_2Sc, Os_2Sm, Os_2Y, Os_2Zr, Re_2Y, Re_2Zr, Ru_2Sc, Ru_2Y, Ru_2Zr, $TiZn_2$?

b.c.c. + b.c.c.:
Be_2Cr, Be_2Fe, Be_2Mn, Be_2Mo, Be_2V, Be_2W, Cr_2Hf (L.T.)?, Cr_2Ta (H.T.), Cr_2Ti (H.T.) Cr_2Zr (H.T. or L.T.?), Fe_2Hf (H.T. and L.T.), Fe_2Mo?, Fe_2Nb, Fe_2Ta, Fe_2Ti, Fe_2W?, $HfMn_2$ (L.T.)?, KNa_2, Mn_2Nb, Mn_2Ta, Mn_2Ti, Mn_2Zr

combinations of different structures:
$BaMg_2$, $CdCu_2$, Ir_2Zr, KPb_2, Ni_2U, Re_2U (H.T.)

(*b*) *$MgCu_2$-type*

f.c.c. + b.c.c.:
Al_2U, Au_2Na, $BaPd_2$, $BaPt_2$, $BaRh_2$, Co_2Hf, Co_2Nb, Co_2Ta, Co_2Ti, Co_2U, Co_2Zr, Cr_2Nb, Cr_2Ta (L.T.), Cr_2Ti (L.T.), Cr_2Zr (H.T. or L.T.?), Fe_2Hf (L.T.), Fe_2U, Fe_2Zr, Ir_2Th, Ir_2U, Mn_2U

b.c.c. + hexa.:
Be_2Ti, $HfMo_2$ (I.T.), HfV_2, HfW_2, Mo_2Zr, Os_2Th, Os_2U, V_2Zr?, W_2Zr, Zn_2Zr

f.c.c. + hexa.:
$AgBe_2$, Al_2Ca, Al_2Ce, Al_2La, Be_3Cu, Be_5Fe, $CaIr_2$, $CaPd_2$, $CaPt_2$, $CaRh_2$, $CeCo_2$, $CeFe_2$, $CeIr_2$, $CeMg_2$*, $CeNi_2$, $CeOs_2$*, $CePt_2$, $CeRh_2$, $CeRu_2$*, Cu_2Mg, Fe_2Gd, $GdIr_2$, $GdMn_2$, $GdPt_2$, $GdRh_2$, Ir_2La, Ir_2Nd, Ir_2Pr, Ir_2Sc, Ir_2Sr, Ir_2Y, $LaMg_2$*, $LaNi_2$, $LaOs_2$*, $LaPt_2$, $LaRh_2$, $LaRu_2$*, Mg_2Th (H.T.), $NdPt_2$, $NdRh_2$, $NdRu_2$*, Ni_2Pr, Os_2Pr*, Pd_2Sr, $PrPt_2$, $PrRh_2$, $PrRu_2$*, Pt_2Sr, Pt_2Y, Rh_2Sr, Rh_2Y

other combinations of different structures:
Au_2Bi, Bi_2K

f.c.c. + f.c.c.:
Au_2Pb

H.T.: high temperature form.
L.T.: low temperature form.
I.T.: intermediate temperature form.

(?) information not confirmed.
* phases involving *f.c.c.* forms of Ce, La, Nd and Pr.

Except the compounds in Al-U, Cd-Cu, Ce-Mg, Cu-Mg, La-Mg, Mg-Th, Mn-Ti, Re-U, Ti-Zn and Zn-Zr systems, the Laves phases in 133 systems are size-factor compounds. Typical of a size-factor compound, the Laves phase is richer in the component of smaller size. According to LAVES[1], with a few exceptions, the sum of $(D_{Mg} - d_{Mg})$ and 2 $(D_X - d_X)$ is positive, where D's are Goldschmidt diameters and d's atomic diameters in the compounds. In other words, there is an overall contraction.

With 7 exceptions, the $MgZn_2$-type is formed from those components having the same crystal structure but the $MgCu_2$-type from those having different structures. It is true that there is ambiguity in specifying crystal structure if one or both components are allotropic. However, in these cases, generally either the distinction between the crystal structures of an allotropic component is not important such as Co_2Nb, Co_2Ta and Co_2U of $MgCu_2$-type; or both types may be present in the same or different temperature ranges, such as the coexistence of both types in Os_2Pr or in the polymorphic transformations in Cr_2Ta, Cr_2Ti and Cr_2Zr. It is known that Cr may possess a high-temperature *f.c.c.* form and Be a high-temperature *b.c.c.* form[19]. Also, Ce, La and Pr are

nown to possess both hexagonal and *f.c.c.* forms, but there is no report on the existnce of an *f.c.c.* form of Nd. Recently doubt has been raised about the existence of ne hexagonal form of Ce[20]. Assumption is made here that Ce, La, Nd and Pr may ossess both hexagonal and *f.c.c.* forms. In Table VII the Laves phases involving the *c.c.* forms of these four elements are marked with asterisks.

TABLE VIII

CsCl-TYPE COMPOUNDS[1,2,21,22]

Solubility-factor compounds

attice expanded:
lCe, CdLa, CdPr, CeMg, LaMg, MgPr, MnPd, MnRh

attice contracted:
gLi, AgMg, AgZn, AlCo, AlFe, AlMn, AlNi, AlPd, AlRh, AuCd, AuMg, AuZn,
Co, BeNi, BiTl, CeHg, CeTl, CuPd, CuZn, FeV, GaNi, HgLa, HgLi, HgMg,
gNd, HgPr, InPd, LaTl, LiPb, LiTl, MgTl, MgRh, NiZn, OsV, PdZn, PrTl,
Si

attice parameters not determined:
Mn, MnPt, RuV, TiZn

attice unchanged:
Fe

Size-factor compounds

attice expanded:
gCe, AgGd, AgLa, AgPr, AlNd, CeZn, HgMn, LaZn, PrZn

attice contracted:
Y, BaCd, BaHg, BaZn, BeCu, BePd, CaCd, CaHg, CaTl, CdSr, CoHf, CoTi,
Zr, CuY, FeTi, HfOs, HfRu, HgSr, InNi, MgSr, NiTi, OsTi, OsZr, RuTi,
Zr, SrRh, SrTl

attice parameters not determined:
bRu, RuTa

Cl-type compounds

As it is seen from Table VIII, the CsCl-type compounds are either solubility-factor size-factor compounds and the lattices show either overall expansions or contracns. By lattice expansion is meant the value of $d_{AB} - D_{AB}$ being positive, where $_{AB}$ is $\frac{1}{2}\sqrt{3}a$, a being the measured lattice parameter and D_{AB} is the average of the o Goldschmidt diameters for coordination number 8. There is no simple correlation tween the dimensional change in the lattice and the predominant effect. However, is noticed that, for those CsCl-type compounds having narrow homogeneity ranges, e expansion occurs only when one component is Ce, Gd, La, Nd or Pr and the other mponent is either an *f.c.c.* metal such as Al or Ag or a hexagonal metal such as Cd, g or Zn.

TYPES OF SIMPLE PHASE DIAGRAMS

r two metals having the same crystal structure and forming no intermediate phases, e simple eutectic, the simple peritectic and the *css* are the three closely-related pes of phase diagrams. The conditions for forming the *css* have been set before and is interesting to ask whether the other two types can be separated according to S d atomic sizes. Because the eutectic type may be pictured as the invasion of the idus by a solid miscibility gap, the size-factor effect is predominant in the eutectic

type. On the other hand, the common expression "peritectic reaction" implies that the solubility-factor effect is predominant in the peritectic type. The pairs of metals forming these two types of phase diagrams are collected in Table IX. It is seen that there is good correlation between the predominant effect and the type of phase diagram. Also, in general, it appears that the two effects are more closely balanced in these systems than in the systems containing *css*.

TABLE IX

TYPES OF PHASE DIAGRAMS OF TWO METALS HAVING THE SAME CRYSTAL STRUCTURE BUT FORMING NEITHER INTERMEDIATE PHASES NOR CONTINUOUS SOLID SOLUTIONS[2]

System				*Predominant effect*	*Type of phase diagram*
Ag–Pb	As–Bi	Au–Co	Cd–Zn	size–factor effect	eutectic
Cr–Th	Cr–U	Ge–Sn	Hf–Th[8]		
Mo–Th[8]	Na–Rb	Nb–Th	Si–Sn		
Ta–Th?	Th–Ti	Th–V	Th–W		
U–V					
Ag–Pt	Au–Fe	Co–Cu	Cu–Fe	solubility-factor effect	peritectic
Cu–Rh	Ta–U	Ti–W	U–W		
Ag–Cu	Cd–Tl			solubility-factor effect	eutectic

(?) information not confirmed.

REFERENCES

1 F. Laves, in *Theory of Alloy Phases*, Am. Soc. Metals, Cleveland, Ohio, 1956, p. 131.
2 M. Hansen, *Constitution of Binary Alloys*, McGraw-Hill, New York, 1958.
3 Y. L. Yao, to be published in *Trans. A. I. M. E.*
4 E. Raub, *J. Less-Common Metals*, 1 (1959) 3.
5 M. K. McQuillan, *J. Inst. Metals*, 88 (1960) 235.
6 H. Lipson, *Progr. Metal Phys.*, 2 (1950) 50.
7 L. S. Darken and R. W. Gurry, *Physical Chemistry of Metals*, McGraw-Hill, New York, 1953, p. 78.
8 F. A. Rough and A. A. Bauer, *Constitution of Uranium and Thorium Alloys*, Battelle Memorial Institute, Columbus, Ohio, 1958.
9 D. T. Peterson and D. J. Beerntsen, *Trans. Am. Soc. Metals*, 52 (1959), preprint No. 158.
10 D. T. Eash and O. N. Carlson, *Trans. Am. Soc. Metals*, 52 (1959), preprint No. 142.
11 E. M. Savitsky and V. F. Terekhova, *Tsvetnye Metal.*, 32 (1959) 48.
12 A. G. Knapton, *J. Inst. Metals*, 87 (1958) 28.
13 G. R. McKingsey and C. M. Faulring, *Acta Cryst.*, 12 (1959) 701.
14 H. P. Stuewe, *Trans. A. I. M. E.*, 215 (1959) 408.
15 E. A. Wood, V. B. Compton, B. T. Matthias and E. Corenzwit, *Acta Cryst.*, 11 (1958) 604.
16 W. B. Pearson, *A Handbook of Lattice Spacings and Structure of Metals and Alloys*, Pergamon Press, New York, 1958.
17 E. A. Wood and V. B. Compton, *Acta Cryst.*, 11 (1958) 429.
18 V. B. Compton and B. T. Matthias, *Acta Cryst.*, 12 (1959) 651.
19 A. J. Martin and A. Moore, *J. Less-Common Metals*, 1 (1959) 85.
20 R. T. Weiner and G. V. Raynor, *J. Less-Common Metals*, 1 (1959) 309.
21 V. B. Compton, *Acta Cryst.*, 11 (1958) 446.
22 A. E. Dwight, *Trans. A. I. M. E.*, 215 (1959) 283.

THE PLUTONIUM–ZIRCONIUM PHASE DIAGRAM

J. A. C. MARPLES

Metallurgy Division, United Kingdom Atomic Energy Authority, Harwell, Berks. (Great Britain)

Received May 14th, 1960)

SUMMARY

The entire plutonium–zirconium phase diagram has been investigated from room temperature to 1300°C. The main features of the diagram are:

(1) Continuous solubility between ε-plutonium and β-zirconium.

(2) A wide δ-plutonium phase field extending across the diagram to 70 at.% zirconium at 600°C.

(3) A maximum solubility of plutonium in α-zirconium of 13 at.% at 618°C.

(4) A depression of the α/β transformation in zirconium to a eutectoid at 618°C.

(5) A compound at about 75 at.% zirconium with an hexagonal $P\,6/mmm$ structure and with $a = 5.055$ Å, $c = 3.123$ Å. On heating to 380°C, this decomposes peritectoidally to α-zirconium and δ-plutonium.

(6) A compound of unknown crystal structure (approx. Pu_6Zr) with a wide composition range from about 12 at.% to about 25 at.% zirconium decomposing congruently to δ-plutonium at 340°C.

(7) Solubilities in α-, β- and γ-plutonium of approximately 1.5, 7 and 3 at.% zirconium respectively.

The δ-plutonium structure may readily be retained by quenching samples with compositions between 5 at.% and 70 at.% zirconium but is not an equilibrium phase below 267°C. ε-plutonium or β-zirconium cannot be retained by quenching at any composition.

Possible valencies of the component metals and Brillouin zones for the α-zirconium and K phases are proposed; these enable the observed composition ranges of the two phases to be explained in terms of zone theory.

INTRODUCTION AND PREVIOUS WORK

n earlier brief survey[1] of the plutonium zirconium system carried out at Harwell d shown that, at about 500°C, δ-plutonium would dissolve 65 at.% zirconium and at α-zirconium dissolved 13 at.% plutonium. At the time of that investigation the ly reference in the open literature to plutonium–zirconium alloys was to a com- und of unknown crystal structure Pu_xZr with $x > 3$. No other details were given[2]. At the 1958 Geneva conference a tentative equilibrium diagram, based on the results this investigation, was published[3]. Russian workers also published[4] an equilibrium agram which for the most part agreed with the results obtained here, but which owed some differences in details; this diagram is referred to again in the discussion.

EXPERIMENTAL METHODS

wing to the well-known toxicity of plutonium[5] all the work had to be carried out sealed glove boxes[6]. Most of the apparatus has already been described[7,8].

The zirconium used was Van Arkel bar containing the usual 2% hafnium. The plutonium had previously been cast into graphite moulds to give discs 1 mm thick, which are very convenient for alloying.

Alloys were made by arc-melting together weighed amounts of the two components; made-up compositions have been taken throughout since melting losses were very small (about 1 part in 1000) and maximum possible composition errors were less than the accuracy to which the phase boundaries have been specified.

Annealing of samples for metallography and stress relief of filings was carried out in sealed glass capsules, under vacuum or in an atmosphere of argon; pyrex was used for temperatures below 600°C and C46 alumina silicate glass for temperatures between 600°C and 900°C. Metallography specimens were usually quenched into water since a little surface oxidation was unimportant; filings for X-ray examination were quenched into silicone oil. Some of the filings for X-ray examination were annealed in about one atmosphere pressure of argon in order to reduce evaporation of plutonium which could alter the alloy composition appreciably.

X-ray examination was carried out with a Guinier focussing camera[9] using Mo $K\alpha$

Fig. 1. The plutonium–zirconium phase diagram.

diation. This camera is sensitive to small traces of a second phase but is not as curate for parameter determination as a normal powder camera; since only low gle lines ($\theta < \sim 50°$) are observed, a Nelson–Riley extrapolation to $\theta = 90$ is not ssible and small errors in specimen positioning can give a variation in apparent lat- e parameters of 1 part in 1000. The accuracy of measurement of any line on a given m is slightly better than this and there is no varying and uncertain absorption rrection to apply; the camera is therefore particulary useful for phase identification d for indexing patterns of complex structures.

Vacuum furnaces were used for the thermal analysis and dilatometry in conjunc- n with chromel-alumel or platinum/platinum 13% rhodium thermocouples. verse heating or cooling curves were plotted for each specimen as the furnace mperature was changed at about 4°C per minute. Simultaneously, readings of a dial uuge showing the expansion or contraction of the specimen could be taken.

When solid state reactions were being investigated, silica and alumina were found be suitable refractory materials for the thermocouple sheaths and crucibles, although e latter was preferred for zirconium-rich alloys; oxidised tantalum was sometimes ployed as a crucible material. When attempting to determine the solidus and liqui- s it was impossible to avoid contamination of the specimen since molten plutonium

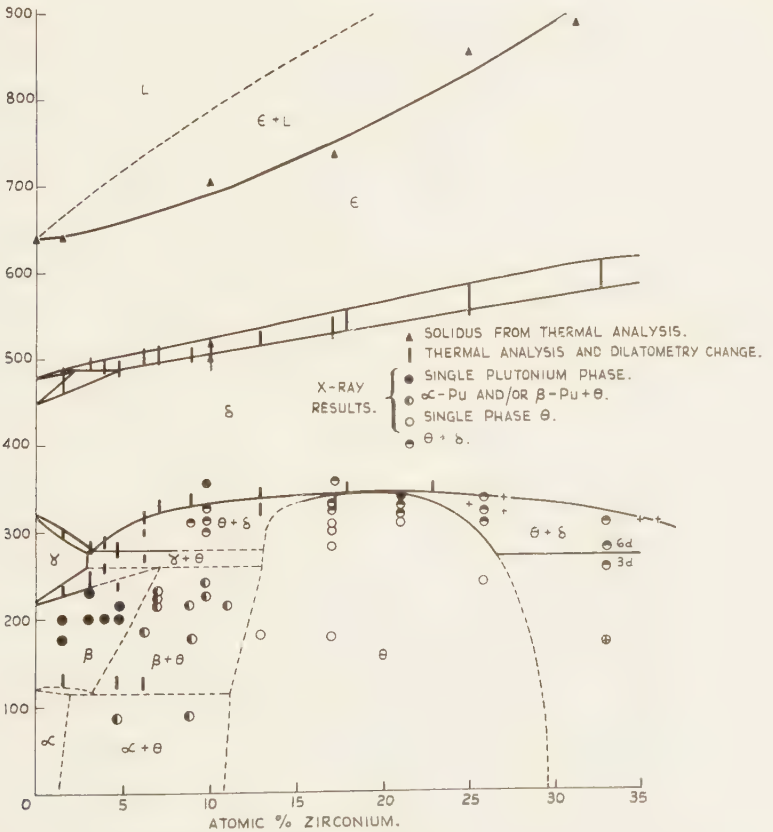

Fig. 2. Plutonium–zirconium equilibrium diagram, 0–35 at.% zirconium.

attacks alumina, molten zirconium attacks tantalum and they both react with silica. Thoria is slightly better thermodynamically than alumina but is not available at present in the form of narrow bore tubes for the thermocouple sheaths.

Densities of some alloys were measured using the displacement technique with ethylene dibromide as the liquid.

For metallographic work the usual polishing methods were used; rough grinding on four grades of silicon carbide paper was followed by polishing on a 0–1 μ diamond wheel or an alumina wheel. Electropolishing was carried out in a solution of 20% perchloric acid in butyl cellusolve, although sometimes an electro-etch using phosphoric acid–sulphuric acid–water mixtures was sufficient.

RESULTS

The completed diagram is shown in Figs. 1, 2 and 3. Accurately determined boundaries are indicated by full lines and tentative boundaries by dashed lines.

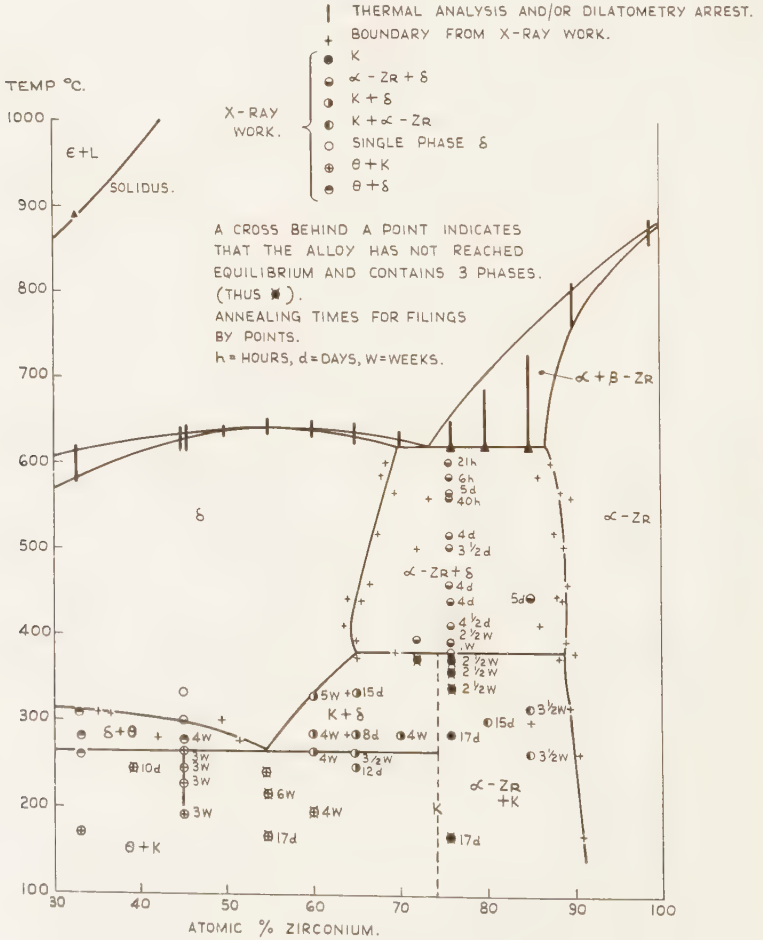

Fig. 3. Zirconium-rich end of the plutonium–zirconium diagram.

The liquidus and solidus

The points on the solidus, shown in Fig. 1, were obtained on heating on the first high temperature run with each alloy; even so, there is a little scatter from a smooth curve.

The two points marked on the liquidus were obtained on cooling at about 5°C per minute with the specimen contained in an alumina crucible with an alumina thermocouple sheath. Considerable reaction between the molten alloy and the alumina was found when the apparatus was subsequently dismantled.

The β-zirconium/ε-plutonium field

No direct evidence has been obtained of the complete miscibility of the two body-centred cubic phases but the smooth curves of the solidus and the δ-plutonium to ε transformation (see below) appear to preclude a miscibility gap.

Filings quenched from this field to room temperature did not retain the body-centred cubic structure and solid specimens quenched from above the eutectoid at 438°C showed a transformed structure (see (*g*) below and Figs. 8, 9 and 10).

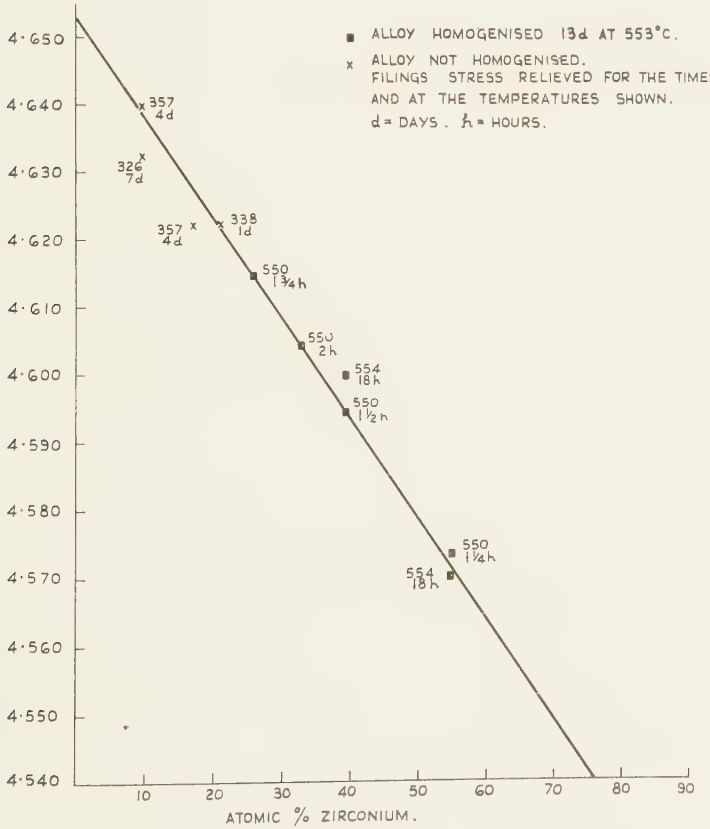

Fig. 4. δ-Plutonium lattice parameter *vs.* composition.

(c) The δ plutonium single-phase field

The range of stability of the face-centred cubic structure of the δ-phase is shown in Figs. 1, 2 and 3.

The lattice parameter *versus* composition curve is shown in Fig. 4. No difficulty was experienced in retaining the δ structure to room temperature except at the extreme plutonium-rich end (less than 5 at.% zirconium); at those compositions the δ-structure broke down to give a mixture of the lower temperature plutonium phases.

(d) The (δ + ε) plutonium field

As can be seen in Figs. 1, 2 and 3 this field is extremely narrow and its extent has been determined by thermal analysis and dilatometry; the two phase regions indicated by these experiments are shown by the vertical bars in Figs. 2 and 3.

The percentage contraction as shown by the dilatometer on transforming from the δ to the ε structure appears to remain constant with composition at about 0.5%. The figures obtained for this in the various experiments do show considerable scatter, however, probably because of specimen creep.

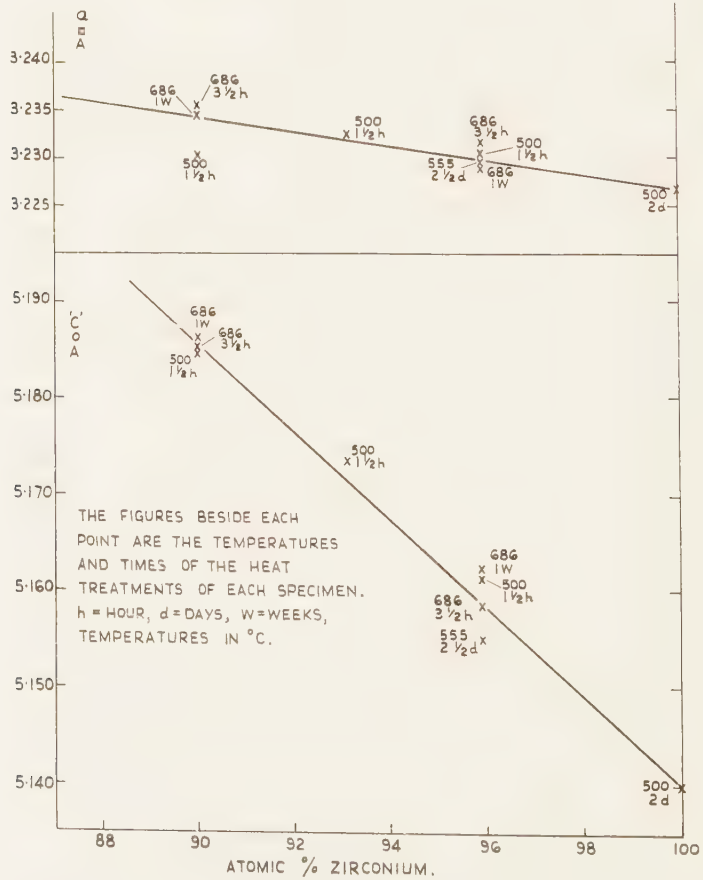

Fig. 5. α-Zirconium lattice parameters *vs.* composition.

) *δ′-plutonium*

No special effort has been made to define the single phase δ′ field. The thermal nalysis and dilatometer results on the 1.5 at.% zirconium alloy indicated a two-nase field, shown by the line in Fig. 2, followed by a sharp arrest at 487°C. The 3.1, 9 and 4.7 at.% zirconium alloys all indicated two-phase fields starting at about this mperature.

The peritectoidal decomposition of δ′ as shown in Fig. 2 is consistent with these sults. The indicated maximum solubility in δ′ of 2 at.% is, however, very uncertain.

The α-zirconium single-phase field

The extent of the single-phase field is shown in Fig. 3. The solubility limit was found the lattice parameter method. For this, filings were taken from the as-cast alloys . I given a brief stress-relieving treatment before being made into X-ray samples. spite the lack of homogenisation there was remarkably little scatter from the nooth parameter curves and the lines on the films were always quite sharp. The tameters obtained from the wide single-phase field are shown in Fig. 5. Solution of utonium had little effect on the '*a*' value but increased the '*c*' parameter by

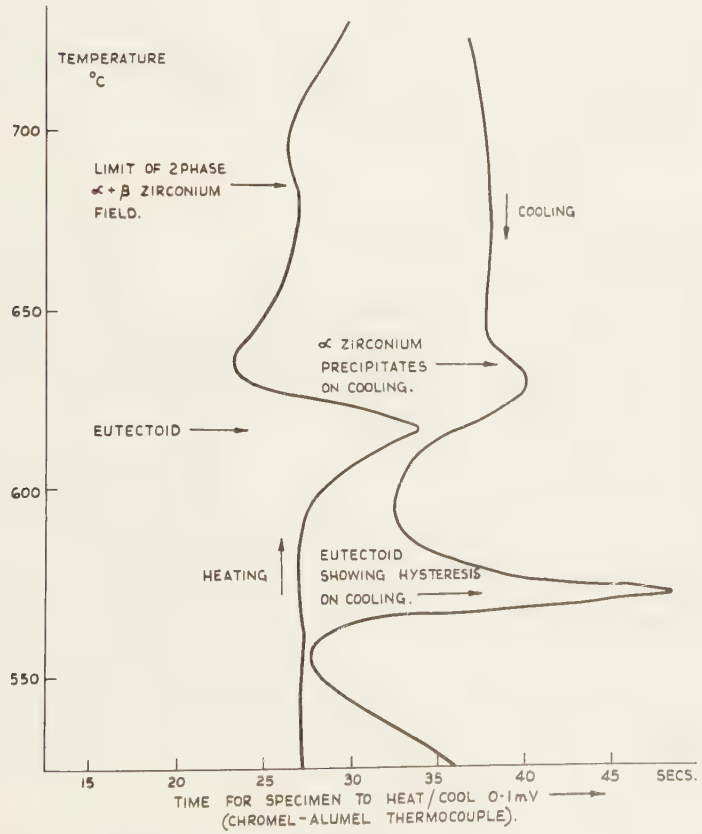

Fig. 6. Inverse rate heating and cooling curves for 80 at.% zirconium alloy.

0.004 Å per atomic percent; accordingly the 'c' parameter was used for determining the phase boundaries (see (h) below).

(g) The α/β-zirconium transformation and the eutectoid

The temperature of the eutectoid and the extent of the ($\alpha + \beta$) zirconium field have been determined by thermal analysis. The extent of the two-phase region found in each thermal analysis run is shown in Fig. 3 by a vertical bar and the eutectoid temperatures determined are shown by small triangles. A typical thermal analysis trace is shown in Fig. 6. This shows considerable hysteresis, as might be expected for a solid state transformation about 800°C below the solidus. The diagram (Fig. 3) is based on temperatures determined from heating runs: this is justified by X-ray and metallographic work just below the eutectoid.

Confirmatory metallographic work is summarised in Fig. 7. Some difficulty was experienced in the interpretation of the results since β-zirconium decomposes on quenching and also because the plutonium used included some impurities which made the detection of small amounts of a second phase uncertain.

Photomicrographs of three alloys quenched from the eutectoid region are shown in Figs. 8 and 9. Fig. 8 is of an alloy containing 60 at.% zirconium quenched from 637°C, and shows β-zirconium, which has decomposed on quenching, together with δ-plutonium. Fig. 9(a) is of an alloy containing 74 at.% zirconium quenched from 633°C. This is almost entirely decomposed β-zirconium with a little α-zirconium in the grain boundaries. Fig. 9(b) is of an alloy containing 76 at.% zirconium and is very similar to Fig. 9(a) but contains rather more α-zirconium, again in the grain boundaries.

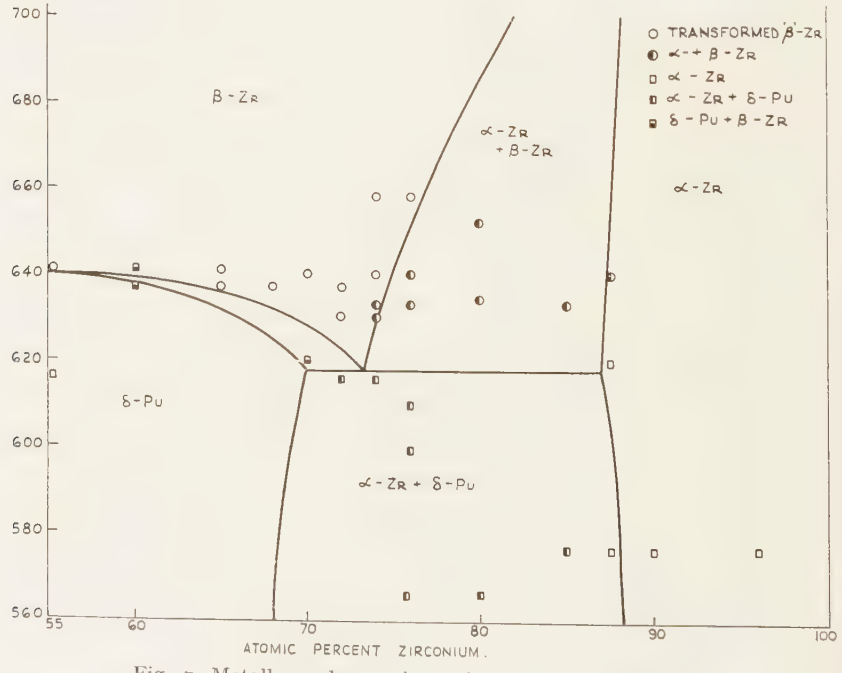

Fig. 7. Metallography specimens in the eutectoid region.

The (α-zirconium + δ-plutonium) two-phase field

The extent of this field is shown in Fig. 3. The boundaries between it and the two-ase field on each side were determined by the lattice parameter method: the points termined are marked as crosses in Fig. 3.

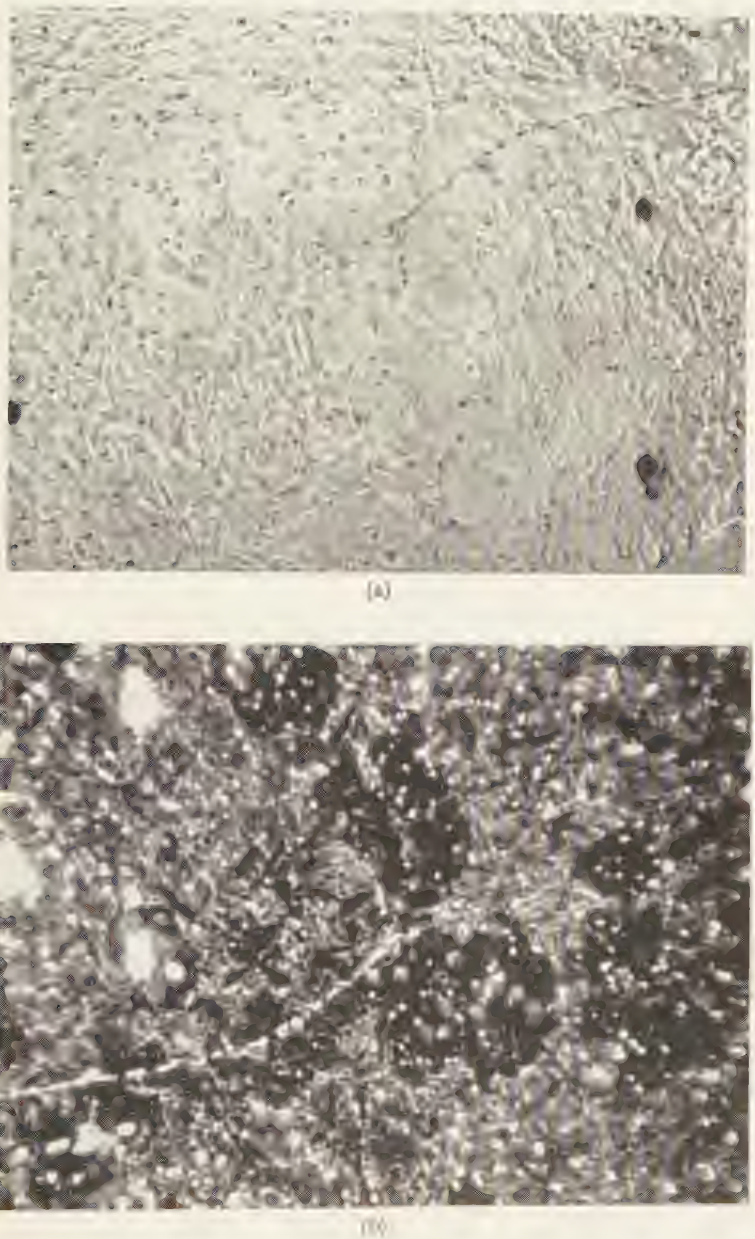

(a)

(b)

. 8. Plutonium 60 at.% zirconium alloy after 2½ days at 637°C. Quenched. Electropolished in 20% $HClO_4$ in butyl cellosolve. × 550. (a) Bright field. (b) Dark field.

(*i*) *The compound K*

This compound has been detected by its X-ray pattern, which was obtained from filings with compositions between 30 and 90 at.% zirconium, annealed at about 200°C. The single-phase region appears to be based on about 75 at.% zirconium and

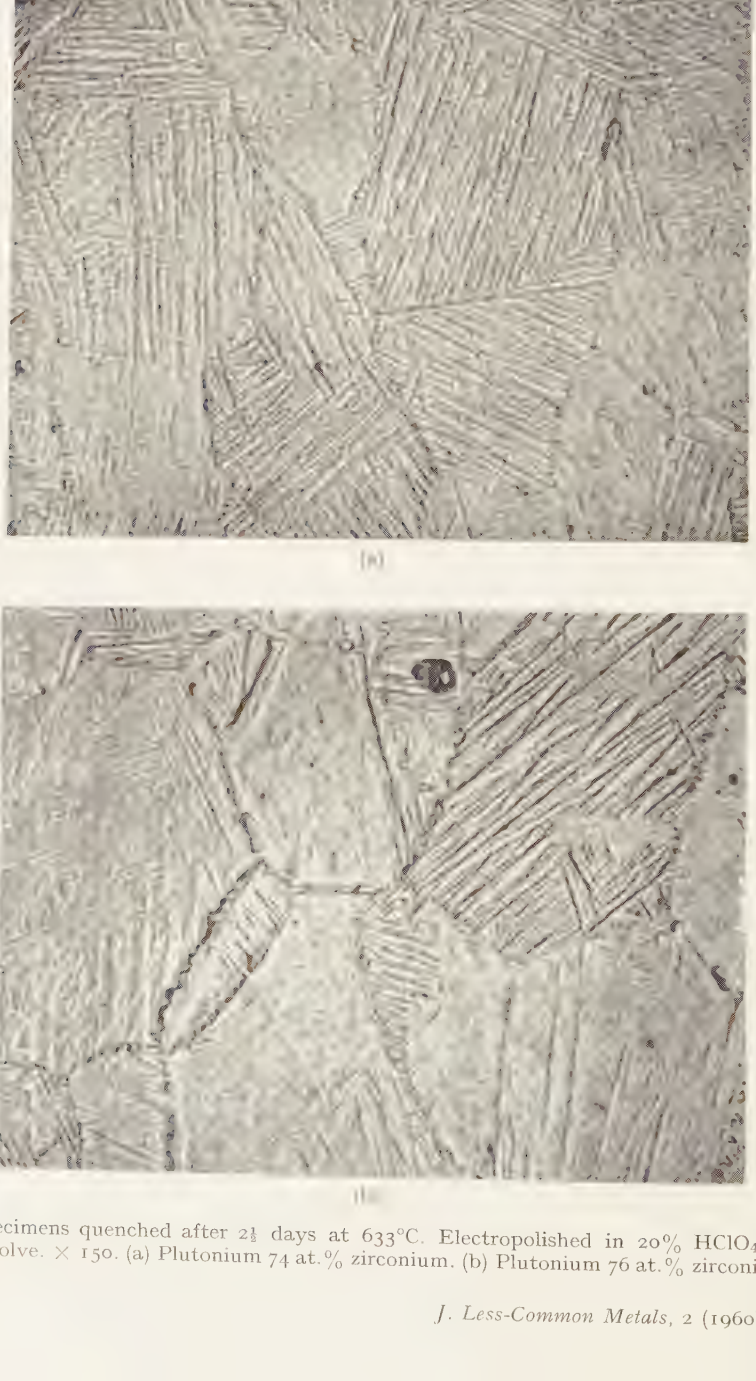

Fig. 9. Specimens quenched after 2½ days at 633°C. Electropolished in 20% $HClO_4$ in butyl cellosolve. × 150. (a) Plutonium 74 at.% zirconium. (b) Plutonium 76 at.% zirconium.

be fairly narrow, but, because of the slow rate at which the alloys reach equilibrium these temperatures, no attempt was made to determine the exact composition range this phase. Furthermore, the plutonium and zirconium atoms are sufficiently similar size to give little change in the lattice parameters of the compound with composi- n so that this effect cannot be used to determine the phase boundaries.

Filings annealed just below the decomposition temperature at 380°C did not form e compound readily and they were therefore annealed first at 200°C at which tem-

TABLE 1

X-RAY DATA FOR COMPOUND K AT 75 AT.% ZIRCONIUM

Line	d(Å)	Index	$Sin^2\theta \times 10^5$ (for Mo Kα radiation)			Intensity (referred to line 2 as 100)		
			Obs.	Calc.	Diff.	Obs.	Calc.	
1	4.395	100	651	656	−5	40	44	
2	3.135	001	1283	1290	−7	100	100	
6	2.544	101	1944	1946	−2	615	507	1160
	2.529	110	1966	1969	−3		653	
8	2.190	200	2623	2625	−2	10	9	
10	1.964	111	3259	3259	0	170	179	
11	1.792	201	3916	3914	+2	218	192	
12	1.655	210	4592	4594	−2	8	8.5	
14	1.562	002	5150	5158	−8	57	55	
		102	—	5815	—		6	
15	1.460	211	5898	5884	+14	345	205	346
		300		5907	−9		135	
17	1.328	112	7129	7127	+2	244	200	256
		301	—	7197	—		56	
		202	—	7784	—	98	4	89
18	1.263	220	7880	7876	+4		85	
		310	—	8532	—		3.4	
19	1.171	221	9166	9166	0	36	38	
20	1.131	212	—	9753	—	102	6	94
		311	9827	9822	+5		88	
		400	—	10501	—		1	
21	1.066	302	11068	11065	+3	88	95	
		003	—	11606	—		4	
22	1.033	401	11793	11791	+2	39	32	
23	1.013	103	12267	12263	+4	31	30	
		320	—	12470	—		2	
24	0.9823	222	13033	13034	−1	55	68	
24A	0.9628	113	13566	13575	−9		19	
		312		13600			3	
25	0.9555	321	13776	13760	+16	138	50	112
		410		13783	−7		62	
26	0.9398	203	14239	14232	+7	18	23	
27	0.9135	411	15070	15073	−3	25	32	
		402		15660	—		1	
28	0.8812	213	16196	16201	−5	40	37	
		500		16408	—		0	
		303		17513	—		12	
		322		17629	—		0	
29	0.8429	501	17700	17698	+2	48	16	36
		330		17721	−21		20	
		420		18377			1	
30	0.8148	412	18944	18941	+3	93	73	84
		331		19011	—		11	
31	0.7995	223		19482	—	27	10	36
		421	19677	19667	+10		26	
32	0.7906	313	20119	20138	−19	22	25	

perature K forms in a few days, and were then heated to successively higher temperatures until a batch of quenched filings no longer gave the X-ray pattern of the K phase. The structures found in this way are shown in Fig. 3 and give the peritectoid decomposition temperature as 380 ± 10°C. Attempts to confirm this by thermal analysis were unsuccessful due to the slow formation of K.

X-ray data for the compound, obtained from an alloy containing 75 at.% zirconium after annealing at 200°C for three weeks, are given in Table I. Molybdenum $K\alpha$ radiation was used with $\lambda(\alpha_1) = 0.70926$ Å. The X-ray pattern was indexed on the basis of an hexagonal cell with $a = 5.055$ Å, $c = 3.123$ Å. This gives good agreement between observed and calculated $\sin^2\theta$ values.

The relative intensities of the lines, shown in the table, were obtained from a recording photometer trace of the film and they are given in terms of line 2 as *100*. The unit cell holds 3 atoms and if these are arranged with a zirconium atom on (*000*) and zirconium and plutonium atoms randomly distributed on (*2/3, 1/3, 1/2*) and (*1/3, 2/3, 1/2*) as in Fig. 10, then the calculated intensities agree well with those observed. Agreement could not be obtained for the other possible atomic arrangements. The space group is *P6/mmm* and the structure is a disordered C32 AlB_2 type, similar to that proposed for UZr_2[10].

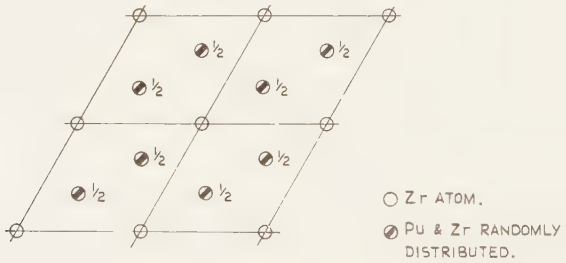

Fig. 10. Arrangement of atoms in compound K.

(j) The (δ-plutonium + K) and (δ-zirconium + K) fields

The boundaries between the two-phase fields and the single-phase δ-plutonium and α-zirconium fields have been found by the lattice parameter method: the points determined are shown as crosses in Fig. 4.

The boundary between the two-phase (α-zirconium + K) field and the α-zirconium field should be considered doubtful as the alloys probably have not reached equilibrium in the time employed at temperatures which are more then 1500°C below their melting points.

Filings annealed in the (K + δ-plutonium) field gave a sharp X-ray pattern of the K phase, but the δ pattern was always blurred, indicating that δ was present either with a range of compositions due to incomplete reaction or was slightly strained. The parameter method therefore did not determine the boundary accurately. Filings from a 60 at.% zirconium alloy after annealing at 200°C to allow K to form, were heated to 328°C for several days. After quenching, the X-ray pattern obtained was mainly that of the δ-phase with only a very small proportion of K. The quenching temperature is

herefore only just inside the $\delta/(\delta + K)$ boundary and so the latter was drawn as own in Fig. 3.

(ii) *The compound θ*

The compound θ which occurs at about 20 at.% zirconium gives a complex X-ray attern. The observed values of d and $\sin^2\theta$ are given in Table II.

TABLE II

X-RAY DATA FOR COMPOUND θ

attern obtained using Mo $K\alpha$ radiation from filings of a 21 at.% zirconium alloy annealed at °C. Calculated $\sin^2\theta$ values computed for the orthorhombic cell $a = 10.39$, $b = 10.44$, $c = 11.18$ Å[5]. See discussion.

Line	d (Å)	Int.	Obs. $\sin^2\theta \cdot 10^5$	Calc. $\sin^2\theta \cdot 10^5$	Index*	Line	d (Å)	Int.	Obs. $\sin^2\theta \cdot 10^5$	Calc. $\sin^2\theta \cdot 10^5$	Index*
1	7.545	W—	221	223	011	24	1.920	W+	3412	3433	152
				224	101	25	1.757	VW	4073	4059	531
2	5.485	M—	418	431	002	26	1.706	VW	4323	4320	253
3	4.646	M—	583	578	120	27**	1.539	M	5308	5311	361
				581	210					5382	236
4	4.412	M—	646	663	112	28	1.529	M	5380	5391	326
5	3.716	W	911	928	220					5392	017
				1036	221					5393	107
6	3.474	M—	1042	1039	030	29	1.515	M	5479	5433	444
				1048	300					5509	117
				1431	023					5694	155
7	2.964	M—	1432	1435	203	30	1.486	M—	5697	5709	700
8	2.715	M	1706	1723	004	31	1.473	M	5798	5798	550
9**	2.596		1865	1864	400	32	1.433	M—	6128	6121	270
0	2.577	S—	1894	1897	223					6126	461
1**	2.555		1926	1936	232	33	1.355	W+	6852		
				1945	322	34	1.296	W	7495		
2	2.535	S—	1957	1954	041	35	1.285	W	7613		
				1955	114	36	1.276	VW	7729		
3	2.481	M+	2043	?		37	1.265	VW	7863		
4**	2.431		2128	2124	133	38	1.229	W+	8329		
				2134	313	39	1.212	VW	8561		
5	2.400	M+	2183	2185	024	40	1.199	VW	8753		
				2189	204	41	1.189	W+	8895		
6	2.354	W+	2274	2277	042	42	1.175	VW	9109		
7	2.251	M	2481	2474	233	43	1.015	W+	12206		
				2483	323	44	0.999	W+	12592		
8	2.182	M—	2641	2651	224	45	0.985	W+	12957		
9	2.147	M	2727	2743	242						
				2885	050						
20	2.086	M+	2890	2888	314						
				2894	340						
					150						
				3002	341						
21	2.044	W	3010	3011	431						
				3020	501						
				3136	511						
22	2.001	W	3141	3154	025						
				3325	342						
23	1.942	W—	3333	3334	432						
				3343	502						

Many more $\sin^2\theta$ values are possible with this cell (the space group was not given). Only those ear observed values are tabulated.

* Indicates a line blurred into the following one.

Various indexing methods tried gave no acceptable results (see discussion).

The density of the θ phase is difficult to determine experimentally since it is impossible to be certain even after quite long anneals that the δ to θ transformation has gone to completion. An as-cast alloy containing 17.9 at.% zirconium had a density of 14.10 which lies on the density composition curve previously determined[1] for δ alloys. After annealing for 15 weeks at about 200°C the density had increased to 15.86 and the true θ density is presumably a little higher than this.

The alloys for which single-phase θ patterns are observed are marked in Fig. 2 by open circles and the extent of the θ single-phase region has been drawn accordingly.

The decomposition temperature has been determined by thermal analysis and dilatometry and the results are marked by vertical bars in Fig. 2. The as-cast arc melted alloys were still in the δ-form and so no θ to δ transformation was observed on the initial heating runs. The alloys were therefore annealed at 200°C for a few hours until the δ to θ transformation had taken place. The thermal analysis and dilatometry results were confirmed by X-ray examination of quenched filings. θ does not form readily at temperatures just below the decomposition temperature of approximately 340°C, and this accounts for some of the single-phase points marked in the two-phase field. Filings from the 21.0 at.% zirconium alloy were annealed for a few days at 200°C to form θ and batches were then quenched from successively higher temperatures. The results of the X-ray examination of these filings are shown in Fig. 2 and indicate a slightly lower decomposition temperature than that determined by thermal analysis, *e.g.*, the batch quenched from 338°C contained very little θ phase. This suggests that there was probably about 10° superheating in the thermal analysis experiments before the θ to δ transformation took place.

(l) The (θ + K) field and the low temperature eutectoid

As mentioned above, the rate of reaching equilibrium at the lower temperatures was very slow and as-cast alloys, or filings from them, annealed just below the eutectoid temperature, retain the δ structure for long periods, or form (θ + δ) (hypoeutectoid alloys) or (K + δ) (hypereutectoid alloys). Several points indicating such specimens that had not reached equilibrium are shown in Fig. 3.

The temperature of the eutectoid was found by annealing batches of filings at 190°C for about 3 weeks until θ and K had formed; these were then heated to successively higher temperatures until the X-ray pattern of a quenched batch of filings showed that the eutectoid had been passed; this occurred between 260°C and 275°C. The eutectoid composition has been determined by the intersection of the (θ + δ)/δ and (K + δ)/δ boundaries with the eutectoid temperature; since neither of these boundaries have been determined with great accuracy the composition given (55 at.% zirconium) must be considered only approximate.

An attempt was made to determine the eutectoid temperature using a dilatometer after the sample (containing 45 at.% zirconium) had been held at 200°C for three weeks. The specimen was slowly heated and slight kinks in the expansion curve occurred at 200°C and 260°C — the explanation of the first of these is not known but both effects were fairly small. When the specimen was well into the δ-field the expansion coefficient dropped to near zero (about $+ 1 \cdot 10^{-6}$). This compares with $-8.6 \cdot 10^{-6}$ for pure δ-plutonium at the same temperature[11].

n) The ($\theta + \delta$) regions

The ($\theta + \delta$) field on the zirconium-rich side of the compound is bounded on the low mperature side by the eutectoid at 267°C (see above). On the high temperature side a sloping boundary separating it from the single-phase δ field; this boundary has een determined by the lattice parameter method, which gives points marked by rosses in Figs. 2 and 3. These points show some scatter from a smooth curve and this probably accounted for by slowness in reaching equilibrium in the filings.

The ($\theta + \delta$) region on the plutonium-rich side of the compound has not been well fined. The X-ray patterns of filings quenched from this field did not show suffiently sharp δ-plutonium lines to enable the lattice parameter method to be used to etermine the boundary.

Thermal analysis changes occur as sharp arrests near the edge of the field, as indiated in Fig. 2 and this is confirmed by dilatometry which was carried out simultaneusly. The normal thermal analysis result for a two-phase field would be a gradual ange across it; if, however, the boundary between the ($\delta + \delta$) field and the θ field ere very convex, as shown, the θ phase in the two-phase alloy would decompose ther suddenly, thus giving a sharp arrest. This would be accentuated by the tendenof the θ phase to superheat before decomposing to δ.

) The low temperature plutonium phases

The main form of this part of the diagram has been determined by thermal analysis nd dilatometry, and by X-ray work. Some specimens for metallography were uenched from various temperatures but polishing them proved to be extremely fficult as they stained so readily.

The phase changes in this part of the diagram all occur rather too slowly for thermal alysis and dilatometry to be entirely reliable and some hysteresis is always appant. The temperatures at which thermal arrests took place are marked in Fig. 2.

The α/β transformation is extremely sluggish: it was not detected by thermal anasis in alloys containing more than 4.7 at.% zirconium and even in more dilute alloys could be suppressed by fast cooling. The transformation was not therefore studied detail but since, from X-ray work, the solubility of zirconium in β appears to be eater than that in α-plutonium the transformation is presumably depressed to a tectoid.

X-ray work in this part of the diagram was complicated by the retention or part ention of β to room temperature even in slowly cooled alloys and by the complexity the diffraction patterns of the three phases involved, *i.e.*, α and β-plutonium and e θ phase.

The solubility of zirconium in β-plutonium has been determined by the disappearing ase method. This is somewhat uncertain since it is difficult to recognise a weak ray pattern of θ when it is masked by a strong β pattern or, worse, a mixture of and β. The points involved are shown in Fig. 2. These include several points repreting alloys in which the β phase had transformed to α. They are marked at their iginal annealing temperatures and are only indicated as two phase when they gave X-ray pattern containing lines of θ phase.

The X-ray patterns of α-plutonium obtained from alloys containing small amounts zirconium show some changes in the $\sin^2\theta$ values of the lines. These values drop

compared with those for pure plutonium until about 1.5–2 at.% zirconium has been added, after which they remain approximately constant for further zirconium additions and this may correspond with the solubility limit. The values obtained were not sufficiently consistent for any work on parameter variations so that this result must be considered very approximate.

DISCUSSION

(*a*) *Comparison with Russian work*

The Russian review article containing their zirconium diagram which was published at Geneva[4] gave no details of the methods by which the diagram was obtained or of the thoroughness with which the work was carried out. As with all the diagrams published in the Russian article the boundary lines drawn between the various phase fields were very thick — about 1 atomic percent or 10°C. The temperatures quoted below were marked on the diagram.

The Russian diagram is of the same form as that proposed here although it shows the following differences in detail:

(i) The α/β zirconium transformation falls to a peritectoid at about 630°C, *cf.* eutectoid at 618°C in the present work.
(ii) The zirconium-rich compound is called $PuZr_2$ by the Russian workers and is marked at that composition, *cf.* 75 at.% in this work.
(iii) The low temperature eutectoid and peritectoid temperatures are both given as 30°C above those found here.
(iv) The δ'/ε transformation is shown depressed to a eutectoid instead of raised to a peritectoid.
(v) The solidus is given as about 100°C above that found in the present work.
(vi) The β/γ peritectoid temperature is given at 238°C, instead of 260°C.

(*b*) *The structure of the compound* θ

The Russian workers stated[4] that this compound has the formula Pu_6Zr and is orthorhombic with cell sides: $a = 10.39$ Å; $b = 10.44$ Å; $c = 11.18$ Å.

It can be seen that this is nearly tetragonal. The cell is very large and a great number of lines are possible. By selection from these most of the observed lines can be explained but the fact that so many lines are not observed does not lend conviction to the proposed cell. The indexing and calculated $\sin^2\theta$ values obtained using this cell are shown in Table II, for $\sin^2\theta$ values less than 0.06500. With coincidences the indexing shows that only 54 of the total of 303 calculated possible lines are observed. For some of the lines the agreement between observed and calculated $\sin^2\theta$ values is not very good, while one line (line 13) cannot be indexed despite the fact that it is fairly strong.

If the experimentally determined density of 15.86 is correct the Russian unit cell will contain 54 atoms, which is not consistent with the formula given: Pu_6Zr, *i.e.* 14.3 at.% zirconium. However, this density, as obtained, is probably too low and if the true density were 16.4 this would give 56 atoms per cell, *i.e.* 8 formula units.

(*c*) *American results*

A list of intermetallic compounds which included "$Pu_{19}Zr$" was recently published

a review article describing plutonium alloy work at Los Alamos[12]. The list did not, owever, include any other plutonium zirconium compounds nor were any details of ne structures of any of the compounds given.

(V) *Theoretical considerations*

Perhaps the most interesting part of the diagram from a theoretical viewpoint is the lubility of plutonium in α-zirconium. The following points are noteworthy.

(1) The solubility extends to about 11–12 at.% plutonium and is remarkably constant with temperature. This suggests that the limitation on solubility is not a size effect.

(2) The size factors of plutonium with respect to zirconium are very small: 3% for δ-plutonium and zero for ε-plutonium.

3) The '*a*' parameter of the zirconium lattice is only slightly increased by solution of plutonium, whereas the '*c*' parameter increases rapidly (*cf.* Fig. 5).

The slight increase in the '*a*' parameter can be ascribed to a size effect. If the '*a*' arameter/composition curve is extrapolated to 100% plutonium, the result, 3.30 Å, equal, within experimental error, to the diameter of the plutonium atom in the δ rm, 3.29 Å. (In h.c.p. structures the '*a*' parameter is equal to the interatomic dis- nce in that direction).

The increase in the '*c*' parameter is proportionally much greater and cannot be counted for in this way and it is suggested that it is due to an electronic effect. has been shown[13] that if an overlap occurs across one face of a Brillouin zone then e zone will be contracted in that direction and the lattice in real space will show an xpansion. The only zone faces that will give effects confined entirely to the *c* direction e of the type (00*l*). In α-zirconium the intensities of the X-ray reflections from these lanes when *l* is odd are zero due to the atoms at $z = 1/2$ in unit cell and so the energy ap across these planes in K-space is presumably zero. Also the planes where $l > 2$ e too far from the origin of K-space to be affected. The Fermi sphere will touch (002) hen it contains about 1.43 electrons per atom.

The transition elements of group IV (a) are usually considered to have a valency 4 but it has recently been suggested that it might well be 2[14]. These elements have ur electrons outside the inert gas core, 2 '*s*' and 2 '*d*' electrons. These do have nergies quite close to one another but there does not seem to be any compelling rea- n why the atoms should be fully ionised in the metallic state.

The X-ray data for the first few lines of the X-ray pattern of α-zirconium are given Table III. *I* is the experimental intensity, $|F|^2/f^2$ is the structure factor divided by he square of the atomic scattering factor for zirconium and $1/2d_{hkl}$ is proportional to he perpendicular distances of the plane *hkl* from the origin in K-space.

TABLE III

X-RAY DATA FOR α-ZIRCONIUM

hkl	d^{15}	I^{15}	$\lvert F\rvert^2/f^2$	$1/2d_{hkl}$
100	2.798	33	1	0.1787
002	2.573	32	4	0.1943
101	2.459	100	3	0.2033
102	1.894	17	1	0.2640
110	1.616	17	1	0.3094

$|F|^2/f^2$ is proportional to the intensity of the X-ray reflected from the appropriate plane and is presumably proportional to the energy gap at that face of the Brillouin zone. [101] is by far the strongest line in the pattern and the structure factor is also large for that line. Thus this will be an important face in the Brillouin zone for zirconium and overlaps across it will only occur reluctantly.

As noted above, when plutonium dissolves in α-zirconium the *c* parameter is increased while the '*a*' parameter is unaffected. Hence it is assumed that in pure zirconium an overlap across the [002] planes has already begun and that, when the electron to atom ratio is increased by dissolving plutonium, the extra electrons are accommodated by increasing this overlap rather than by forming a new overlap across the [101] planes. If an overlap across these [101] planes does not occur then the [002] overlap will increase until the electrons fill the zone, shown in Fig. 11, consisting of the hexagonal pyramids formed by the [101] planes truncated by the [102] pyramids. In zirconium this zone contains 2.416 electrons per atom — in titanium it contains slightly less: 2.410 electrons per atom.

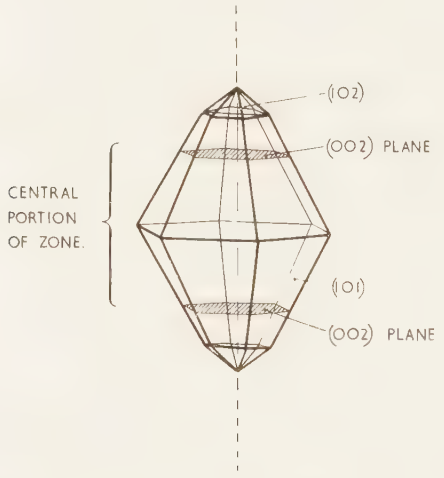

Fig. 11. Proposed zone for α–zirconium containing 2.416 electrons per atom.

If the zone could be filled exactly up to the bottom of the [102] pyramids it would contain 2.38 electrons per atom: this is of course strictly impossible since the Fermi surface will have some complex curved form but it gives an idea of the approximate electron to atom ratio in that region, where the zone starts to become unstable.

Assuming the valency of zirconium to be 2 and that for plutonium to be 4.8[16] then the electron to atom ratio will be 2.31 at 11 at.% solubility, 2.34 at 12% and 2.36 at 13% solubility. The solubility found in practice has a peak value of 13 at.% plutonium at 618°C and the solubility at 400°C is about 11 at.%. These solubility limits are consistent with the rapid fall off in the density of states when the main part of the zone has been filled but they occur considerably before the whole zone is filled at 2.42 electrons per atom.

This fall off in the density of states means that when an element of valency more

han 2 is dissolved in either zirconium or titanium the stability of the single phase ructure will drop, gradually at first and then more rapidly as the zone fills. Thus the lectron to atom ratio of 2.42 when the zone is full is an upper limit: in most cases nother phase will become more stable long before this. Not many elements dissolve o any extent in α-titanium or α-zirconium so that the value of this zone is difficult to heck. The solubilities of those that do dissolve are tabulated in Table IV[17,18,19], but one of these elements show much evidence either for or against the proposed zone, except aluminium, for which the electron to atom ratio at maximum solubility (2.43) very close to that for the full zone (2.42).

TABLE IV

SOLUBILITIES OF VARIOUS ELEMENTS IN TITANIUM AND ZIRCONIUM

Alloy system	*Size factor* (%)	*Maximum solubility* (*at.*%)	*Valency*	*Electron to atom ratio at maximum solubility*	*Effect on c/a ratio of Zr or Ti*
TiAl	—4.4	43	3	2.43	increased slightly
Nb	0	1.6	5	2.08	increased slightly
Ag	—2.0	7	1 5.44	1.93 2.24*	increased
Ta	0	2	5	2.06	slightly decreased
Sn	+7	13	4	2.26	increased
Ga	—8	12	3	2.12	
In	+8	10	3	2.10	
ZrSn	—3	7	4	2.14	increased
Pb	+9	6	4	2.12	
Nb	—8	7	5	2.21	
Al	—11	7	3	2.07	
In	—1.6	9	3	2.09	
Cd	—2	>10	2	2 (assuming Zr and Ti valencies to be 2).	

Silver dissolving in titanium increases the c parameter while decreasing the a value. This would be expected if the valency of silver were greater than 2; if it were less the reverse would be expected. 5.44 is the valency given by L. PAULING for silver (*J. Am. Chem. Soc.*, 69 (1947) 3.)

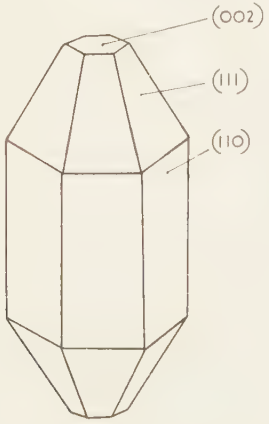

Fig. 12. Brillouin zone for compound K. This contains 2.97 electrons per atom.

Another interesting feature of the diagram which can be accounted for by zone theory is the formation of the compound K at zirconium concentrations higher than those indicated by the formula $PuZr_2$. Consideration of the X-ray scattering factors of the first few lines in the diffraction pattern suggests that an important zone for this structure is that shown in Fig. 12, bounded by the [110], [111] and [002] planes. This contains 2.97 electrons per atom and, assuming valencies of 2 and 4.8 for zirconium and plutonium, would be completely filled when the compound contains 35 at.% plutonium. However, when completely full this zone will be relatively unstable and so the compound will not occur at compositions near the "ideal" $PuZr_2$. If zirconium is assumed to have valency 4, there is no well-defined zone which will explain this effect.

The existence of the other wide single-phase fields based on δ-plutonium and ε-plutonium/β-zirconium is not surprising in view of the small size factors involved; β-zirconium atoms are almost exactly the same size as those of ε-plutonium, while the size factor of zirconium with respect to β-plutonium is only —3%.

The solubility of zirconium in the other three plutonium phases is larger than the negligible values reported for most other elements. This again is presumably accounted for by the small size factor. For α-, β- and γ-plutonium these will be about + 4%, + 1% and zero respectively. The only other elements so far investigated which have very low size factors and which, from electronegativity considerations, will not be likely to form compounds stable enough to limit solubility, are uranium and neptunium. The former dissolves appreciably in β-plutonium (2 at.%) and γ-plutonium (1 at.%)[20] while the latter appears to form a wide field with the λ-plutonium structure extending to about 50% neptunium[21]; these observations lend support to a simple size factor approach.

ACKNOWLEDGEMENTS

Thanks are due to many members of the Plutonium Metallurgy Group for help and advice. In particular, the author acknowledges the metallographic work by H. Haines, D. J. Hodkin and T. Thoday and many useful discussions with Dr. D. M. Poole and Dr. M. B. Waldron. Dr. J. A. Lee and Mr. R. O. A. Hall carried out the dilatometry experiment described on page 344.

REFERENCES

1 G. K. Williamson, D. M. Poole, J. A. C. Marples and M. B. Waldron, *Alloys of Plutonium with Zirconium*, A.E.R.E. Rept. M/R 2085, 1956.
2 A. S. Coffinberry and F. H. Ellinger, *International Conference on the Peaceful Uses of Atomic Energy, Geneva, 1955*, A/Conf. 8/P/826.
3 M. B. Waldron *et al.*, *Second United Nations Conference on the Peaceful Uses of Atomic Energy Geneva, 1958*, A/Conf. 15/P/71.
4 A. A. Bochvar *et al.*, *Second United Nations Conference on the Peaceful Uses of Atomic Energy Geneva, 1958*, A/Conf. 15/P/2197.
5 H. J. Dunster and E. J. Bennellick, *Atomics*, 6 (1955) 312.
6 G. N. Walton, *Glove Boxes and Shielded Cells*, Butterworths Sci. Publ., London, 1958.
7 G. K. Williamson, D. M. Poole and J. A. C. Marples, *Some Facilities for the Study of Plutonium and its Alloys*, A.E.R.E. Rept. M/R 1990, and *J. Inst. Metals*, 85 (1956–57) 431.
8 D. M. Poole, G. K. Williamson and J. A. C. Marples, *A Preliminary Investigation of the Plutonium-Thorium System*, A.E.R.E. Rept. M/R 2156, April, 1957.
9 R. W. M. D'Eye, *Some Remarks on the Guinier-Type X-ray Focussing Camera*, A.E.R.E. Rept. C/R 1524, October, 1954.
10 J. M. Silcock, *J. Metals*, 9 (1957).

A. S. Coffinberry and M. B. Waldron, *Progress in Nuclear Energy*, Vol. 1, Pergamon Press, London and New York, 1956, series V, chap. 4.
Plutonium, *Nucleonics*, 16 (1958).
H. Jones, *Proc. Roy. Soc. (London)*, 147A (1934) 396.
J. A. Betterton and J. H. Frye, *Acta Met.*, 6 (1958) 205; and G. M. Adamson *et al.*, *Second United Nations Conference on the Peaceful Uses of Atomic Energy, Geneva, 1958*, A/Conf. 15/P/1993.
H. E. Swanson and R. K. Fuyat, *Natl. Bur. Standards Circ.*, 539, 1953.
W. H. Zachariasen, in G. T. Seaborg and J. J. Katz, *The Actinide Elements*, McGraw-Hill, New York, 1954, p. 769.
A. D. and M. K. McQuillan, *Titanium*, Butterworths Sci. Publ., London, 1956.
G. L. Miller, *Zirconium*, 2nd edit., Butterworths Sci. Publ., London, 1957.
B. Lustman and F. Kerze, *The Metallurgy of Zirconium*, McGraw-Hill, New York, 1955, chap. VII.
A. S. Coffinberry *et al.*, The physical metallurgy of plutonium and its alloys, *Second United Nations Conference on the Peaceful Uses of Atomic Energy, Geneva, 1958*, A/Conf. 15/P/1046.
H. A. C. McKay *et al.*, The chemistry and metallurgy of neptunium, *Second United Nations Conference of the Peaceful Uses of Atomic Energy, Geneva, 1958*, A/Conf. 15/P/304.

THE VARIATION OF UNIT-CELL EDGE OF URANIUM MONOCARBIDE IN ARC MELTED URANIUM–CARBON ALLOYS

J. WILLIAMS, R. A. J. SAMBELL AND D. WILKINSON

Metallurgy Division, United Kingdom Atomic Energy Authority, Harwell, Berks. (Great Britain)

(Received May 14th, 1960)

SUMMARY

The unit-cell edge of uranium monocarbide in arc melted uranium–carbon alloys varies between 4.9600 ± 0.0005 Å and 4.9520 ± 0.0002 Å in a systematic manner with carbon content up to approximately 4.8 wt.%. Annealing at 1300°C *in vacuo* causes all cell edges to approach the former value slowly. The compositions studied ranged from 2.5 wt.% C up to 7.0 wt.% C but beyond approximately 4.8 wt.% the cell edge varied little with composition.

The variations in cell edge are believed to be due to structural variation in the monocarbide itself, and not to contamination with oxygen or nitrogen.

INTRODUCTION

A range of values for the unit-cell edge of uranium monocarbide are given in the literature. RUNDLE *et al.*[1] quoted a cell edge of 4.951 ± 0.001 Å for monocarbide prepared by heating carbon with uranium or a uranium oxide *in vacuo* at about 1800°C. LITZ *et al.*[2] gave a value of 4.955 Å for carbide also prepared as above. In *Structure Reports* Vol. 11, p. 84, these values of cell parameters were assumed to have been in kX units and were re-quoted as 4.961 ± 0.001 Å and 4.965 Å respectively: the same results were quoted as 4.961 Å and 4.955 Å by SALLER AND ROUGH[3]. For fused carbide MALLETT *et al.*[4] quoted 4.951 Å whilst BURDICK *et al.*[5], for the alloys prepared by MALLETT subsequently heated at 1700°C for 2 h and quenched, gave a cell edge of 4.962 Å. BOETTCHER[6] quoted a value of 4.951 ± 0.004 Å for monocarbide prepared by carbon reduction of the oxide and sintered at 1800°C. One of the present authors[7] quoted the cell edge of monocarbide, prepared by solid state reaction of uranium and graphite, as 4.963 ± 0.001 Å, and more recently AUSTIN[8] has given the parameter for monocarbide prepared by arc melting under helium as 4.9598 ± 0.0003 Å.

During investigations of the U–C–UN system[9] the authors obtained U–C alloys in which the monocarbide, in an alloy of nominally stoichiometric composition prepared by solid-state reaction of the mixed elemental powders, had a unit-cell edge of 4.9605 ± 0.0004 Å. When melted in an argon-arc furnace on a water-cooled copper hearth the cell edge of the monocarbide fell to 4.9544 ± 0.0003 Å but on annealing at 1200°C *in vacuo* for 72 h the cell edge increased again to 4.9606 ± 0.003 Å.

The investigations described in this report were undertaken in an attempt to resolve these apparent anomalies in the unit-cell of uranium monocarbide.

EXPERIMENTAL METHODS

The materials used were freshly-leached calcium-reduced uranium powder (—300 mesh B.S.S.) and ultrafine graphite powder (Acheson Dag 624). Mixtures containing from 2.5 wt.% to 7.0 wt.% C were prepared and cold-compacted at 40 tons/in². The resulting 25 g pellets were arc melted in argon on a water-cooled copper hearth using a tungsten electrode. Samples were turned over and re-melted twice to minimise segregation. Portions of the melted button were annealed *in vacuo* ($< 10^{-5}$ mm Hg) for totals of 12 and 88 h at 1300°C and furnace cooled.

X-ray powder diffraction patterns were obtained for all alloys. Specimens containing more than 4 wt.% C were ground in an agate mortar and pestle under trichlorethylene to give powder in the size range 75–55 μ. Powder samples were obtained from those specimens containing less than 4 wt.% C by drilling with a diamond-tipped tool under trichlorethylene. Exposures were made in a Straumanis type of Debye-Scherrer camera using a copper radiation (Cu $K\alpha_1$, 1.54050 Å, Cu $K\alpha_2$ 1.54434 Å). The cell edges were determined from a Nelson–Riley plot. The temperature of the camera was not deliberately controlled but temperature records for the period of exposure (2 h) showed that the observed maximum variation was 2°C, which would cause changes of lattice parameter well within the error due to other factors. Chemical analysis for carbon was carried out after melting and after annealing for 88 h.

RESULTS

Carbon contents are given in Table I for all the specimens used. Melting caused a loss of up to 0.17 wt.% C, but negligible change in carbon content resulted from annealing.

TABLE I

VARIATION OF UNIT-CELL EDGE WITH COMPOSITION AND ANNEALING TREATMENT

Nominal wt.% C	Analysed wt.% C		Unit-cell edge (Å)		
	As-melted	Annealed 88 h at 1300°C	As-melted	Annealed 12 h at 1300°C	Annealed 88 h at 1300°C
2.5	2.40	2.40	4.9562 ± 0.0007	4.9570 ± 0.0004	4.9570 ± 0.0003
3.0	2.85	2.83	4.9544 ± 0.0005	4.9568 ± 0.0003	4.9570 ± 0.0002
3.5	3.40	3.41	4.9531 ± 0.0005	4.9562 ± 0.0002	4.9574 ± 0.0003
4.0	3.83	3.83	4.9520 ± 0.0002	4.9558 ± 0.0002	4.9578 ± 0.0002
4.4	4.35	4.35	4.9550 ± 0.0003	4.9576 ± 0.0003	4.9592 ± 0.0003
4.6	4.48	4.46	4.9555 ± 0.0003	4.9582 ± 0.0003	4.9592 ± 0.0003
4.8	4.65	4.64	4.9568 ± 0.0005	4.9601 ± 0.0002	4.9601 ± 0.0003
5.0	4.85	4.85	4.9600 ± 0.0005	4.9601 ± 0.0002	4.9601 ± 0.0002
5.2	5.12	5.12	4.9607 ± 0.0003	4.9605 ± 0.0003	4.9603 ± 0.0003
5.4	5.35	5.35	4.9602 ± 0.0003	4.9598 ± 0.0003	4.9597 ± 0.0003
6.0	5.85	5.86	4.9605 ± 0.0004	4.9605 ± 0.0004	4.9605 ± 0.0004
6.4	6.28	6.30	4.9610 ± 0.0005	4.9611 ± 0.0005	4.9608 ± 0.0003
7.0	6.85	6.86	4.9616 ± 0.0005	4.9600 ± 0.0004	4.9600 ± 0.0004

Within the limits of spectrographic analysis no tungsten was detected, indicating that contamination, if it occurred, was <100 p.p.m.

The cell edges for various compositions in the three conditions of treatment are given in Table I and plotted in Fig. 1. In alloys containing more than 4.85 wt.% C the cell edge remains sensibly independent of annealing treatment and composition. Below 4.85 wt.% the cell edge for cast specimens diminishes with decreasing carbon

content from 4.9600 ± 0.0005 Å to 4.9520 ± 0.0002 Å at 3.8$_3$ wt.% C. Further decrease of carbon content to 2.4 wt.% causes the cell edge to increase to 4.9562 ± 0.0004 A. Annealing at 1300°C causes the cell edges to increase progressively to values lying between 4.9570 ± 0.0003 A and 4.9601 ± 0.0002 A, lower values being associated with lower carbon contents.

The only effect of annealing upon the appearance of the specimens was to cause exudation of uranium.

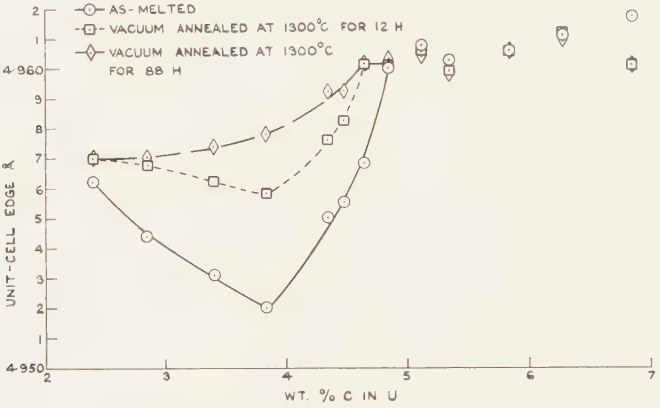

Fig. 1. Variation of cell edge with carbon content and annealing treatment.

DISCUSSION

Variation in cell edge could be, and has been, ascribed to variation in impurity content of the monocarbide. Both the mononitride and 'monoxide' are isomorphous with the monocarbide and also have smaller cell edges[7,9]. Increase of either of these constituents with increased uranium content could therefore be responsible for the decrease of lattice parameters of those alloys containing 4.8 wt.% C. A number of facts argue against this explanation.

(a) Assuming a linear relationship of lattice parameters and composition for the UC–UN system, 10 wt.% UN would be needed to give rise to the difference in cell sizes between the 4.8$_5$ wt.% and the 3.8$_3$ wt.% C alloys: depending upon the parameter assumed for UO, *viz.* 4.93 Å or 4.953 A, 15–50 wt.% UO would be needed. For this quantity of contaminant to be associated with 1 wt.% U is impossible.

(b) When UO_2 and UC are melted together in an argon arc mutual elimination of carbon and oxygen occur[10] and at such temperatures uranium mononitride dissociates.

Reaction between UO_2 and graphite proceeds at an appreciable rate at temperatures above 1500°C. The uranium powder used contained 0.15% O_2 which would combine with 0.11% C to give carbon monoxide. The difference of 0.05 to 0.17% C between analysed and nominal carbon contents could therefore be roughly accounted for by this reaction.

Melting therefore probably reduces the nitrogen and oxygen contents of the alloys.

(c) Considering nitrogen and/or oxygen contamination as being responsible for the parameter changes on melting, annealing presumably reduces the variation in cell

ge by elimination of impurities. This process would have been expected to be far ore effective at 2400°C than at 1300°C unless contamination is introduced by the elting technique.

(d) The systematic variation of cell edge with composition coupled with the success- l use of the technique for melting reactive metals, *e.g.*, zirconium, titanium, argues ainst introduction of impurities during melting. Nitrogen analyses of the U–C loys have shown ~100 p.p.m. N_2 to be present.

The variation of cell edge with composition seems therefore to be a true feature of U–C system and is probably associated with deviation from stoichiometry of nium monocarbide in the direction of increased proportion of metal at elevated peratures.

Systematic decrease of cell edge of NbC[11], TiC[12], VC[13], and TaC[14] with decrease of bon content below the stoichiometric composition has been reported but not com- ited upon. There is no reported parallel to the subsequent increase in cell edge h further decrease of carbon content below 3.8$_3$ wt.% and an obvious explanation not apparent. One possibility is a change of structural type of the monocarbide. NDLE[1] showed that if the monocarbide possessed a sodium chloride structure *(420)* should be about 14% greater than *I(331)*, whilst for a zinc blende structure *(331)* should be greater by about 7%. He found *I(420)* > *I(331)* for stoichiometric showing that it had the sodium chloride structure. This finding was confirmed by STIN[8] using neutron diffraction. To establish whether or not a change from NaCl ZnS type of structure occurs, the relative intensities of the *(420)* and *(331)* lines of e UC in arc cast alloys of varying carbon content were measured on a Philips fractometer using copper radiation. With decreasing carbon content the definition the two lines decreased considerably. The results given in Table II show that there probably a slight variation in relative intensities of the ratio of intensities of the *31)* and *(420)* lines with carbon content of the U–C alloys, but that the ratio is never eater than unity.

TABLE II

VARIATION OF I(*331*/*420*) WITH CARBON CONTENT

Wt.% C	2.40	3.41	3.8$_3$	4.35	4.46	5.35	6.30
I(331/420)	0.82	0.85	0.80	0.85	0.85	0.93	0.87

When satisfactory methods for preparation of samples have been evolved, neutron fraction studies will be made on selected alloys to determine the position of the rbon atoms in a less equivocal fashion.

The monocarbide structures that have been examined and reported upon here for oys containing less than 4.8 wt.% C are obviously non-equilibrium structures. e extent to which they are truly representative of structures at the quenching mperature will depend upon the efficacy of the quenching technique. Values of it-cell edge quoted therefore must not be regarded in any sense as "standard lues". Variation in specimen size or quenching method could, for example, yield a onocarbide having a different unit-cell edge from that reported here. What this vestigation shows is that uranium monocarbide probably deviates from stoichio-

metry in the direction of a metal : carbon ratio greater than unity, and further work is needed to determine the extent and nature of the deviation.

CONCLUSIONS

The unit-cell edge of uranium monocarbide in cast and rapidly cooled uranium-carbon alloys containing up to 4.8 wt.% C varies between 4.9600 ± 0.0005 Å and 4.9520 ± 0.0002 Å, in a systematic manner with carbon content. Annealing at 1300°C *in vacuo* causes all cell edges to approach the former figure at a slow rate. These variations in cell edge are believed to be due to structural variation in uranium monocarbide itself, *e.g.* departure from stoichiometry in the direction of an increased metal : carbon ratio and not to contamination with oxygen or nitrogen. X-ray diffraction techniques by themselves do not, however, indicate the nature of these structural changes.

REFERENCES

1 R. E. RUNDLE, N. C. BAENZIGER, A. S. WILSON AND R. A. MCDONALD, *J. Am. Chem. Soc.*, 70 (1948) 99.
2 L. M. LITZ, A. B. GARRETT AND F. C. CROXTON, *J. Am. Chem. Soc.*, 70 (1948) 1718.
3 F. A. ROUGH AND R. E. BAUER, *Battelle Memorial Inst. Rept. No. 1300.*
4 M. W. MALLETT, A. F. GERDS AND D. A. VAUGHAN, *J. Electrochem. Soc.*, 98 (1951) 505.
5 M. D. BURDICK, H. S. PARKER, R. S. ROTH AND E. L. MCGANDY, *J. Research Natl. Bur. Standards*, 54 (1955) 217.
6 A. BOETTCHER, AND G. SCHNEIDER, *Second United Nations Atomic Energy Conference, Geneva, 1958*, A/Conf. 15 /P/ 964.
7 J. WILLIAMS, *Rev. mét.*, 13 (1956) 189.
8 A. E. AUSTIN, *Acta Cryst.*, 12 (1959) 159.
9 J. WILLIAMS AND R. A. J. SAMBELL, *J. Less-Common Metals*, 1 (1959) 217.
10 J. WILLIAMS AND R. A. J. SAMBELL, unpublished work.
11 G. BRAUER, H. RENNET AND J. WERNER, *Z. anorg. Chem.*, 277 (1954) 249.
12 P. ERLICH, *Z. anorg. Chem.*, 259 (1949) 1.
13 N. SCHONBERG, *Acta Chem. Scand.*, 8 (1954) 624.
14 V. SMIRNOVA AND B. F. ORMONT, *Doklady Akad. Nauk S.S.S.R.*, 96 (1954) 557.

THE MELTING POINT OF OSMIUM

A. G. KNAPTON, J. SAVILL AND R. SIDDALL

Research Laboratory, Associated Electrical Industries, Aldermaston, Berks. (Great Britain)

(Received June 2nd, 1960)

SUMMARY

In the literature the accepted melting point of osmium metal is reported as 2750°C. It has now been established that this value is low and a redetermination gives 3045 ± 30°C.

INTRODUCTION

he melting point of osmium has been variously reported as 2500°C by TAMMANN[1] 2750 ± 100°C by FROHLICH[2]. The generally accepted value appears to be 2700°C[3]. an empirical arc furnace method[4,5], results were obtained in this laboratory which gested that these reported melting points are low, and that 3000 – 3100°C is almost tainly a more correct value.

he melting point of osmium has now been redetermined by direct measurement of black-body radiation from a hole near the centre of an electrically heated bar, as he method originally used by PIRANI AND ALTERTHURN[6] In this method, the bar perature is raised steadily, and the temperature at which the hole fills with liquid noted.

EXPERIMENTAL

experimental arrangement is shown schematically in Fig. 1. Small cylindrical is of the metal (A), approximately 5 mm in diameter, and 10–15 mm long, were pported between two water-cooled electrodes (B). The electrodes were mounted in a oratory arc furnace chamber (C), which could be evacuated before being filled with

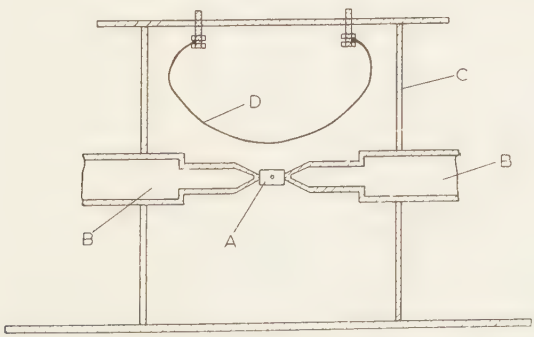

Fig. 1. Melting point apparatus.

cylinder argon. The argon was gettered with a titanium strip (D) and heated to redness by direct passage of an electric current prior to the melting point determinations.

The optical pyrometer, a Cambridge disappearing filament type, was sighted on a 1 mm hole 4-5 mm deep drilled centrally in the specimen along a diameter. Readings were taken through a 1/4 in. thick silica viewing window in the port of the arc furnace chamber. Low tension d.c. was supplied by two 600 A Lincoln welding generators in parallel.

The osmium metal used was supplied in the form of powder, by Johnson Matthey and Co., Ltd. and by the Mond Nickel Company. The metal was consolidated by argon-arc melting for the determinations, and its purity is considered to be better than 99.7% after melting.

Molybdenum, tantalum and tungsten were used as standard specimens. These metals were electron-bombardment zone-melted in a high vacuum, and were of high purity. The melting points of certain rhenium specimens, arc-melted from 99.9% pure Johnson Matthey sponge, were also measured during this investigation. Holes in the harder materials, osmium, rhenium and tungsten were formed by spark-machining.

The melting temperatures of the molybdenum, tantalum and tungsten standards were taken as 2620°, 3000° and 3380°C respectively[3].

CONCLUSIONS

The observed melting points for the pure metal standards are given in Table I, and were used to plot the correction curve given in Fig. 2.

TABLE I

OBSERVED MELTING POINTS OF STANDARD ELEMENTS

Metal	*Observed melting points* (°C)	*Accepted melting point* (°C)
Molybdenum	2610	2620
	2610	
Tantalum	3030	3000
	3010	
Tungsten	3360	3380
	3390	

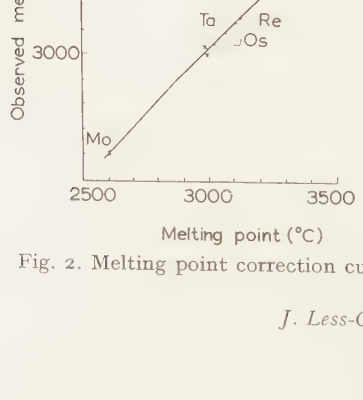

Fig. 2. Melting point correction curve.

The observed melting temperatures of osmium and rhenium (Table II) are interpolated in Fig. 2, giving the osmium melting point as 3045° ± 30°C, and rhenium 3140° ± 20°C.

TABLE II

MELTING POINTS OF OSMIUM AND RHENIUM

Metal	*Observed melting points* (°C)	*Melting point* (°C)
Osmium	3040	
	3080	3045 ± 30
	3065	
Rhenium	3140	
	3130	3140 ± 20
	3135	

The latter is in fair agreement, but slightly lower than the generally accepted value, 3170°C[3], and it is obvious that the previously used osmium melting point is seriously in error.

ACKNOWLEDGEMENTS

The authors wish to thank Dr. G. A. Geach for his encouragement and interest in the work, and Dr. T. E. Allibone, Director of the Laboratory, for permission to publish this paper.

REFERENCES

G. Tammann, *Z. Elektrochem.*, 14 (1908) 800.
F. Frohlich, *Gmelin's Handbuch der Anorganischen Chemie*, System No. 66, Osmium, 1939, p. 11.
G. W. C. Kaye and T. H. Laby, *Tables of Physical and Chemical Constants*, 12th Edit., Longman's, London, 1959.
J. D. Baird, G. A. Geach and A. G. Knapton, *Plansee Proc.*, 3rd Plansee-Seminar, Reutte, June, 1958, p. 371.
F. O. Jones, A. G. Knapton and J. Savill, *J. Less-Common Metals*, 1 (1959) 80
M. Pirani and H. Alterthurn, *Z. Elektrochem.*, 29 (1923) 5.

SOME STUDIES ON INORGANIC PEROXY-ACIDS

I. PEROXYMOLYBDIC AND PEROXYTUNGSTIC ACIDS

E. RICHARDSON

Dept. of Chemistry, Whitehaven College of Further Education, Cumberland (Great Britain)

(Received May 24th, 1960)

SUMMARY

The reaction between hydrogen peroxide and molybdic acid and tungstic acid has been studied by conductometric, potentiometric and spectrophotometric methods over a wide concentration range. Direct evidence is presented for the existence in solution of peroxymolybdic acids of active oxygen: Mo ratios of 1 : 1 and 2 : 1. Some properties of these acids are discussed. Two peroxytungstic acids are formed in a solution of active oxygen: W ratios of 1 : 1 and 4 : 1. Both acids are simpler in structure than the original tungstic acid.

INTRODUCTION

Two peroxymolybdic acids of empirical formulae H_2MoO_5[1,2] and H_2MoO_6 have been described in the literature. Evidence for these formulae has been obtained from cryoscopic[5] and thermochemical studies[3,4] on acidified molybdate solutions containing various quantities of hydrogen peroxide. MoO_3 and molybdic acids prepared by conventional techniques are only sparingly soluble in cold dilute peroxide but a spectrophotometric study has been made by TREADWELL[6] on the effect of peroxide on MoO_3 dissolved in concentrated sulphuric acid, and a thermogravimetric study by TRIDOT[7] on the products obtained by dissolving MoO_3 in concentrated peroxide at 100°C. The existence of condensed peroxymolybdates in acid solution has been claimed by JAHR[8] from diffusion studies but CSANYI[9] claims that excess peroxide inhibits the aggregation process. TRIDOT[7] claims that the acid of empirical formula H_2MoO_5 is a complex containing anionic and cationic molybdenum (Mo_2O_{11})-H (HMo_2O_6) which forms the peroxydic ion $Mo_2O_{11}^{2-}$ and on partial neutralisation $Mo_4O_{13}^{2-}$ and MoO_4^{2-}. According to TRIDOT[7] no simple anion of active O : Mo ratio 1 : 1 exists. The existence of the condensed ion $Mo_2O_{11}^{2-}$, now accepted by most authors[10,11] to be formed in peroxide-rich solutions, has recently been disputed by CSANYI[9] who claims the ion is $(HMoO_6)^-$

$$2(HMoO_6)^- \rightleftarrows H_2O + Mo_2O_{11}^{2-}$$

In the present study the reaction of hydrogen peroxide with molybdic acid prepared by ion exchange has been investigated. This approach offers 3 advantages.

(1) Molybdic acid prepared by ion exchange is known to be a poly-acid[12] and if peroxypolymolybdates do exist will presumably favour their formation.

2) Ion-exchange molybdic acid is more soluble[12] than other varieties, allowing dies to be made at higher molybdenum concentrations than hitherto.

3) Molybdic acid-peroxide interaction can be studied in the absence of foreign ·s.

n contrast to peroxymolybdic acids little information is available on peroxy-ngstic acids, due largely to the low solubility in water of WO_3 and of tungstic acids pared by precipitation from acidified tungstate solutions. These materials will solve in concentrated hydrogen peroxide at 100°C to form a compound of empirical mula H_2WO_5 although, according to REMY[13], this could be a peroxyhydrate $)_3H_2O_2$ and not a peroxy acid. RACISZEWSKI[14] has used H_2WO_5 as a catalyst in epoxidation of allyl alcohol and has proposed a mechanism incorporating this and its ions. More information is available on peroxytungstates. MARTINEZ[15] has pared salts containing various tungsten-active oxygen ratios and JAHR[8] and co-kers have made spectrophotometric, conductometric and freezing point measure-ts on peroxytungstate solutions using acidified sodium tungstate. Since a soluble tungstic acid can be prepared at room temperature by ion exchange[16] it was ught of interest to investigate its reaction with dilute hydrogen peroxide.

EXPERIMENTAL

molybdic acid was prepared by dissolving AnalaR $Na_2MoO_4O \cdot 2H_2O$ in distilled er and passing the solution slowly through a prepared column containing sufficient Karb 225 (a sulphonated polystyrene cation-exchange resin) in the hydrogen form, nsure complete exchange. The liquid collected was clear to the naked eye and with-any trace of "Molybdenum blue". To ensure complete removal of the sodium column was regenerated and washed until the liquid emerging had a conductivity than 3 μmhos; the molybdic acid was then recycled through the column. In eral the first bed-volume was rejected and the first volume of washings collected; 85% recovery of molybdenum was achieved by this method, the actual percentage ending upon the excess of resin used. A small quantity of molybdenum was retain-tenaciously by the resin and even after washing with 1 l of water formed a blue oration within the column after standing 2–3 weeks.

The concentration of molybdic acid was determined both gravimetrically by cipitation with 8-hydroxyquinoline after careful buffering, and directly by nductometric or potentiometric titration with standard NaOH. All concentrations expressed in terms of MoO_3.

Tungstic acid was prepared similarly. AnalaR sodium tungstate, $Na_2WO_4 \cdot 2H_2O$, as used as a source of tungsten. This salt is readily soluble in cold water. Since gstic acid is unstable it was prepared immediately before use. All tungsten con-ntrations are expressed as WO_3.

Hydrogen peroxide solutions were prepared by dilution of pure 20-volume un-bilised hydrogen peroxide kindly supplied by Laporte Chemicals Ltd. The concen-tion of the peroxide was determined by titration in acid solution (H_2SO_4) with N $KMnO_4$. The $KMnO_4$ was standardised using specially prepared sodium alate.

All pH measurements were made using a Cambridge pH meter with a glass–calomel ctrode system, calibrated by 0.05 M potassium hydrogen phthalate at 4.00. The

pH scale calibrated in this fashion loses some theoretical significance when used in non-aqueous solvents. MITCHELL AND WYNNE-JONES[17] have shown that the glass electrode is reversible in solutions of hydrogen peroxide, and standard E° potentials required to set up pH scales over the whole range of composition H_2O–H_2O_2 have been determined by these workers. Most of the peroxide, solutions used in the present study were so dilute, however, that no interrelation has been attempted.

All conductivity measurements were made using a Mullard Conductivity Bridge, operating in the most sensitive range, using a cell with a constant of 1.54. Since water and hydrogen peroxide have similar dielectric constants, the interionic effects in peroxide solution should be similar to those in water, and the conductivity should be unaltered by small changes in solvent composition.

Spectrophotometric measurements were made using either a Hilger Uvispek or a Unicam S.P. 500 with 1 cm cells. Appropriate blank solutions were used. All experiments were conducted at 20°C.

RESULTS AND DISCUSSION

Peroxymolybdic acids

Potentiometric and conductometric titration studies together with measurements of the u.v. absorption spectra have shown that molybdic acid prepared by ion exchange even in dilute solution is a poly acid whose simplest formula is probably

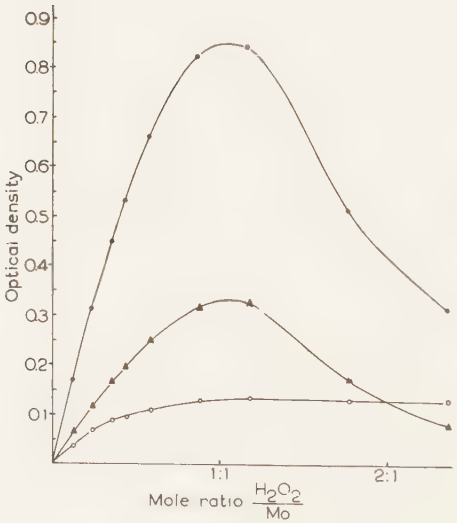

Fig. 1. The effect of hydrogen peroxide on the optical density of molybdic acid, mole ratio method. ●, 0.048 *M* w.r.t. Mo read at 4500 Å; ▲, 0.048 *M* w.r.t. Mo read at 4700 Å; ○, 0.0048 *M* w.r.t. Mo read at 4200 Å. Plot: optical density against mole ratio H_2O_2/Mo.

Fig. 2. The effect of hydrogen peroxide on the optical density of molybdic acid, method of continuous variations. ●, Concn. of Mo at maximum 0.087 *M* read at 4600 Å; ▲, Concn. of Mo at maximum 0.022*M* read at 4600Å. Plot: optical density against mole fraction H_2O_2.

$[_2Mo_4O_{13}]^{12}$. In concentrated solution further aggregation occurs, producing a more complex acid. In the present study experiments have been performed over a wide range of concentrations to examine the effect of concentration changes on the peroxide complex formed.

Evidence for the existence of a peroxymolybdic acid of active oxygen : Mo ratio 1 : 1 (hereafter known as 1 : 1 acid) in previous studies has been obtained either indirectly by cryoscopic or thermochemical studies on acidified molybdate solutions or by analysis of the solid obtained by dissolving MoO_3 in 110 volume peroxide at 100°C [2, 5,7]. The results of a direct spectrophotometric study of the effect of peroxide using both the mole ratio and the method of continuous variations[18] are shown in Figs. 1 and 2. From these figures it is clear that a compound of empirical formula $MoO_3 \cdot H_2O_2$ exists in solution. The numerical values of the optical density at various concentrations as shown in Fig. 2, curves (a) and (b), appear also to indicate that some polymerization process occurs in solution. TRIDOT[7] has suggested from potentiometric studies that H_2MoO_5, a solid obtained by evaporation of MoO_3 dissolved in 110 volume peroxide, that simple MoO_5^{2-} ions are not formed in solution. In a later spectrophotometric study in very dilute solution containing mineral acid, TRIDOT AND SOUCHAY[19] interpret the shape of their absorption curves in terms of a complex (Mo_2O_{11})–H–

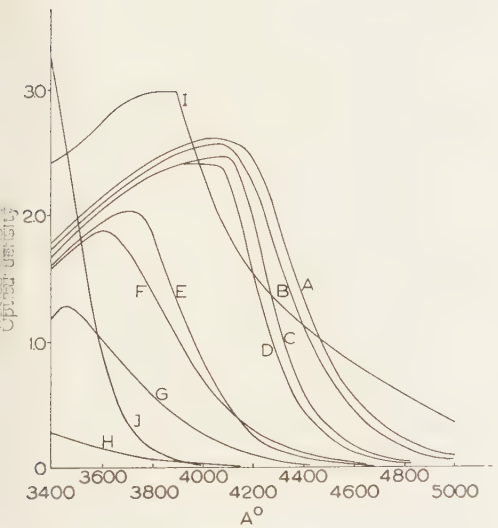

Fig. 3. Absorption spectra of various molybdic acid – H_2O_2 mixtures. Standard solution 1 : 1 Mo : active O, 0.042 *M* w.r.t. Mo and H_2O_2: (A) in 0.1 *N* $HClO_4$; (B) in water; (C) in 0.1 *N* $HClO_4$ and excess peroxide (10 vol.); (D) in excess peroxide (10 vol.); (E) 1 → 5 diln. of standard in 4 vol. peroxide; (F) 1 → 5 dilution water; (G) 1 → 10 dilution water; (H) 1 → 50 dilution water; (I) Excess peroxide (10 vol.) Na : Mo ratio 3 : 2; (J) Molybdic acid – no peroxide, 0.05 *M*. Plot: optical density against wavelength Å.

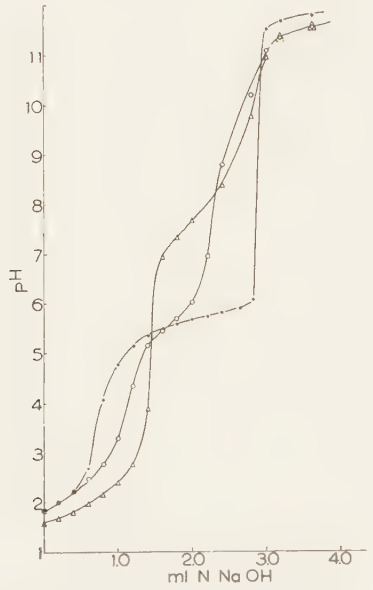

Fig. 4. The effect of hydrogen peroxide on the potentiometric titration of molybdic acid: ● 10 ml 0.145 *M* molybdic acid + 10 ml H_2O; ○ ml 0.145 *M* molybdic acid + 10 ml 0.145 *M* H_2O_2; △ 10 ml 0.145 *M* molybdic acid + 10 ml 20 vol. H_2O_2. Plot: pH against ml *N* NaOH.

(HMo_2O_6) containing both cationic and anionic molybdenum. These workers claim that $H_2Mo_2O_{11}$, formed quantitatively in excess peroxide, is the only peroxy acid which exists in solution.

The effect of excess peroxide on the spectrum of molybdic acid at various concentrations is shown in Fig. 3. In concentrated solutions, addition of excess peroxide to the 1 : 1 acid causes a shift in the spectrum to the u.v.; in more dilute solutions however, (1–5 dilution) the opposite effect occurs. The maximum optical density of the 1 : 1 complex (and the solution containing excess peroxide) shown in Fig. 3 shows a considerable shift to the visible when compared with the maximum at 3200 Å obtained in dilute solution by TRIDOT AND SOUCHAY. These results are inconsistent with any theory involving only one acid $H_2Mo_2O_{11}$. Studies of this type have previously been prevented by the low solubility of molybdic acid prepared by AUGER'S[20] method. Spectrophotometric studies of molybdates in mineral acids have shown that aggregation causes a shift in the absorption edge to the visible[21]. If similar considerations apply to peroxy acids the above results would appear to indicate that at least four peroxy acids exist in solution: at high concentrations in the presence of excess peroxide, an acid $H_2Mo_2O_{11}$, and at similar concentrations at 1 : 1 acid of the type $H_2Mo_4O_{17}$. On dilution $H_2Mo_2O_{11} \rightarrow H_2MoO_6$ ($K_1 \gg K_2$) while $H_2Mo_4O_{17}$ depolymerises to form a simpler acid of the type $H_2Mo_2O_9$. Both of the 1 : 1 acids appear to be unstable on addition of alkali (Figs. 4 and 7).

Additional evidence for the absence of cationic molybdenum in the 1 : 1 acids has been obtained from paper electrophoresis, ion exchange and ion migration studies. No exchange of hydrogen ion for the ion $(HMo_2O_6)^+$ (postulated by TRIDOT AND SOUCHAY[19] occurs when 10 ml of the 1 : 1 acid (0.042 *M* w.r.t. Mo) is passed slowly through a 10 g column of Zeo Karb 225 in the hydrogen form. The pH of the solution obtained by collecting the 10 ml, plus washings to a total volume of 50 ml, is similar to that obtained merely by diluting 10 ml of the 1 : 1 acid to 50 ml with distilled water (2.45 column, 2.44 direct dilution). The conductances of the solutions are also similar. The very small amount of molybdenum retained on the column after a 40 ml wash is similar to that retained by passing 10 ml of peroxide-free molybdic acid through the same column under similar conditions, then washing with 40 ml of distilled water. In both cases the adhering molybdenum was removed by treating the column with 50 ml 1.0 *N* KCl, then estimated colorimetrically with gallic acid. Insufficient molybdenum was present to colour acidified peroxide. Under similar conditions, the unstable red-brown complex formed by addition of peroxide to vanadic acid and believed to be due to the $(VO_3)^+$ ion, is exchanged quantitatively[22].

The absence of cationic molybdenum was also indicated in a paper electrophoresis study using a Shandon vertical type apparatus with Whatman No. 31 paper, a carrying electrolyte of 0.01 *N* $HClO_4$, a current of 30 mA at an e.m.f. of 300 V. Spots of

TABLE I

	Volume (ml)	*Conc. Mo before electrolysis (M)*	*Conc. Mo after electrolysis (M)*
Anode compartment	10.25	0.044	0.054
Cathode compartment	9.85	0.044	0.035
Centre compartment	—	0.044	0.044

th the 1 : 1 acid and the acid in excess peroxide migrated as a diffuse bullet-shaped me some 5 cm to the anode in 3 h. The spots were developed using either H_2S or kaline gallic acid.

Ionic migration studies were also performed on the 1 : 1 acid using a small specially ade Hittorf tube with loosely fitting platinum electrodes. Analysis of the compartents after 2 h 50 min at a current of 4.0 mA gave the following results (Table I).

It is clear from Table I that the molybdenum content of the anode compartment creases while that of the cathode decreases. These results are best explained by the esence in solution of only negatively charged molybdate ions.

From these studies it seems reasonable to suppose that the 1 : 1 acid formed in centrated solution is of the type $H_2Mo_4O_{17}$. The potentiometric evidence produced TRIDOT[7] to support the complex nature of H_2MoO_5 (later suggested to be $(Mo_2O_{11}H)_2Mo_2O_6$)), namely points of inflexion at Na : Mo ratios of 0.75 : 1 and 1.50 : 1, is pable of other interpretations.

$$8\ H_2MoO_5 + 6\ NaOH \rightarrow 2\ Na_2Mo_2O_{11} + Na_2Mo_4O_{13} + 11\ H_2O \quad (1)$$

$$Na_2Mo_4O_{13} + 6\ NaOH \rightarrow 4\ Na_2MoO_4 + 3\ H_2O \quad (2)$$

$$2\ Na_2Mo_2O_{11} + 4\ NaOH \rightarrow 4\ Na_2MoO_4 + 2\ H_2O + 4\ O_2 \quad (3)$$

ne points of inflexion found at the same ratios in the present study (Fig. 4) may be ue to reactions of the type

$$2\ H_2Mo_4O_{17} + 6\ NaOH \rightarrow Na_2Mo_4O_{13} + 2\ Na_2Mo_2O_{11} + 5\ H_2O$$

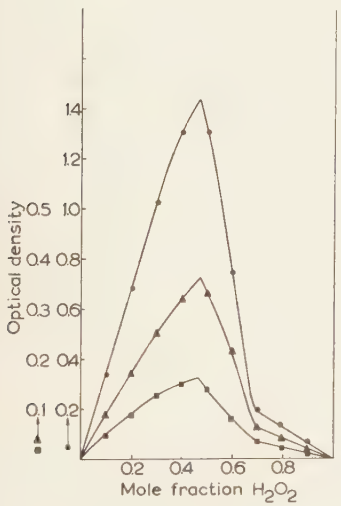

g. 5. The effect of concentration on the tical density of acidified molybdate–drogen peroxide mixtures: ● Concn. of olybdic acid at maximum 0.08 *M* inner ale 4700 Å; ■ Concn. of molybdic acid at aximum 0.016 *M* outer scale 4700 Å; Concn. of molybdic acid at maximum 032 *M* outer scale 4600 Å. Plot: optical density against mole fraction H_2O_2.

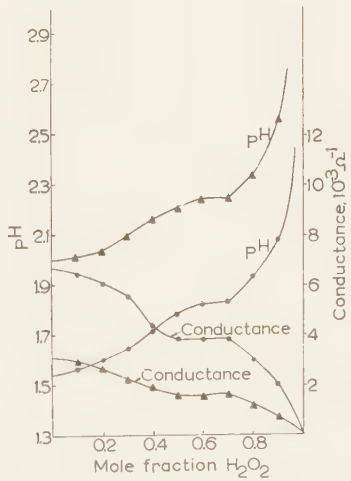

Fig. 6. The effect of hydrogen peroxide on the conductance and pH of molybdic acid, method of continuous variations: concn. symbols as in Fig. 2. Plot: conductance, $10^{-3}\ \Omega^{-1}$, against mole fraction H_2O_2; pH, against mole fraction H_2O_2.

followed by reactions (2) and (3) It is reasonable to assume that the 1 : 1 and 1 : 2 acids vary in stability with pH.

Further evidence to support the acid $H_2Mo_4O_{17}$ is obtained from conductance studies. Addition of hydrogen peroxide has only a small effect on conductance or pH of molybdic acid until the Mo : O ratio exceeds 1 : 1 (*e.g.*, initial section of Figs. 4 and 7) thereafter the change becomes pronounced. Presumably therefore, $H_2Mo_4O_{17}$ is only slightly stronger than $H_2Mo_4O_{13}$. Addition of small amounts of peroxide to either vanadic acid or tungstic acid where appreciable reactions occur (*i.e.* the formation of VO_3^+ in the former and a depolymerised acid in the latter) is accompanied by appreciable changes in conductance.

It is fortunate that the two peroxy acids formed have sufficiently different optical densities measured at a suitable wavelength for the empirical formula of the 1 : 1 complex to be obtained by the mole ratio method (Fig. 2). Even to the naked eye the 1 : 1 complex is appreciably more coloured than the 1 : 2. While the empirical formula of the 1 : 2 complex cannot be obtained by the former method it is indicated quite clearly by the latter (Fig. 2). A sharp change occurs in the optical density – mole fraction curve at a Mo : O ratio of 1 : 2, indicating the presence of a second complex of lower optical density. This effect is also found in molybdate solutions acidified to the same pH with $HClO_4$ (Fig. 5). This second peroxy acid was suggested earlier from spectrophotometric studies to be simpler in structure than $H_2Mo_4O_{17}$. This is confirmed by both pH and conductance studies (Fig. 6). After a 1 : 1 ratio the rise in pH and the fall in conductance is arrested obviously due to some simplification occurring in solution. The reaction is complete by the ratio 1 : 2; thereafter the curves again rise and fall respectively,

$$H_2Mo_4O_{17} + 4\ H_2O_2 \rightarrow 2\ H_2Mo_2O_{11} + 3\ H_2O$$

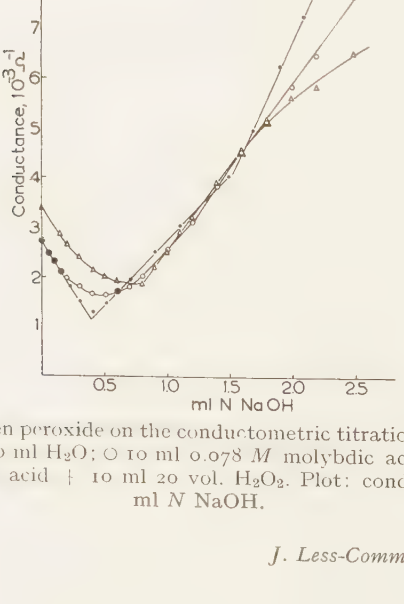

Fig. 7. The effect of hydrogen peroxide on the conductometric titration of molybdic acid: ● 10 ml 0.078 *M* molybdic acid + 10 ml H_2O; ○ 10 ml 0.078 *M* molybdic acid + 10 ml 0.137 *M* H_2O_2; / 10 ml 0.078 *M* molybdic acid + 10 ml 20 vol. H_2O_2. Plot: conductance, $10^{-3}\ \Omega^{-1}$, against ml *N* NaOH.

ANYI[9] has shown that addition of excess peroxide to polymolybdates produces a fall pH. From the results described it is clear

$$Na_2O.xMoO_3 + 2\ xH_2O_2 \rightleftarrows xHMoO_6^- + 2\ Na^+ + (x-2)H^+ + (x+1)\ H_2O$$

y no peroxypolymolybdates were found by CSANYI, who worked with solutions ntaining excess peroxide.

Points of inflexion or breaks in the potentiometric and conductometric titration ves (Figs. 4 and 7) at an Na : Mo ratio of 1 : 1 indicate that the 1 : 2 peroxyacid is of type $H_2Mo_2O_{11}$ or H_2MoO_6 ($K_1 \gg K_2$). Application of the Henderson equation its simplest form (pH = pK at Na : Mo ratio 1 : 2) neglecting activity coefficients d making no allowance for the high concentrations of peroxide, gives a value of $\cdot 10^{-3}$ for the first dissociation constant of the acid used in the present study, in mparison with $3 \cdot 10^{-3}$ obtained by CSANYI, in both cases assuming the acid under se conditions to be H_2MoO_6.

The colour changes found during the titration of molybdic acid in excess H_2O_2 with OH are worthy of mention. Initially the colour is yellow green, changing suddenly brown at a Na : Mo ratio of 1 : 1 darkening and then becoming lighter, and gradu- changing to yellow in the presence of excess NaOH. The half-way stage can readily determined by the appearance of the brown coloration. This colour is only transient gradually disappears if the titration is carried out extremely slowly. An absorption ctrum of the system containing the brown colour is shown in Fig. 3 at an Na : Mo io of 3 : 2.

roperties of the peroxymolybdic acids

The thermal stability of the 1 : 1 (Mo : H_2O_2) acid was investigated by mixing equal antities of 0.035 *M* molybdic acid and peroxide, allowing the mixture to stand 1 h reach equilibrium, then heating measured aliquots to 18, 35, 43, 52 and 82°C, in rmostatic baths for 1 h. After removal from the baths the samples were cooled and ter was added to replace that lost by evaporation. The optical density of each solu- n was then measured at 4600 Å. No change was observed in any sample.

This same material is also remarkably stable to potassium permanganate. Solutions H_2O_2 : Mo ratios less than 1 : 1 which required from 5–30 ml of 0.1 *N* $KMnO_4$ to sorb the available peroxide required from 3–4 h to discharge the colour of 1 ml of rmanganate in the absence of sulphuric acid. Addition of sulphuric acid caused the

TABLE II

	10 ml $BaCl_2$ 0.5 N	*10 ml $CaCl_2$ 0.5 N*	*10 ml $Pb.Ac_2$ 0.5 N*	*Excess $AgNO_3$ 0.1 N*
10 ml 0.078 M molybdic acid + 10 ml H_2O	No ppt. until 2 h white	Clear	White ppt.	Pale yellow ppt.
10 ml 0.078 M molybdic acid + 10 ml 0.17 M H_2O_2	Turbid after after 2 h	Clear	No ppt. until 3–4 h	No ppt. until 12 h
10 ml 0.078 M molybdic acid + 10 ml 20 vol. H_2O_2	Turbid after 2 h	Clear	Pale yellow ppt. Vigorous liberation of O_2	Faint turbidity

reaction to proceed normally. Peroxide in excess of an Mo : H_2O_2 ratio of 1 : 2 could however, be titrated readily although a quantitative end-point was not achieved.

An acid of the same Mo : H_2O_2 ratio buffered with ammonia to pH 8.5 (using a pH meter) gave an immediate iodine coloration on addition of 30% KI solution. A little oxygen was also formed. Unbuffered acid gave an iodine coloration more than 10 times as dense as a similar solution containing the same quantity of peroxide acidified to the same pH with sulphuric acid.

The masking effect of excess peroxide on the precipitation of some molybdates is shown in Table II. Dilute peroxide initially prevents the precipitation of silver molybdate and lead molybdate. The lead solution gradually becomes turbid and a precipitate forms after a few hours. The lead solution appears to have a great catalytic effect on the decomposition of the peroxide in both dilute and concentrated solution. A precipitate also forms in the silver solution on leaving overnight. For comparison solutions containing similar amounts of peroxide were prepared using sodium molybdate acidified to the same pH with HNO_3. The reactions were all similar with the exception of that in the lead solution where precipitation occurred immediately even in the presence of peroxide.

Peroxytungstic acids

Tungstic acid prepared by ion exchange is a polyacid whose simplest formula is probably $H_3(H_3W_6O_{21})$. When just prepared the solution is clear to the naked eye, but further aggregation soon occurs giving a turbid solution, then a white paste and ultimately after a few days a yellow solid. A full discussion of the properties of this acid can be found elsewhere[16]. Addition of even a small amount of hydrogen peroxide (Active O : W ratio less than 1 : 4) retards the aggregation process. Solutions with ar

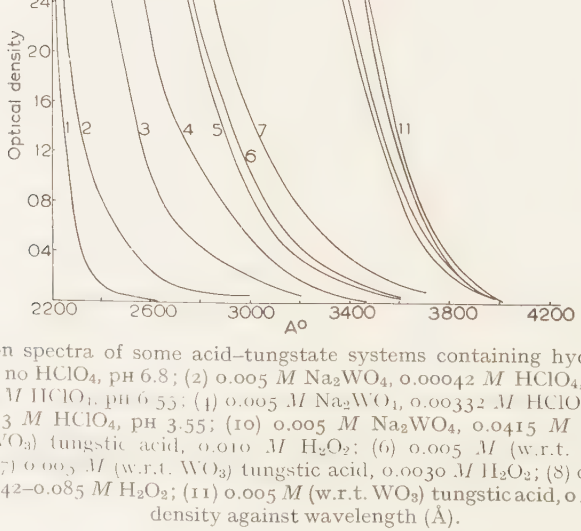

Fig. 8. Absorption spectra of some acid–tungstate systems containing hydrogen peroxide: (1) 0.005 *M* Na_2WO_4, no $HClO_4$, pH 6.8; (2) 0.005 *M* Na_2WO_4, 0.00042 *M* $HClO_4$, pH 6.7; (3) 0.005 *M* Na_2WO_4, 0.00166 *M* $HClO_4$, pH 6.55; (4) 0.005 *M* Na_2WO_4, 0.00332 *M* $HClO_4$, pH 6.35; (9) 0.005 *M* Na_2WO_4, 0.0083 *M* $HClO_4$, pH 3.55; (10) 0.005 *M* Na_2WO_4, 0.0415 *M* $HClO_4$, pH 1.60; (5) 0.005 *M* (w.r.t. WO_3) tungstic acid, 0.010 *M* H_2O_2; (6) 0.005 *M* (w.r.t. WO_3) tungstic acid 0.0070 *M* H_2O_2; (7) 0.005 *M* (w.r.t. WO_3) tungstic acid, 0.0030 *M* H_2O_2; (8) 0.005 *M* (w.r.t. WO_3) tungstic acid, 0.0042–0.085 *M* H_2O_2; (11) 0.005 *M* (w.r.t. WO_3) tungstic acid, 0 *M* H_2O_2. Plot: optical density against wavelength (Å).

W ratio of 1 : 1 have been stored for months without any visible sign of aggregation. *M* tungstic acid which becomes turbid on standing 1–2 h readily clears on addition 0.1 *M* peroxide. A sample of 0.1 *M* peroxide which had become a white paste on nding 24 h, partially redissolved on adding twice the volume of 0.1 *M* H_2O_2 but the ution retained a faint turbidity even after several hours. Yellow tungstic acid once med did not dissolve appreciably in 0.1 *M* peroxide at room temperature.

The results of a spectrophotometric study at various O(active) : W ratios is shown ig. 8. Addition of mineral acid to sodium tungstate causes a progressive shift in absorption edge from the u.v. to the visible. This shift is thought to be due to gressive aggregation of the tungstate ion. Tungstic acid prepared by ion exchange a similar spectrum to that of acidified tungstate of similar pH. Addition of per- ide to freshly prepared tungstic acid causes a shift in the spectrum back to the u.v., ch suggests that some depolymerisation of the tungstate ion has occurred. A simi- ffect is produced on adding α-hydroxy acids[23]. This simplification is confirmed by nductance studies. Aged tungstic acid reacts much more slowly with hydrogen roxide. Addition of 0.5–10 ml of 0.17 *M* peroxide to 10 ml of 0.01 *M* tungstic acid

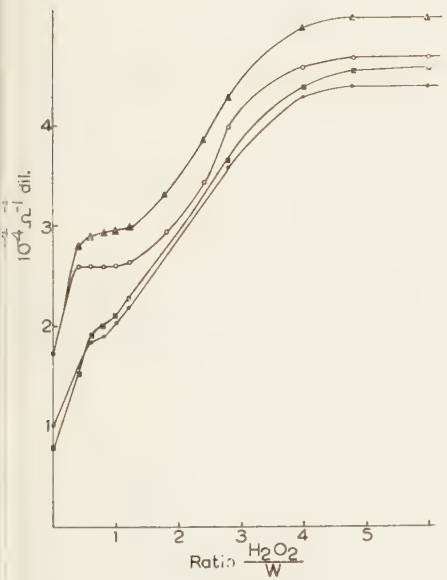

9. Effect of hydrogen peroxide on the nductance of tungstic acid: ▲, 0.002 *M* ngstic acid conductance after 6 and 13 days; 0.002 *M* tungstic acid conductance after 3 ys; ■, 0.02 *M* tungstic acid conductance er 6 and 13 days; ●, 0.02 *M* tungstic acid nductance after 3 days. Plot: conductance, $^{-4}\,\Omega^{-1}$ dilute against ratio H_2O_2/W; con- tance, $10^{-3}\,\Omega^{-1}$ conc. against ratio H_2O_2/W.

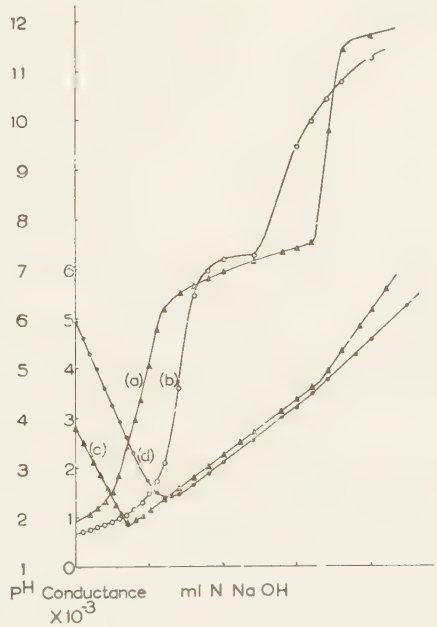

Fig. 10. Conductometric and potentiometric titration of peroxytungstic acid: 20 ml 0.082 *M* tungstic acid + either 20 ml H_2O or H_2O_2. H_2O_2 = 0.085 *M*. ▲, potentiometric titration without peroxide; ○, potentiometric titration in peroxide; ▲, conductometric titration without peroxide; ○, conductometric titration in peroxide. Plot either pH or conductance ·. $10^{-3}\,\Omega^{-1}$ against ml 1*N* $NaOH_3$; smaller amounts of peroxide produce curves between those shown.

aged for 1 day causes only a slight shift to the u.v. even after standing for 2 h (Fig. 8 curve 8).

The effect of varying hydrogen peroxide concentration on the conductance o freshly prepared tungstic acid at two absolute concentrations is shown in Fig. 9 Addition of a small quantity of peroxide causes a large increase in conductance whicl levels off at an O (active) : W ratio of 1 : 1. Addition of more peroxide causes a pro nounced increase in conductance to a limiting ratio of 4 : 1. This effect is quite repro ducible. Mixtures of peroxide and tungstic acid prepared from solutions of simila concentrations, using the method of continuous variations[18] also show a maximun conductance at this latter ratio.

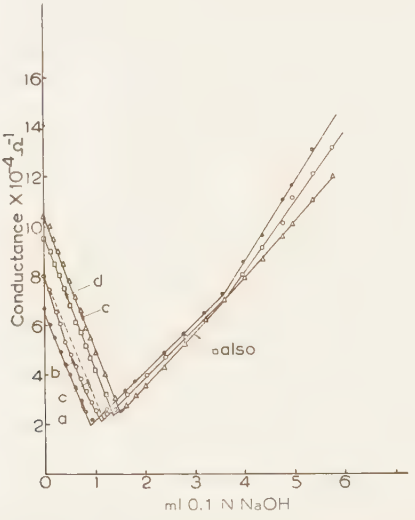

Fig. 11. Conductometric titration of tungstic acid in the presence of excess hydrogen peroxide (a), 20 ml 0.009 M tungstic acid, 0 ml 0.172 M H_2O_2, 10 ml H_2O; (b) 20 ml 0.009 M tungstic acid 0.5 ml 0.172 M H_2O_2, 9.5 ml H_2O; (c), possible shape of (b) if unaffected by pH change; (d 20 ml 0.009 M tungstic acid, 2.0 ml 0.172 M H_2O_2, 8.0 ml H_2O; (e), 20 ml 0.009 M tungsti acid, 10 ml 0.172 M H_2O_2, 0 ml H_2O. Plot: conductance, 10^{-4} Ω^{-1}, against ml 0.1 N NaOH.

It is clear from the shape of the conductometric and potentiometric titration curve (Fig. 10) that strong peroxy acids are formed at all W : O ratios. The increase in cor ductance on addition of peroxide can only be due to depolymerisation. In comparisor molybdic acid prepared by ion exchange exhibits little change in conductance o addition of small amounts of peroxide. Since several ions are probably present i solution and the equilibrium is probably pH dependent (see Fig. 11, curve (b)) it is nc possible to obtain the number of readily replaceable hydrogen atoms in the first perox acid formed using either conductance or pH techniques but it is obviously more tha the 1 : 2 H : W ratio of $H_3(H_3W_6O_{21})$. Information on the 1 : 4 peroxy acid is easier t obtain. The great increase in conductance on adding excess peroxide suggests tha this acid is simpler than the 1 : 1 acid. From the trend in the conductometric titratio curves of a dilute solution of tungstic acid containing excess peroxide, it would appea that this acid is either H_2WO_8 with one strong and one weak hydrogen or $H_2W_2O_1$

No evidence has been found by pH or conductance studies for a peroxytungstic acid W : O ratio 1 : 2 corresponding to the various peroxytungstates described in the erature. It is probable therefore that this free acid is unstable and disproportionates form mixtures of the two acids described above.

Paper electrophoresis studies using conventional techniques have been unsuccessful gely due to the difficulty of obtaining a spot reagent for tungsten in the presence of roxide. However, it is hoped to present soon information obtained using radioactive acer techniques.

ACKNOWLEDGEMENTS

he author wishes to thank Dr. G. TRIDOT for a copy of his thesis and Mr. W. P. ISTLETHWAITE for the use of a valuable collection of reprints.

REFERENCES

1 K. CAMMERER, *Chem. Ztg.*, 15 (1891) 957.
2 E. PECHARD, *Ann. chim. et phys.*, 28 (1893) 537.
3 L. PISSARJEWSKI, *Z. anorg. Chem.*, 24 (1900) 115.
4 G. BRODE, *Z. physik. Chem.*, 37 (1901) 299.
5 A. MAZZUCHELLI AND A. ZANGRILLE, *Gazz. chim. ital.*, 40 (1910) 49.
6 W. D. TREADWELL, *Helv. Chim. Acta*, 31 (1948) 577.
7 G. TRIDOT, *Thesis*, Paris, 1955.
8 K. F. JAHR, *Ber. Freunden techn. Hochsch., Berlin*, 91 (1939) and later references.
9 L. J. CSANYI, *Acta Chim. Acad. Sci. Hung.*, 14 (1958) 69.
10 P. SOUCHAY, *Bull. soc. chim. France*, 16 (1949) 122.
11 K. F. JAHR AND M. BLANKE, *Z. anorg. Chem.*, 272 (1953) 45.
12 E. RICHARDSON, *J. Inorg. Nucl. Chem.*, 9 (1959) 267.
13 H. REMY, *Treatise on Inorganic Chemistry*, Vol. II, Elsevier Publishing Co., Amsterdam, 1956, p. 179.
14 Z. RACISZEWSKI, *J. Am. Chem. Soc.*, 82 (1960) 1267.
15 J. B. MARTINEZ, *Anales fis. y quim. (Madrid)*, 40 (1944) 358.
16 E. RICHARDSON, *J. Inorg. & Nuclear Chem.*, 12 (1959) 79.
17 A. G. MITCHELL AND W. F. K. WYNNE-JONES, *Trans. Faraday Soc.*, 51 (1955) 1690.
18 P. JOB, *Ann. chim.*, 6 (1935) 97.
19 F. CHAUVEAU, P. SOUCHAY AND G. TRIDOT, *Bull. soc. chim. France*, 22 (1955) 1519.
20 V. AUGER, *Compt. rend.*, 206 (1938) 913.
21 I. LINDQVIST, *Acta Chem. Scand.*, 5 (1951) 568.
22 E. RICHARDSON AND J. MAGEE, *J. Inorg. & Nuclear Chem.*, in press.
23 E. RICHARDSON, *J. Inorg. & Nuclear Chem.*, in press

SOME OBSERVATIONS ON URANIUM–MOLYBDENUM–NIOBIUM ALLOYS

G. H. BANNISTER* AND J. R. MURRAY**

Metallurgy Division, Atomic Energy Research Establishment, Harwell, Berks. (Great Britain)

(Received June 1st, 1960)

SUMMARY

The constitution of U–Mo–Nb alloys at 1100°, 1200°, and 1300°C has been studied, mainly by metallographic and X-ray methods, and isothermal sections have been obtained. The decomposition of the body-centred cubic γ-phase in alloys containing 5 at. % Mo and approximately 50 at. % U occurred very slowly at temperatures near the maximum of the miscibility gap. Additions of Mo have been found to decrease the rate of the monotectoid reaction $\gamma_1 \rightarrow \alpha + \gamma_2$. Room temperature lattice parameters of quenched homogeneous γ alloys were obtained and a hardness survey of the same alloys showed that a maximum occurred at approximately 50 at. % Nb and a minimum at 85 at. % U.

The effect of Mo on the maximum temperature of the miscibility gap has been discussed in terms of the strain energy in the solid solution from which it is formed.

INTRODUCTION

The U–Nb system has been studied by PFEIL, BROWNE AND WILLIAMSON[1], by ROGERS, ATKINS, MANTHOS AND KIRKPATRICK[2], and by DWIGHT AND MUELLER[3]. The results differ in some details, but agree that a complete range of solid solubility exists below the solidus between niobium and the body-centred cubic γ modification of uranium. This breaks down, at lower temperatures, to form a $\gamma_1 + \gamma_2$ miscibility loop which has a maximum at $\sim$ 50 at. % U and 950 $\pm$ 10°C.

Extensive studies of the U–Mo system have also been carried out and the results have been summarized by ROUGH AND BAUER[4]. While considerable difficulties have attended the establishment of the true equilibrium conditions below about 650°C there is agreement that Mo dissolves in γ-U up to about 35 at. % at 1000°C.

A logical next step towards an understanding of the alloying behaviour of U was to study the U–Mo–Nb system. EREMENKO[5] has reported that Mo and Nb form a complete series of solid solutions. LUSHMAN[6] investigated ternary alloys containing 13–34 at. % Mo and 1–19 at. % Nb after annealing at 500°C and IVANOV AND BADAJEVA[7] studied the phase relationships which exist up to 1000°C over the whole range of compositions in the ternary U–Mo–Nb system. The present paper is complementary to these results since it is concerned mainly with temperatures above 1000°C, the emphasis being on the range of stability of the body-centred cubic phase.

* Now at the Australian Atomic Energy Commission Research Establishment, Sutherland, Australia.

** Now Mrs. J. R. THOMSON at the Metallurgy Department, Imperial College of Science and Technology, London, S.W.7.

EXPERIMENTAL METHODS

The U used in the early experiments was Ca-reduced bar containing approximately 100 p.p.m. carbon, other impurities, metallic and non-metallic totalling less than 200 p.p.m.; Mg-reduced billet material was used for the main part of the work and this had a carbon content of approximately 300 p.p.m., other impurities being again low. Johnson Matthey "spec-pure" Mo and Nb were used throughout.

All alloys were prepared by arc-melting in a Zr-gettered argon atmosphere. Each of the materials was first melted until no surface "gassing" was observed and then weighed up for alloying. In this way weight losses on alloying were negligible and final compositions have been accepted throughout. Except for two alloys with high hardness (see section on results) all the material was too hard and brittle for cold-working as solid specimens. For heat treatment below 1200°C specimens were wrapped in a foil, while for higher temperatures Mo foil was used; solid samples were sealed in silica capsules under a vacuum of better than 10^{-5} mm mercury or a low pressure of argon, depending on the annealing temperature, and were quenched by breaking the silica under water. Powders for X-ray examination were wrapped in Ta or Mo capsules, sealed in evacuated silica tubes, and after annealing were cooled by plunging into water without breaking the silica. For the determination of lattice parameters of the homogeneous body-centred cubic phase, powders were strain-relieved at the annealing temperature of the parent material, while for the X-ray investigation of the breakdown of the homogeneous phase cold-work was introduced by filing prior to annealing at the lower temperatures.

For γ stabilization studies on U-rich material, specimens were cradled in Mo wire and suspended on thin "kanthal" wire in a vertical, evacuated silica tube with a 6 in. depth of Hg at its lower end. A small "kanthal"-wound furnace surrounded the silica tube and, after the anneal, the suspending kanthal wire was fused, allowing the samples to fall directly into the Hg; a U sinker was employed to ensure a rapid quench. Standard methods of metallographic preparation were used, the final polish being obtained on a diamond wheel. Surfaces for examination under polarised light were obtained by attack-polish using a γ alumina abrasive in a solution of 1 part by volume nitric acid: 2 parts chromic oxide: 1 part water. Hardness measurements were made with a standard Vickers diamond pyramid indentor using a 20 kg load; results quoted are the average of at least 5 readings.

Cu $K\alpha$ radiation was used for all X-ray work and lattice parameters for the determination of the pseudo-binary section containing 5 at. % Mo were obtained with a precision 19 cm diameter powder camera[8]. Other parameters were obtained with a Philips camera of 11.46 cm diameter and solid specimens were examined using a camera of similar diameter in which the sample could be continuously rotated and oscillated enabling a powder photograph to be obtained.

Thermal analysis was carried out in equipment which has been described elsewhere[9] and dilatometric examination in an evacuated silica tube using a silica comparator and a linear variable differential transformer system to detect the length change of the sample. The output from the transformer was fed into a millivolt recorder so that the progress of slow transformations could be observed without the fatigue of manual readings.

RESULTS

Isothermal sections at 1100°, 1200°, and 1300°C are shown in Figs. 1–3; the liquidus

and solidus compositions in the binary U–Mo and U–Nb systems and the limits of solubility of molybdenum in uranium at the relevant temperatures have been taken from ROUGH AND BAUER[4]. Results on the ternary alloys were obtained from metallo-

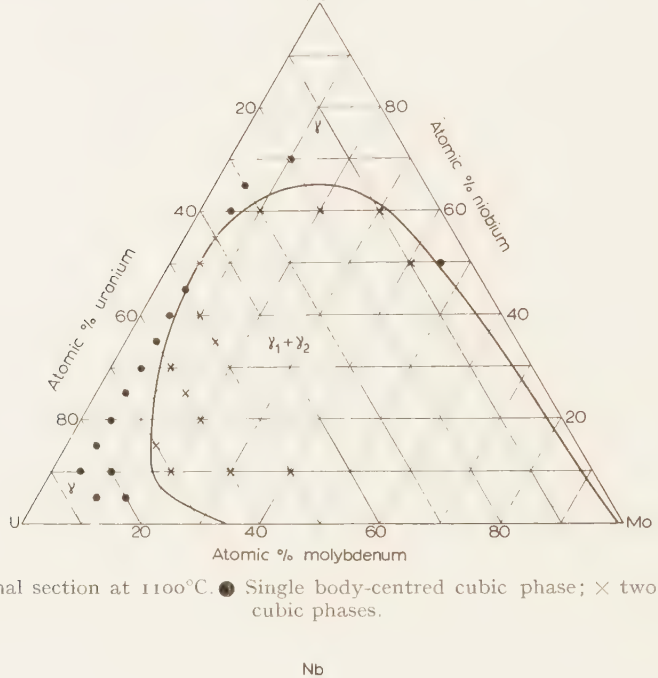

Fig. 1. Isothermal section at 1100°C. ● Single body-centred cubic phase; × two body-centred cubic phases.

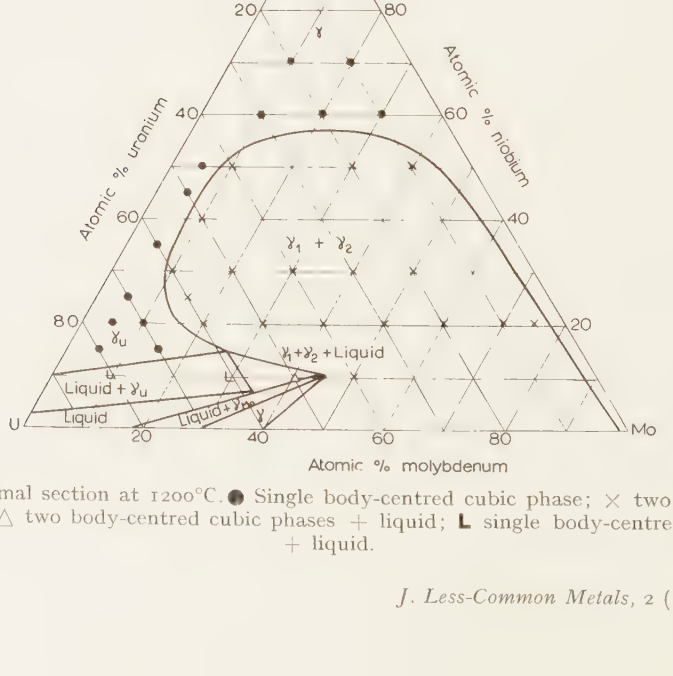

Fig. 2. Isothermal section at 1200°C. ● Single body-centred cubic phase; × two body-centred cubic phases; △ two body-centred cubic phases + liquid; **L** single body-centred cubic phase + liquid.

graphic examination of quenched specimens. Annealing times of 4, 14 and 21 days were employed for solid specimens in the determination of the $\gamma/\gamma_1 + \gamma_2$ phase boundary at 1300°, 1200°, and 1100°C, respectively. Boundaries involving a liquid

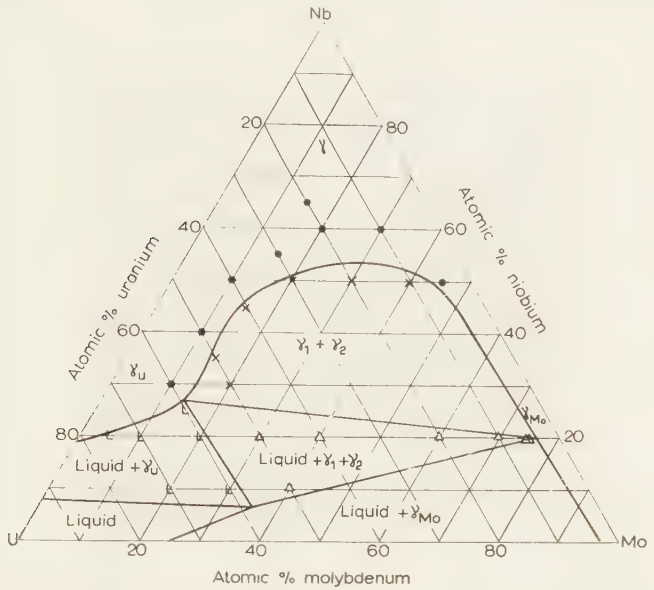

. 3. Isothermal section at 1300°C. ● Single body-centred-cubic phase; × two body centred bic phases; △ two body-centred cubic phases + liquid; L single body-centred cubic phase + liquid.

ase were obtained by taking the specimens annealed at 1100°C and re-annealing 2 h at 1200° or 1300°C. A few alloys were annealed at temperatures in excess of 00°C but reaction with the Mo wrapping foil frequently occurred. This caused rtial liquation, which led to misleading microsections and insufficient unambiguous sults were obtained for isothermal sections to be drawn. However, it is worth reding that an alloy containing 15 at. % Mo and 45 at. % Nb became homogeneous after annealing for 2 days at 1350°C, while a specimen of 40 at. % Mo and 50 at. % b became γ after 6 h at 1500°C. No liquation had occurred in samples containing at. % Mo and 50 at. % Nb or 30 at. % Mo and 60 at. % Nb after 12 h at 1560°C. The extent of the homogeneous γ field increased gradually as the annealing temperature was raised, the increase in U-rich and Nb-rich alloys being greater than in Mo-rich alloys. Liquation at 1200°C prevented the γ-field of U–Mo alloys joining that of U–Nb alloys at this temperature and a small three-phase ($\gamma_1 + \gamma_2$ + liquid)-field was observed. At 1300°C the composition range over which liquation occurred had increased considerably, covering most alloys containing less than 20 at. % Nb. No evidence was obtained that suggested ordering of alloys near the monotectoid composition which had been quenched from the γ-field although the relevant X-ray films were not of high quality; such ordering has been reported to occur non-reproducibly quenched binary U–Nb and U–Nb–Zr alloys [6].

On water-quenching from 1100°C small areas of the alloy containing 10 at. % Mo and 5 at. % Nb showed deformation markings when examined under polarised light, while all of the alloy with 5 at. % Mo and 10 at. % Nb showed a similar structure. The metallographic appearance of the latter alloy was unchanged after quenching into mercury from 900°C and is shown in Fig. 4. An X-ray film of the polished surface

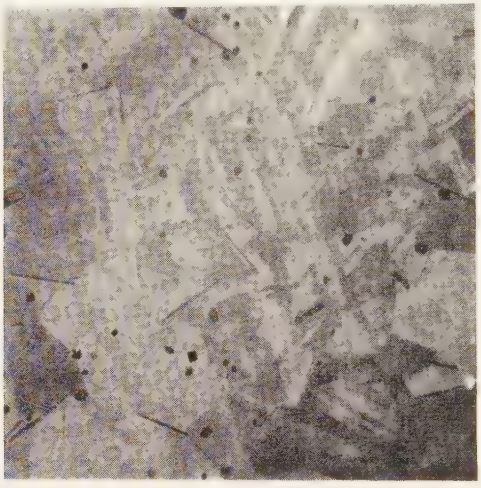

Fig. 4. Deformation markings in an alloy containing 5 at. % Mo and 10 at. % Nb after quenching into mercury from 900°C (dark needles and angular particles are inclusions). Polarised light (× 150)

of the former alloy showed a close resemblance to γ-U, while a film of the latter alloy was more similar to α-U. These results are in agreement with those of MURRAY AND JAGGER[10], who found that in binary alloys Mo was a more effective γ stabilizer than Nb. No attempt was made to classify the quenched, non-γ, ternary alloys into γ_0, α', α'' etc. since similar structures in binary U–Mo and U–Nb alloys are known to be complex[11] and it was felt that the unambiguous identification of the non-equilibrium structures obtainable in ternary U–Mo–Nb alloys was outside the scope of the present investigation.

Lattice parameters of γ alloys were determined from X-ray patterns of powders from alloys quenched from the relevant temperatures and the results are plotted in Fig. 5. parameters of binary Mo–Nb alloys are taken from EREMENKO[5], while those for U–Mo and U–Nb alloys are taken from PFEIL, BROWNE AND WILLIAMSON[1]. A pseudo binary section for alloys containing 5 at. % Mo is shown in Fig. 6; this was obtained mainly from X-ray lattice parameter measurements, assuming that the tie-lines are along lines of constant Mo content. The results of metallographic examination of solid specimens annealed in the temperature range 900–1200°C confirm the general shape of this boundary. It was noted that even in heavily cold-worked powders, for temperatures below 900°C, annealing times of several weeks were required before the X-ray patterns became reasonably sharp.

PFEIL, BROWNE AND WILLIAMSON[1] reported that powdered alloys of 50 at. % U *i.e.*, the composition at which the maximum on the miscibility loop occurs, when

quenched from 1000°C (the γ-field) gave diffuse X-ray patterns which in some cases were resolvable into two γ phases, while solid specimens showed only the presence of a single phase. No such effects have been observed in the ternary alloys.

As observed with solid binary U–Nb alloys[1] decomposition of the gamma phase in alloys containing approximately 50 at. % U and 5 at. % Mo occurred very slowly

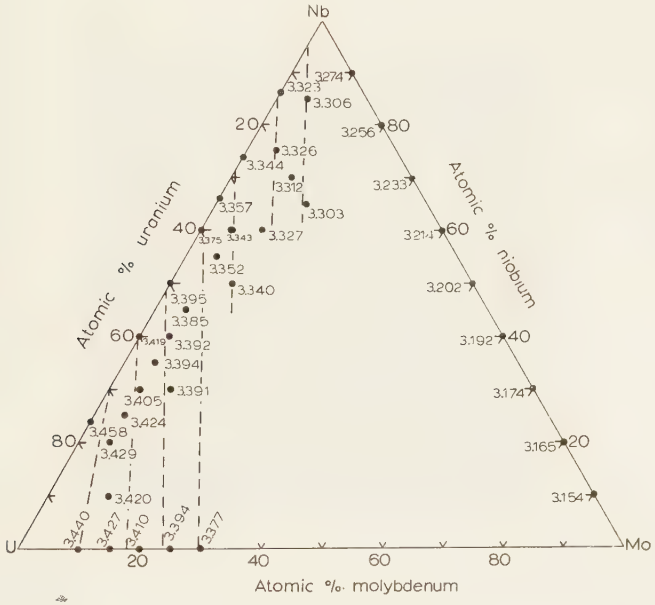

Fig. 5. Lattice parameters of quenched γ solid solutions (in A°). — — — Isoparametric lines.

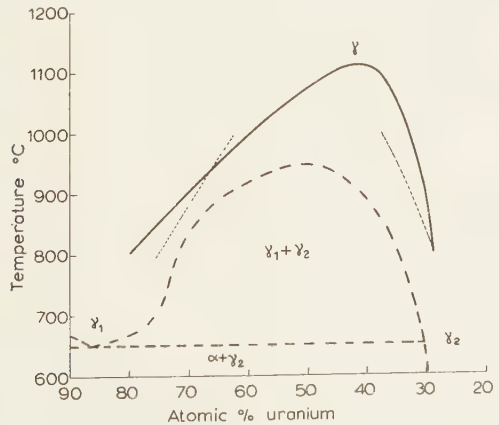

Fig. 6. Extent of $\gamma_1 + \gamma_2$ miscibility gap in binary uranium–niobium alloys and in uranium–molybdenum–niobium alloys containing 5 at. % molybdenum. — — Binary uranium–niobium alloys (PFEIL, BROWNE AND WILLIAMSON); ———uranium–molybdenum–niobium alloys containing 5 at. % molybdenum (present results); - - - - - - containing 5 at. % molybdenum (IVANOV AND BADAJEVA).

at temperatures near the maximum of the miscibility gap and this part of the equilibrium phase boundary was therefore determined by annealing two-phase alloys at successively high temperatures. Decomposition of γ was observed after 7 days at 750° or 900°C, yielding a fine eutectoid-like structure of $\gamma_1 + \gamma_2$ (see Fig. 7) but no decomposition occurred in 10 weeks at 1050°C although a small increase in hardness (from 363 to 393 V.P.N.) had taken place. A γ alloy containing 30 at. % U and 10 at. % Mo required 4 weeks to decompose to $\gamma_1 + \gamma_2$ at 1100°C.

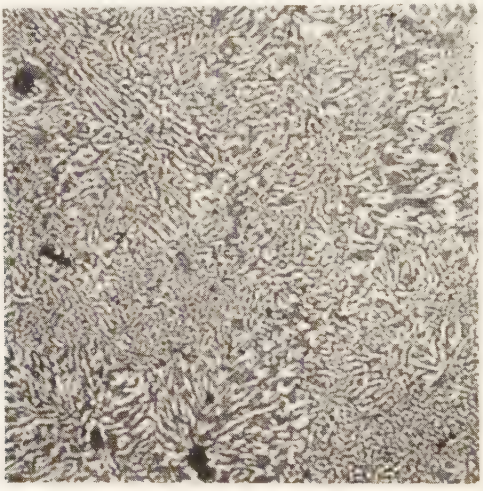

Fig. 7. Breakdown of γ to 2 body-centred cubic phases in alloy containing 5 at. % Mo and 45 at. % Nb annealed 14 days 1150°C, quenched then annealed 14 days 900°C and quenched, attack-polished and air-tarnished. (× 500)

The monotectoid transformation which occurs at 650 ± 5°C in binary U–Nb alloys was more sluggish in those containing 5 at. % Mo. It could readily be detected by thermal analysis of binary alloys at heating and cooling rates of approximately 1°C/min but was not observed on thermal analysis of an alloy containing 70 at. % U and 5 at. % Mo. However, dilatometric examination of this ternary alloy showed that the transformation of $\alpha + \gamma_2 \rightarrow \gamma_1$ occurred in 1 h at 650°C when the temperature was raised in steps of 10°C every 2 h and transformation of $\gamma_1 \rightarrow \alpha + \gamma_2$ occurred in 2 h at 618°C when the temperature was lowered in the same way. Subsequent metallographic examination confirmed that the ternary alloys had not transformed after thermal analysis and that γ_1 had transformed to $\alpha + \gamma_2$ after the dilatometer run.

Hardness results on alloys quenched from the γ field are shown in Fig. 8; the values for binary U–Nb alloys are taken from PFEIL, BROWNE AND WILLIAMSON[1]. A hardness maximum occurred at approximately 50 at. % Nb, while a minimum was observed at approximately 85 at. % U, the minimum occurring at the composition at which an equiaxed microstructure was just not retained on quenching. This is in good agreement with results on binary alloys, where a hardness minimum was found in U–Mo and U–Nb alloys and where the quenched structure changed from γ_0 (body-centred tetragonal) to α_b'' (monoclinic variation of α-uranium)[11], *i.e.*, at approximately 11 at. % Mo or 16 at. % Nb[12].

DISCUSSION

e results obtained on the ternary U–Mo–Nb alloys are consistent with published ormation on the three binary systems and show general agreement with the work Ivanov and Badajeva (Fig. 9). The latter's miscibility loop for specimens con- ning 5 at. % Mo is more symmetrical about the 50 at. % U composition (Fig. 6).

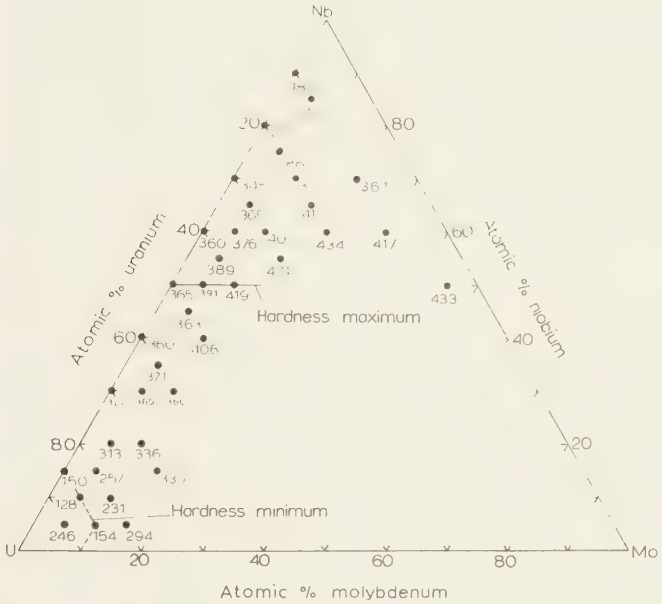

. 8. Vickers diamond pyramid hardness results on quenched body-centred cubic alloys (20 kg load). ———— Hardness maximum; - - - - - - - hardness minimum.

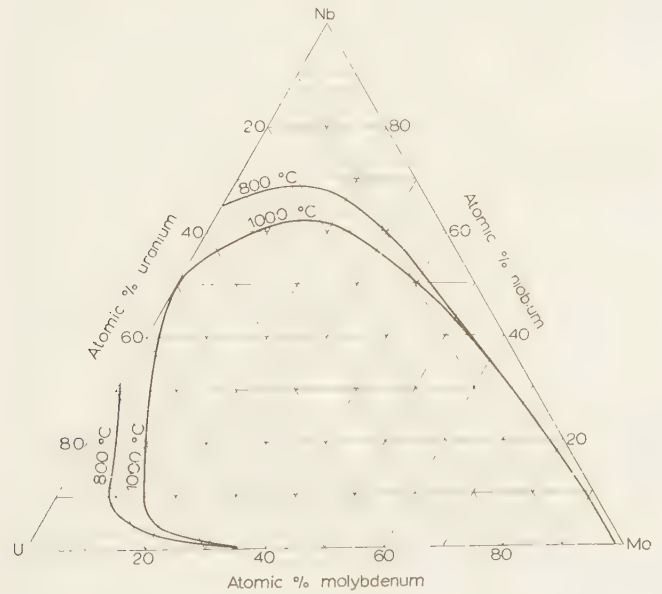

Fig. 9. Isothermal section at 1000°C and 800°C. (Ivanov and Badajeva[7])

The extent of the γ field in Nb-rich alloys observed in the present work was less than that indicated at 1000°C by IVANOV AND BADAJEVA, but the latter gave no information on their experimental techniques.

HOWLETT[13] has recently discussed miscibility gaps in random body-centred cubic solid solutions with particular reference to U alloy systems and has suggested that the temperature at which a miscibility gap forms is a function of the strain energy in the solid solution from which it is formed. To a first approximation, the strain energy depends on the size difference between the atoms and the relative number of different kinds of atoms present; the latter may be expressed as the ratio of the number of bonds between each kind of atom, taken in pairs, to the total number of bonds. HOWLETT then derived the following expression for the strain factor (*S.F.*) in a ternary solid solution:

$$S.F. = 2\left[\frac{(d_A - d_B)\ c_A c_B + (d_B - d_C)\ c_B\ (1 - c_A - c_B) + (d_C - d_A)\ c_A\ (1 - c_A - c_B)}{d_C + c_A\ (d_A - d_C) + c_B\ (d_B - d_C)}\right]$$

where d_A = Goldschmidt's atomic diameter of pure A
d_B = Goldschmidt's atomic diameter of pure B
d_C = Goldschmidt's atomic diameter of pure C
c_A = Atomic fraction of A atoms
c_B = Atomic fraction of B atoms

If, in the present case one assumes that A is U then all three terms in the numerator of the size-factor expression will be of the same sign, since Mo and Nb are both smaller than U and each term increases the strain energy. Using these parameters and the present isothermal sections at 1100°C, 1200°, and 1300°C, the strain factors at the observed compositions of the peaks of the miscibility gaps for alloys containing 5 and 10 at. % Mo were obtained and are given in Table I together with HOWLETT's value for the strain factor for the corresponding binary U–Nb alloy. The strain factors are plotted against the temperatures of the maxima on the miscibility gaps in Fig. 1c.

TABLE I

STRAIN FACTORS FOR U–Mo–Nb ALLOYS AT MAXIMA ON THE MISCIBILITY GAPS

At. % Mo	*At. % Nb*	*Temp. of max. on miscibility gap (°C)*	*Strain factor ($\times 10^{-2}$)*
0	50	950	2.49
5	50	1100	2.91
10	45	1250	3.38
15	40	—	3.68
20	35	—	3.96

It will be observed that the 3 points are a good fit to a straight line, the slope of which is slightly less than that of a line obtained by HOWLETT when U alloys containing Nb, Ti, Zr, Ti + Zr and Nb + Zr were considered. The present deviation from HOWLETT's line increases with Mo content, suggesting that some additional factor, possibly short-range ordering or clustering, should be included when considering the bonds with Mo. Recent results obtained by WILLIAMS AND TANGRI[14] suggest that the γ_0 produced

quenching a U-15 at. % Mo alloy is ordered while that obtained by quenching U-20 at. % Nb alloy is not ordered.

The U composition corresponding to the miscibility peaks for 5 and 10% Mo is ose to 45 at. %. If we assume that this remains constant for equivalent peaks in oys of 15 and 20 at. % Mo, we can calculate the strain factors corresponding to ose compositions (Table I). From Fig. 10 these strains correspond to temperatures 1360° and 1450°C respectively for the relevant peaks of the miscibility gaps. These mperatures are in general agreement with the available evidence, since an alloy taining 15 at. % Mo and 45 at. % Nb was γ at 1350°C but two-phased at 1300°C;

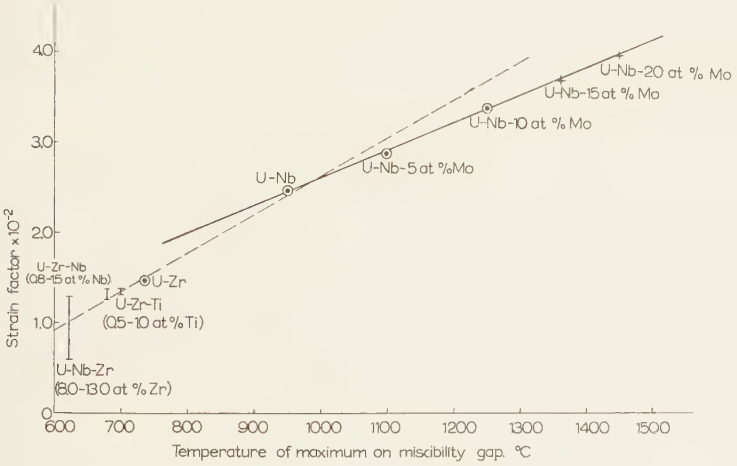

g. 10. Maximum temperature of the miscibility gaps plotted *vs.* strain factor for body-centred ic solid solutions of uranium alloys (after HOWLETT). — — — — — HOWLETT's line; ———— line based on present results; ⊙ experimental points; + points obtained from this line.

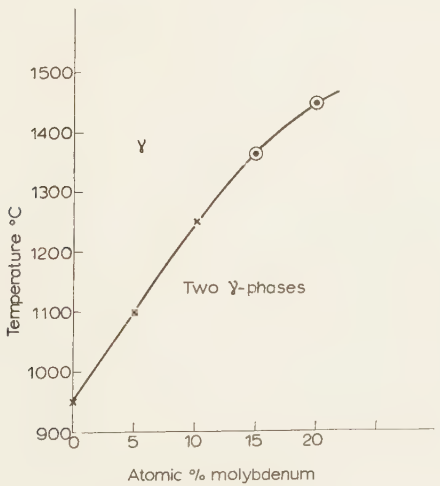

g. 11. Temperature of maximum of $\gamma_1 + \gamma_2$ phase field *vs.* molybdenum content of alloy. × Experimental points; ⊙ points derived from Fig. 10.

also, the shape of the relevant boundary of the γ phase field is not unreasonable as shown in Fig. 11.

On the simple strain-factor approach, Ti added to U–Nb alloys might increase the maximum temperature of the miscibility gap but its effect should be less marked than that of Mo while V might be expected to have a more pronounced effect than Mo. Hf should also be an interesting ternary addition since, although its room temperature lattice parameter is similar to that of Zr, the available evidence suggests that its effective atomic diameter in body-centred cubic alloys of Th is considerably smaller than that of Zr[15].

ACKNOWLEDGEMENTS

The authors would like to thank Mr. C. H. THOMAS for assistance with the preparation and heat treatment of the alloys and Mr. J. D. BROWNE and Dr. G. K. WILLIAMSON for many helpful discussions.

REFERENCES

1 P. C. L. PFEIL, J. D. BROWNE AND G. K. WILLIAMSON, *J. Inst. Metals*, 87 (1958–59) 264.
2 B. A. ROGERS, D. F. ATKINS, E. J. MANTHOS AND M. E. KIRKPATRICK, *Trans. A.I.M.E.*, 212 (1958) 387.
3 A. E. DWIGHT AND M. H. MUELLER, *U.S. Atomic Energy Comm. Publ. ANL. 5581*, (1957).
4 F. A. ROUGH AND A. A. BAUER, *U.S. Atomic Energy Comm. Publ. BMI. 1300*, (1958).
5 V. N. EREMENKO, *Ukrain. Khem. Zhur.*, 20 (1954) 227.
6 B. LUSTMAN, *U.S. Atomic Energy Comm. Publ. WAPD. MM. 491*, (1955).
7 O. S. IVANOV AND T. A. BADAJEVA, *Proc. Intern. Conf. Peaceful Uses Atomic Energy, Geneva, 1958*, A/CONF. 15/P/2043.
8 J. ADAMS, *J. Sci. Instr.*, 32 (1954) 131.
9 S. J. LLOYD AND J. R. MURRAY, *J. Sci. Instr.*, 35 (1958) 252.
10 F. L. JAGGER AND J. R. MURRAY, *Atomic Energy Research Estab. (Gt. Brit.), Rept. M/M. 182*, 1958.
11 J. LEHMANN AND R. F. HILLS, to published in *J. Nuclear Materials*.
12 R. F. HILLS *et al.*, *Atomic Energy Research Estab. (Gt. Brit.), Rept. M/R 2840*, (1959).
13 B. HOWLETT, *Associated Electrical Ind. Research Rept. A. 890*, (Feb. 1959).
14 G. I. WILLIAMS AND K. TANGRI, private communication.
15 B. A. LOOMIS AND O. N. CARLSON, *Trans. Am. Soc. Metals*, 50 (1958).

RESEARCH ON THE ALLOYS OF NOBLE METALS WITH THE MORE ELECTROPOSITIVE ELEMENTS

III. MICROGRAPHIC AND X-RAY EXAMINATION OF SOME MAGNESIUM–PLATINUM ALLOYS

RICCARDO FERRO AND GABRIELLA RAMBALDI

General Chemistry Institute and Physical Chemistry Institute of Genoa University, Genoa (Italy)

(Received July 19th, 1960)

SUMMARY

About 20 Mg–Pt alloys were prepared in the portion of the system included between 0% and 78 wt. % Pt (*ca.* 30 at. % Pt). They were subjected to chemical analysis, specific gravity determination, X-ray and micrographic examinations.

In the range of composition stated, the existence is deduced of an eutectic point (*ca.* 7.6 at. % Pt and 575°C, in close analogy with what occurs in the Mg–Au system) and of at least 2 intermediary phases (analogous with those previously found in the Mg–Pd system), *viz.*: ζ phase (solid solution region around a composition such as Mg_6Pt, face-centered cubic); δ phase (corresponding to the Mg_3Pt compound).

The crystal structure of Mg_3Pd and Mg_3Pt (both hexagonal Na_3As type) was determined and the results are briefly discussed.

INTRODUCTION AND METHODS OF STUDY

formation concerning the Mg–Pt alloys is limited to some measurements of the riation in the lattice distances produced by adding small quantities of Pt to Mg[1]. this paper results are described which were obtained during the study of alloys ging from 100% Mg/0% Pt to 22% Mg/78% Pt (*ca.* 30 at. % Pt).

eparation and general properties of the alloys

The alloys were prepared by placing the two metals (> 99.9% pure) in the proirtions desired in Fe crucibles, which were then sealed by electric welding. (Over the nge of composition studied there was no appreciable dissolution of Fe by the melted oys). The various samples were then heated to *ca.* 1400°C and then slowly (over a ek) cooled to about 300°C. During the heating and cooling they were frequently rred in order to avoid sedimentation*.

The quantities prepared were usually about 2–3 g. Thermal analysis to determine the orientation was carried out on only a few samples owing to the weak thermal effects which can be observed in small quantities.

The alloys obtained were in compact form, completely homogeneously melted, ually brittle and stable toward atmospheric oxidation.

*See, for example, Fig. 7, which shows an alloy that was cooled very slowly without stirring.

Chemical analysis

Analyses of all the alloys prepared were carried out by dissolution in aqua regia, determination of the Pt by electrolytic precipitation and determination of the Mg as pyrophosphate.

Specific gravity determination

This determination was carried out on all the alloys by use of a piknometer, which was filled *in vacuo* with rectified benzene dried over sodium.

Micrographic examination

After dry-polishing, the alloys containing up to approx. 50% Pt were etched with water and the remainder with 20% HNO_3.

X-ray examination

This was carried out by the powder method (Straumanis arrangement) using Fe $K\alpha$ radiation.

DESCRIPTION OF THE DATA OBTAINED FROM THE ALLOY EXAMINATION

The results obtained from the examination of about 20 alloys in the range of composition stated can be summarised as follows. At low Pt percentages the formation of a eutectic point occurs, whereas at higher platinum contents the existence is

TABLE I

PROPERTIES OF ALLOYS CONTAINING LOW PERCENTAGES OF Pt

% Mg found	% Pt found	Pt at. %	ϱ exp. (g/cm^3)	Microphotographs	Powder photograph appearance
89.38	10.76	1.48	1.95	Fig. 1	Mg reflex. + ζ (very weak)
77.41	22.40	3.48	2.23	Fig. 2	Mg + ζ
72.05	28.50	4.69	2.43		Mg + ζ
60.41	40.05	7.63	2.87	Figs. 3 and 4	Mg (very weak) + ζ

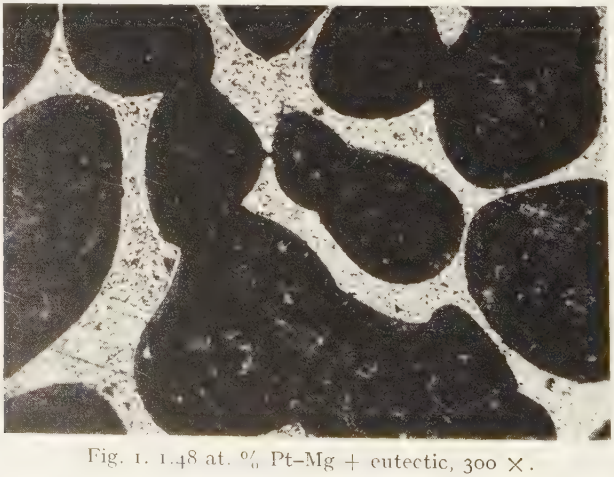

Fig. 1. 1.48 at. % Pt–Mg + eutectic, 300 ×.

uced of at least 2 intermediary phases, which, in analogy with the isostructural ses previously found in Mg–Pd alloys[2], can be indicated respectively by ζ (solid ation region around a composition such as Mg_6Pt) and δ (corresponding to the $_3$Pt compound).

m the first part of the system the alloys formed are those shown in Table I.

The eutectic composition can be estimated (as we see in Fig. 4) to be about 7.5–7.6 % Pt.

In order to gain an idea of the order of magnitude of the eutectic temperature, ther alloys (*ca.* 10 g containing 19 and 29 wt. % Pt respectively) were prepared.

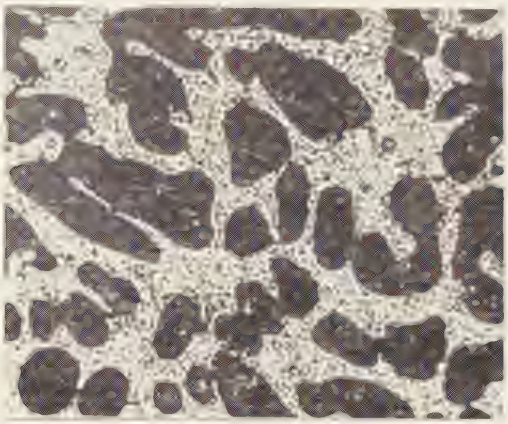

Fig. 2. 3.48 at. % Pt–Mg + eutectic, 150 ×.

Fig. 3. 7.63 at. % Pt, nearly pure eutectic, 60 ×.

er having been melted and homogenized at a high temperature, as previously ted, they were submitted to thermal analysis (in Fe crucibles, under 99.8% argon nosphere). The arrests observed point to a eutectic temperature of *ca.* 575°C. hough this value is not very accurate, it may be interesting to note that it corre-

sponds to an average lowering of the melting point of Mg of about 10°C for every 1 at % of the secondary metal, a value very near to that which can be observed in severa other Mg systems. Particularly remarkable from this point of view is the analogy with the Mg–Au alloys[3], for which the Mg-rich eutectic has composition and temper ature practically equal to those of the Mg-rich eutectic in the Mg–Pt system

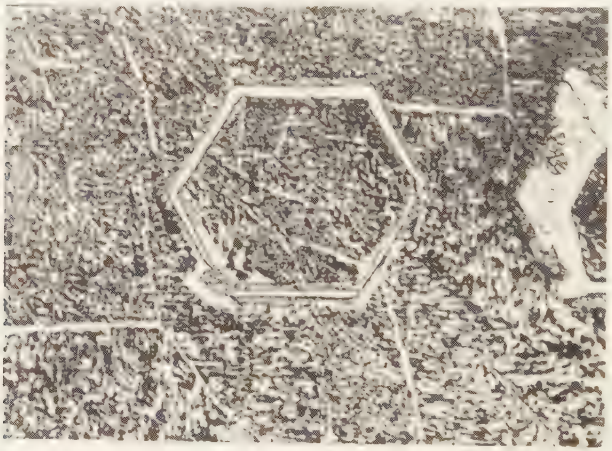

Fig. 4. The same as in Fig. 3 with higher magnification. 150

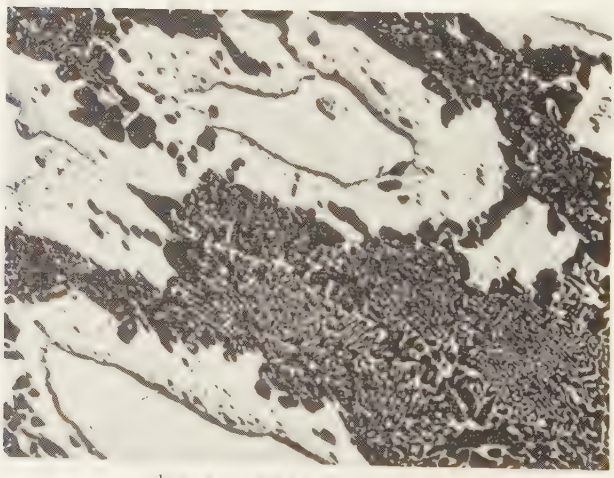

Fig. 5. 11.50 at. % Pt. 50

As far as the alloys with higher Pt contents are concerned, in the range 50–70 wt. % P the powder photographs show (for the method of preparation stated) reflexions o the ζ phase mixed with those (more or less intense) of the subsequent δ phase. Th microgaphic appearance of these alloys shows the eutectic in the vicinity of bi white heterogeneous masses.

The alloys given in Table II serve as examples.

TABLE II

PROPERTIES OF ALLOYS CONTAINING HIGH PERCENTAGES OF Pt

% Mg found	*% Pt found*	*Pt at. %*	*Microphotographs*
47.92	51.48	11.80	Fig. 5
42.12	58.44	14.75	Fig. 6

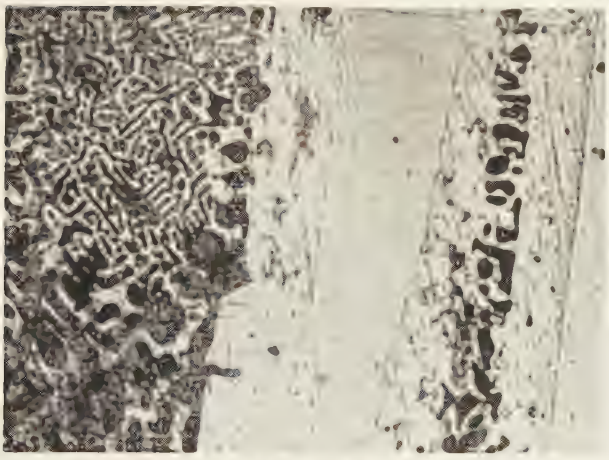

Fig. 6. 14.75 at. % Pt, 150 ×.

Fig. 7. 9.25 at. % Pt, eutectic + ζ phase, 70 ×.

This non-equilibrium condition of these samples is confirmed by the irregular variation of their specific gravity.

Since this state of incomplete equilibrium has appeared already in alloys immediately after the eutectic point (see Fig. 4), although in a very small extent, it was thought useful to make an extremely slow and gradual cooling around that temperature. For such a purpose, some alloys, after being quickly cooled from 1400° to 650°C, were further cooled down to 530°C during 10 days and then removed from the furnace. Fig. 7 shows the appearance of an alloy containing 45 wt. % Pt after such treatment; we note the existence of only 2 phases and the sedimentation of the primary crystals owing to the long duration of the crystallisation and the large excess of liquid. Figs. 8 and 9 show the micrographic appearance, after the same treatment, of 2 alloys containing 49.5$_0$ and 60.9$_0$ wt. % Pt (10.9$_0$ and 16.2$_5$ at. % Pt) respectively; we observe the presence of the ζ phase near small quantities of Mg or of the subsequent δ phase. On the powder photographs of these alloys only the ζ phase reflexions are ob-

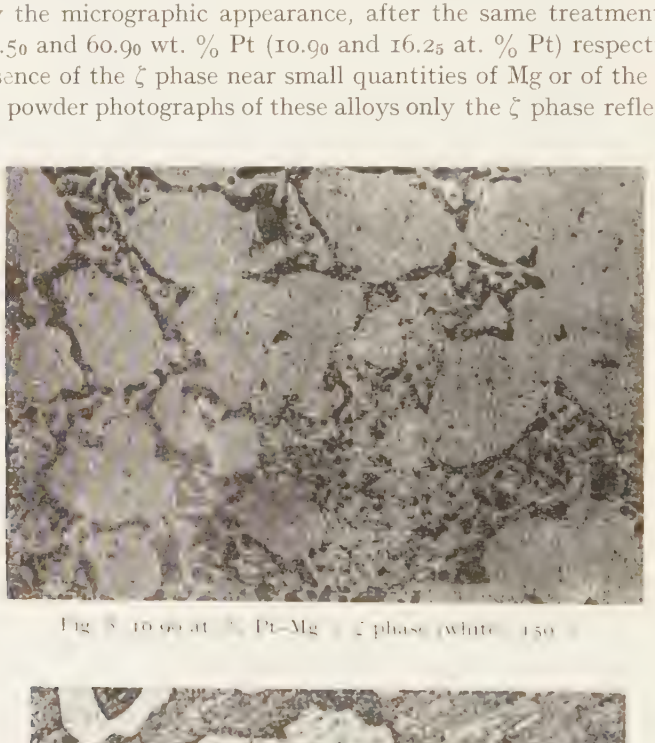

Fig. 8. 10.9$_0$ at. % Pt–Mg, ζ phase (white), 150 ×

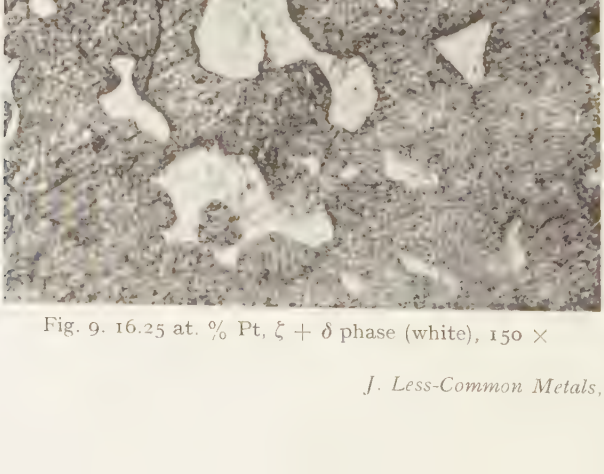

Fig. 9. 16.25 at. % Pt, $\zeta + \delta$ phase (white), 150 ×

ved; a slight change in the lattice distances shows for this phase (to which, as a ple stoichiometric ratio, a formula like Mg_6Pt can be given) the existence of a tain solid-solution ranges.

For still higher Pt percentages the results shown in Table III were obtained.

TABLE III

PROPERTIES OF ALLOYS CONTAINING LIGH PERCENTAGE OF Pt

Mg found	*% Pt found*	*Pt at. %*	*ϱ exp. (g/cm³)*	*Microphotographs*	*Powder photograph reflexions*
32.97	67.31	20.29	5.05	Fig. 10	$\zeta + \delta$
30.01	69.33	22.35	5.37		ζ (weak) + δ
27.95	72.07	24.31	5.81	Fig. 11	δ
25.86	74.62	26.44	6.14	Fig. 12	δ
24.95	78.33	30.77	6.92		δ + other reflex.

Fig. 10. 20.29 at. % Pt, $\zeta + \delta$ phases, 70 · .

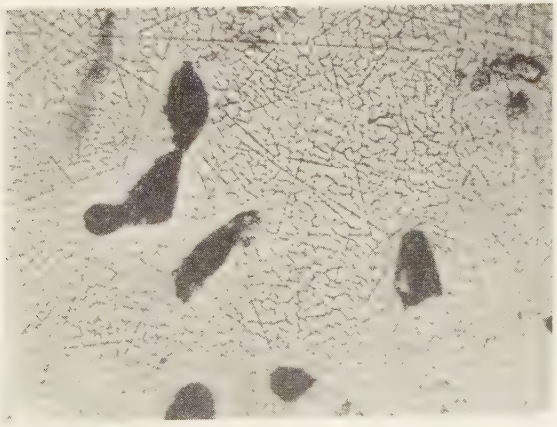

Fig. 11. 24.31 at. % Pt, nearly pure δ phase, 300 · .

We deduce that the δ phase is homogeneous for a composition like Mg_3Pt (theor 72.79% Pt). On the powder photographs variations of the lattice distances of this phase with changing composition are not observed.

DESCRIPTION OF THE VARIOUS PHASES

ζ phase

From powder photographs it appears that this phase is isostructural with the analogous one found in the Mg–Pd system (which is face-centered cubic, space group O_h^5, T_d^2 or O^3)[2] and with this hypothesis it is possible to index the reflexions.

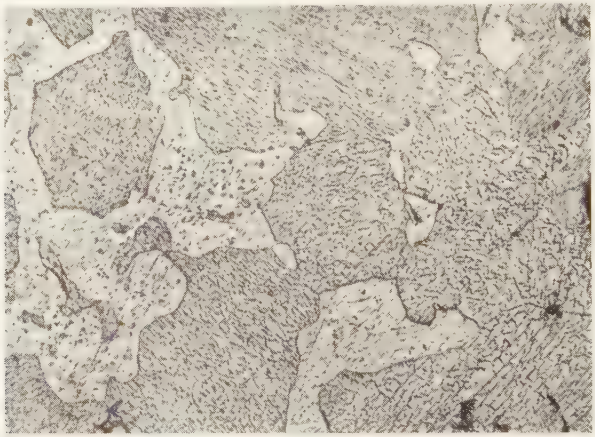

Fig. 12. 26.44 at. % Pt, δ phase + another Pt-richer phase, 150 ×.

On varying the composition the constant changes slightly around the valu $a_0 = 20.11$ Å*, decreasing with an increase of the Pt percentage. (For the metho of preparation stated, the variations noted are of the order of $\pm$ 0.01 Å.) For th composition corresponding to Mg_6Pt, using the value of the constant stated and th experimental specific gravity $\varrho = 4.00$ g/cm³, we obtain $Z = 402$ for the number o atoms in the unit cell, which is in good agreement with the ζ phase of the Mg–P system (for which $Z = 394$–398).

δ phase

This phase, corresponding to the Mg_3Pt compound, is hexagonal with constants

$$a = 4.577 \text{ Å}; \qquad c = 8.322 \text{ Å}; \qquad c/a = 1.818.$$

Using 2 molecules in the unit cell we obtain for the X-ray specific gravity ϱ = 5.90 g/cm³, while the experimental value, interpolated for Mg_3Pt, is 5.92 g/cm³.

This phase is isostructural with Mg_3Pd[2]. Both these compounds have a structur of the Na_3As type[4] with space group D_{6h}^4:

2 Pd (or Pt)	in (*c*)	$\frac{1}{3}, \frac{2}{3}, \frac{1}{4}$; $\frac{2}{3}, \frac{1}{3}, \frac{3}{4}$
2 Mg′	in (*b*)	0, 0, $\frac{1}{4}$; 0, 0, $\frac{3}{4}$
4 Mg″	in (*f*)	$\frac{1}{3}, \frac{2}{3}, z$; $\frac{2}{3}, \frac{1}{3}, \overline{z}$; $\frac{2}{3}, \frac{1}{3}, \frac{1}{2}+z$; $\frac{1}{3}, \frac{2}{3}, \frac{1}{2}-z$.

* The values of the constants were obtained by a graphical method using the extrapolatio function: $\frac{1}{2}(\cos^2\theta/\sin\theta + \cos^2\theta/\theta)$.

s is confirmed by the comparison of the observed intensities of the powder re-
ions and the calculated values. For both the compounds (and for all the reflexions
ch can be obtained with Fe $K\alpha$ radiation) the intensities were calculated using 5
ferent values of z between $z = 0.51$ and $z = 0.63$. The best agreement with the
erved values is obtained in the range: $0.57 \geq z \geq 0.60$. An exact determination
he z parameter cannot be achieved owing to the low atomic scattering factor of
; nevertheless the value $z = 0.583$, indicated for several compounds having this
ucture, is possible also in these 2 cases.
his structure is shown by a number of intermetallic compounds of magnesium
ch are given in Table IV.

TABLE IV

PARAMETERS OF COMPOUNDS HAVING THE FORMULA Mg_3X

Mg_3X	a (Å)	c (Å)	c/a	V_m (cm^3)	ΣV_a	ΔV	ΔV(%)
Pd[2]	4.613	8.410	1.823	46.68	50.81	4.13	8.13
Hg[5]	4.868	8.656	1.778	53.51	56.74	3.24	5.71
Au[6]	4.64	8.46	1.82	47.51	52.15	4.64	8.90
Pt	4.577	8.322	1.818	45.48	51.03	5.56	10.90

he molar volumes of all the above-mentioned compounds are given, both those
ained from crystallographic data (V_m) and those obtained by adding the atomic
umes (ΣV_a). The particularly high value of the volume contraction (ΔV) which
btained for the platinum compound should be noted and which probably indicates
reater stability of the compound itself.

REFERENCES

. S. Busk, *Trans A.I.M.E.*, 188 (1950) 1460.
. Ferro, *J. Less-Common Metals*, 1 (1959) 424.
. Hansen and K. Anderko, *Constitution of Binary Alloys*, McGraw-Hill Co., New York, 1958,
214.
. Brauer and E. Zintl, *Z. physik. Chem.*, B37 (1937) 323.
. Brauer, H. Nowotny and R. Rudolph, *Z. Metallk.*, 38 (1947) 81.
. Schubert and K. Anderko, *Z. Metallk.*, 42 (1951) 321.

HARDENING OF A MOLYBDENUM ALLOY BY NITRIDE DISPERSIONS

A. K. MUKHERJEE AND J. W. MARTIN

Department of Metallurgy, University of Oxford (Great Britain)

(Received July 8th, 1960)

SUMMARY

A highly stable dispersion of TiN has been produced in Mo by the isothermal heat-treatment in nitrogen of a 1% Ti–Mo alloy in the temperature range 1100°C to 1500°C. The dispersed phase has been studied metallographically, and microhardness traverses made of the diffusion layer. The hardness of the surface layers is approximately doubled, but the microhardness falls on passing inwards from the surface. The results are discussed in terms of the relationship between hardness, particle sizes, and diffusion rates.

INTRODUCTION

The work described forms part of a general study of dispersion hardening in metals, with particular emphasis on high temperature mechanical properties. Since the production of a dispersed phase by precipitation from supersaturated solid solution may not in general confer high temperature strengthening, owing to coalescence of the particles, other methods of producing highly stable dispersions have been considered.

Dispersed refractory oxides would obviously provide a stable system, and such materials have been produced by powder metallurgical techniques[1] and their mechanical properties studied. The dispersion hardening produced is, in general, related to the interparticle spacing of the oxide phase, and in such powder metallurgical methods of physically mixing the oxide and metal powders the ultimate interparticle spacing must be of the order of the original powder granule size. This must clearly limit the degree of dispersion hardening effected by such means.

The technique of internal oxidation, although capable of producing much more highly dispersed oxide phases than the above method, is hardly appropriate for Mo-base alloys. In this technique oxygen is allowed to diffuse at elevated temperatures into an alloy consisting of a dilute solid solution of a base metal in a more noble metal, the solute metal is oxidized and the resulting structure consists of a dispersion of base metal oxide in a matrix of the more noble metal. For its successful application there must be a large difference in the free energy of formation of the oxides of the solvent and solute metals. MoO itself has a fairly high negative free energy of formation, although some success has been reported in the case of a Mo–0.5% Ti alloy[2].

It was therefore decided to attempt to produce dispersions of stable nitrides in Mo by methods analogous to those of internal oxidation. Reference to the appropriate Ellingham diagram[3] (Fig. 1) suggests that Mo should form a suitable basis metal, and Ti, with its relatively high negative free energy of formation of nitride, was selected

suitable solute element. The conditions for the production of a dispersed nitride se are that nitrogen should be soluble in the matrix, and that the rate of diffusion itrogen into the surface of the specimen should be greater than the rate of diffusion olute outwards, otherwise a surface scale of nitride would result.

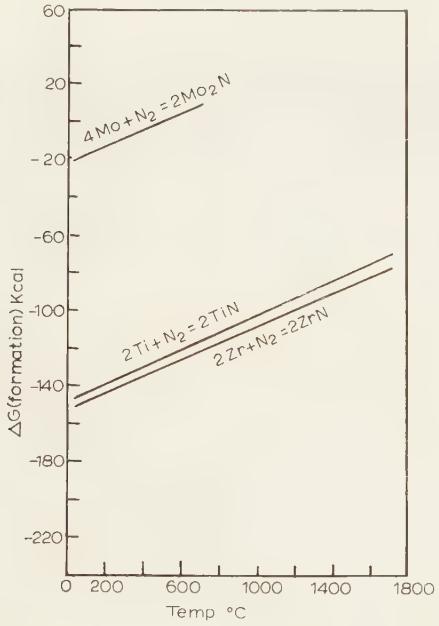

Fig. 1. Standard free energies of formation of nitrides.

EXPERIMENTAL

paration of alloy

n alloy of 1% Ti in Mo was prepared in an argon arc furnace, using a water-cooled nearth, a W electrode, and 24 cm Hg argon pressure. The arc-cast Mo used had C tent of 0.015%, and the Van Arkel Ti was of 99.97% purity.

t-treatment

pecimens were isothermally annealed in deoxidized nitrogen for varying times. heating up and cooling down took place *in vacuo*, and during the actual process itriding the nitrogen was led to the furnace through a glass tube which had been iously evacuated, thus ensuring no contamination with atmospheric oxygen. trol specimens containing no Ti were given similar heat-treatment.

allography

fter heat-treatment, specimens were mounted and sectioned for metallographic mination. Electrolytic polishing was not successful and mechanical polishing, using amond paste, has been employed throughout, followed by chemical etching in lution containing 10 g NaOH, 30 g $K_3Fe(CN)_6$ and 100 ml water. The speci-s were etched by immersion at room temperature for 1–1½ min.

Examination of Mo–1% Ti specimens sectioned after nitriding showed features of which Fig. 2 is typical. A relatively light-etching outer rim (A) was present, beneath this in the specimens nitrided only at 1500°C there was a thinner darker-etching zone (B), and between this and the unaffected interior of the specimen was a zone

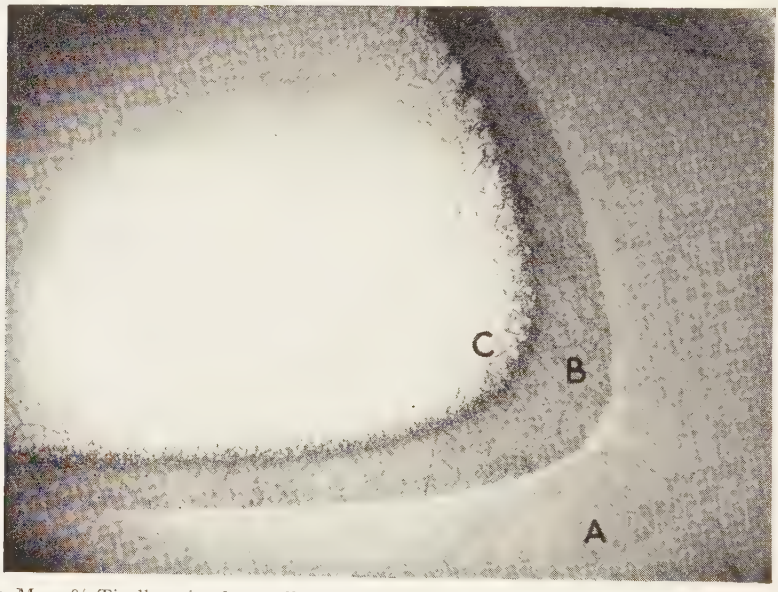

Fig. 2. Mo–1% Ti alloy, isothermally nitrided for 27 h at 1500°C. Etched section, × 150.

Fig. 3. Mo–1% Ti alloy, isothermally nitrided for 9 h at 1300°C. Etched section, × 450.

ntaining relatively coarse particles which also delineated a sub-boundary structure . This darker zone of coarse particles is shown more clearly in Fig. 3, together with rt of the light-etching rim.

The rate of formation of these nitrided zones is shown in the curves of Fig. 4. A rabolic law appears to be obeyed for the times and temperatures studied; the ex-

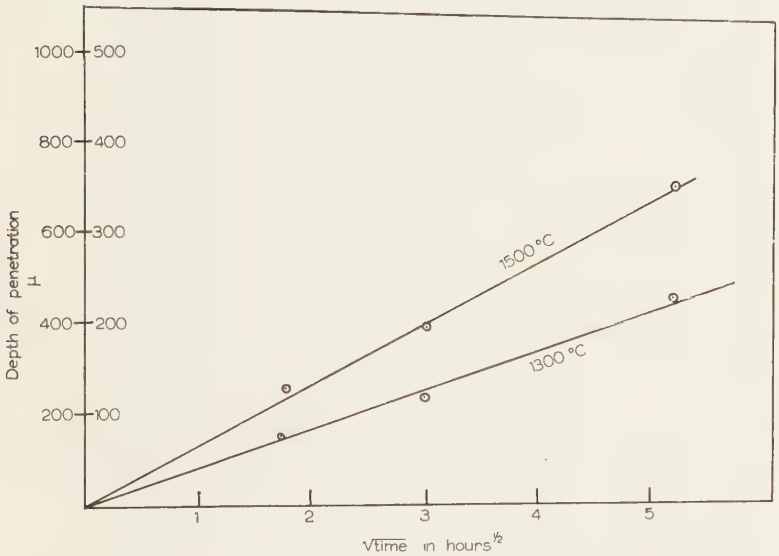

g. 4. Rate of nitriding of Mo–1% Ti alloy. The outer scale of the ordinate corresponds to the 1500°C plot, the inner scale to the 1300°C plot.

rimental points were obtained by measurements on metallographic sections of ecimens such as Fig. 2. Although it was attempted to establish a penetration-rate

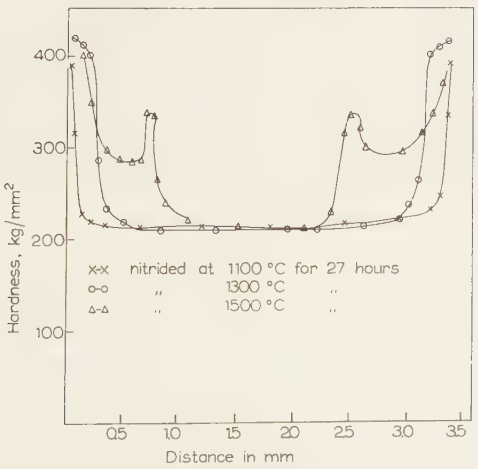

Fig. 5. Reichert microhardness traverses, load 20 g.

time curve for nitriding at 1100°C, the rate of diffusion was so low that insufficient points were obtained.

Microhardness traverses were made over all sectioned specimens, using a Reichert micro-hardness indenter and a load of 20 g. Typical results appear in Fig. 5. It was observed that the hardness of the lighter-etching outer rim was higher by a factor of 2 than the normal hardness of the solid solution of Ti in Mo. The microhardness falls on passing inwards from the surface, the zone of coarse particles and subgrains being unhardened. The specimens nitrided at 1500°C exhibited the intermediate darker zone and this was reflected in a small peak in the microhardness traverse. The heat-treatment in nitrogen of unalloyed Mo produced no observable effect upon microstructure or upon microhardness.

Fig. 6. Mo–1% Ti nitrided 27 h at 1300°C. Electron micrograph of carbon extraction replica, × 9000.

After nitriding at 1100 C or 1300 C, no particles were visible in the optical microscope in the hard, light-etching rim. In the material annealed in nitrogen at 1500°C, however, small particles could just be resolved. Carbon extraction replicas were prepared from the region of the rim and examined in the electron microscope; typical photomicrographs are reproduced in Figs. 6 and 7. Electrolytic etching was found to be most satisfactory for specimens from which carbon extraction replicas were made. The electrolyte contained 10 ml of HCl, 4 ml of H_2SO_4 and 110 ml of methyl alcohol

nd was immersed in an ice bath and operated at 4–6 V. A fine dispersion of approxi-nately equiaxed particles is resolved and from their transmission electron diffraction attern a lattice parameter closely resembling that of face-centred cubic TiN (4.257 kX)

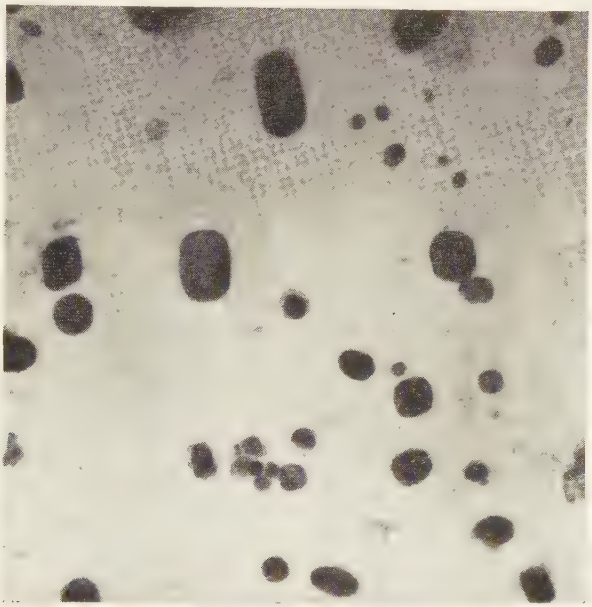

Fig. 7. Mo–1% Ti nitrided 27 h at 1500°C. Electron micrograph of carbon extraction replica, × 25,000.

was obtained. A second series of experiments was conducted using powder X-ray diffraction techniques. The particles were extracted from the specimens by electro-lysing the nitrided specimen within a semi-permeable membrane and collecting the particles. A Debye-Scherrer photograph, using Cr$K\alpha$ radiation, gave high angle reflections which were definitely interpreted as reflections from a face-centred cubic lattice with a value closely resembling that of TiN. TiC is isomorphous with the structure of TiN, and the small amount of C present as an impurity in the Mo could conceivably be present in these nitrides thus causing slight changes in lattice para-meter.

From thermodynamic considerations the TiN dispersion would be expected to be extremely stable. This was confirmed by further isothermally annealing a nitrided alloy for 9 h at 1500°C when no observable change in microstructure or microhardness was detected.

DISCUSSION AND CONCLUSIONS

The work described has demonstrated the possibility of effecting dispersion hardening in Mo by producing diffusion layers of TiN. Their thermal stability has been confirmed and similar effects could be predicted in the case of Mo–Zr alloys, which will, in due course, also be studied.

Diffusion and growth of nitride particles can take place only after dissociation of

the molecules ('MN'). The dissociation MN → M + N is inhibited by a high nitrogen content in the metal and dissociation and growth take place rapidly only at the advancing inner boundary; once this boundary has passed some distance beyond the particles the dissociation is reduced greatly and the particles are effectively "frozen".

Since a parabolic law of penetration has been demonstrated a coarsening of the structure with depth is to be expected. As the front slows down the time available for dissociation, diffusion, and growth of the nitride is increased, and the observed changes may be interpreted on these lines. With regard to the microhardness, the general picture seems to be one of increasing hardness with decreasing particle size for the same total volume of nitride per unit volume of metal.

The appearance of the darker-etching layer in the specimens nitrided at 1500°C cannot readily be explained. It is possible that it is associated with the outward diffusion of Ti, as there will be an increasing concentration gradient of Ti towards the centre of the specimen owing to the progressive removal of dissolved Ti as the nitriding proceeds. The phenomenon may be due to the achievement of optimum conditions for interaction between the nitrogen and Ti diffusing in opposite directions producing a locally more intense precipitate. The local peak in the microhardness traverse implies the presence of a finer dispersion. Unfortunately, no data have been found in the literature on the relative diffusivity of nitrogen and Ti in Mo that would permit such reasoning to be placed on a more quantitative basis.

In view of the stability of the dispersed phase the high temperature properties of these materials should be of interest and it is intended to examine their mechanical properties by carrying out creep tests, high temperature tensile tests and hot hardness tests. The results of these investigations will be published in due course.

ACKNOWLEDGEMENT

The authors are grateful to Professor W. HUME-ROTHERY, Isaac Wolfson Professor of Metallurgy at Oxford, for his encouragement, and for the laboratory facilities made available.

REFERENCES

[1] J. B. HUFFADINE, L. LONGLAND AND N. C. MOORE, *Powder Metallurgy*, 1/2 (1958) 235.
[2] J. WULFF, private communication.
[3] C. J. SMITHELLS, *Metals Reference Book*, Butterworths, Sci. Publ., London, 1955, p. 589.

Short Communications

Grain boundary migration in niobium

eretofore, virtually all evidences of grain boundary migration have been surface arkings. This note reports on some observations of a distinctive internal structure lieved to result from grain boundary migration in niobium.

A 65 g button of niobium produced by non-consumable electrode arc melting was ld-rolled 50% and then annealed for 3 h at 1700°C in a vacuum of less than to $^{1}/_{10}\mu$. is temperature, well above the recrystallization temperature, about 1200°C, was osen in order to produce large grains. The surface of the slab was ground, polished etallographically, and etched with the 10 ml H_2O, 10 ml H_2SO_4, 10 ml HF, 1 ml $_2O_2$ reagent reported by MICHAEL AND HUEGEL[1] to produce etch pits at the emer-nce points of dislocations. Figs. 1 and 2 show typical structures produced. The dark, d-like particles in the grains where the etch pits are most clearly revealed are car-ides of niobium which have been over-etched in the generation of the etch pits. The atures of interest, however, are the regular lines of etch pits which appear related by eir contours to certain nearby grain boundaries.

Many of the arrays of etch pits were single lines of pits (Fig. 1), while others were

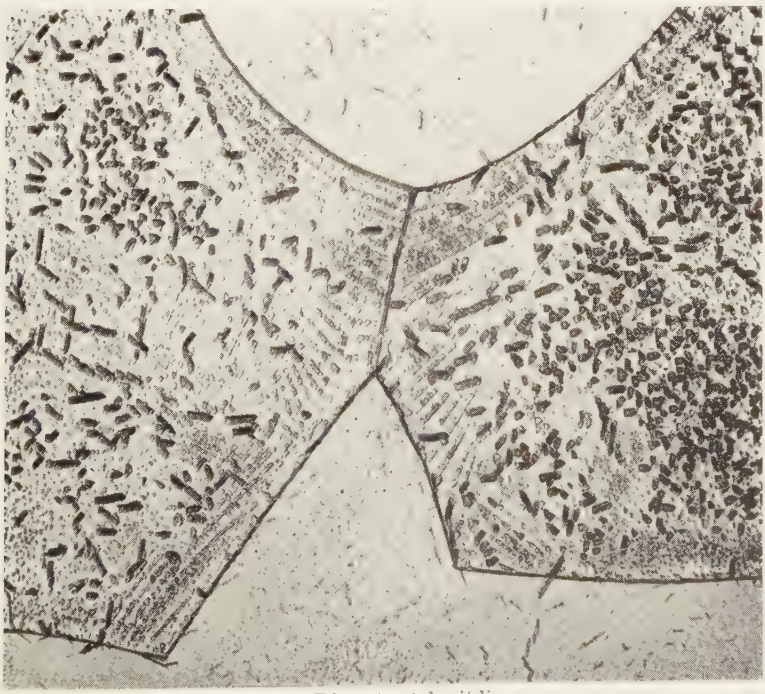

Fig. 1. Discrete etch pit lines.

more diffuse lines (Fig. 2). In virtually all families of etch pit lines, the shape of the lines progressively became more similar to the shape of the associated grain boundary, the nearer they were to this grain boundary. This similarity to the many observations of thermal grooving occurring on the surface of a metal in which the grain boundaries are migrating has led to the conclusion that these lines of etch pits delineate periodic positions of migrating grain boundaries.

There are two possible internal structures which would cause the positions of the migrating grain boundaries to be marked by etch pits. These etch pits may form either on dislocation emergence points or on precipitate sites. If the former is true, this means that as a high-angle grain boundary changes orientation during migration, its structure alters in such a way that it must periodically "precipitate" dislocations in a regular sub-boundary array. The second possibility is that the solubility of carbon in the neighbourhood of grain boundaries at 1700°C is greater than in the interior of the grains, so that as a migrating grain boundary sweeps through a grain it dissolves the carbides in the grain being consumed and periodically precipitates them in the growing grain. Conditions for this are favourable since the analyzed carbon content of the sample, 0.030 wt.%, is very close to the solid solubility of carbon at 1600–1700°C[2]. Although an electron microscope study of the etch pits at high magnification did not reveal these precipitates, there is insufficient evidence to dismiss this mechanism. The author is inclined to favour the first mechanism, however, because this observation has been made in a number of other samples of both alloyed and unalloyed niobium; one would expect that the second mechanism would require rather special

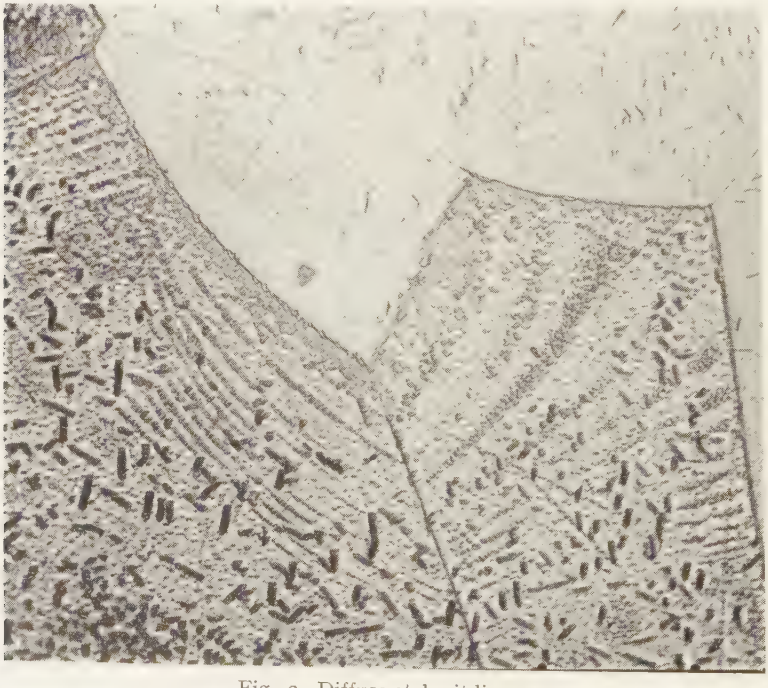

Fig. 2. Diffuse etch pit lines.

mposition–temperature conditions. The nearly regular periodicity of the rows ggests that in the case of either mechanism, the rate of motion of the boundaries is continuous.

)ccurrence of this phenomenon opens the possibility of studying in three dimensions change in shape of an entire grain during grain boundary migration. Its shape could revealed by successively removing layers of metal and etching to reveal the various sitions of the grain boundaries.

ion Carbide Metals Company,
agara Falls,
Y. (U.S.A.)

W. F. SHEELY

1 B. MICHAEL AND F. J. HUEGEL, *Acta Met.*, 5 (1957) 339.
2 L. POCHON, C. R. MCKINSEY, R. A. PERKINS AND W. D. FORGENG, *Regional Conference on Reactive Metals*, Am. Inst. Mech. Engrs., 1958.

Received May 23rd, 1960

J. Less-Common Metals, 2 (1960) 399–401

The ammonolysis of zirconium(IV) chloride

nsimetric studies made by FOWLES AND POLLARD[1] showed that one mole of ammo- m chloride was formed in the reaction of zirconium(IV) chloride with ammonia at 3 and —36 °C. However, although these experiments suggested the formation of ammonobasic zirconium(IV) chloride $ZrCl_3(NH_2)$, xNH_3, this compound was not lated, and in comparable experiments with vanadium(IV) chloride[2,3], where $l_2(NH_2)_2$, xNH_3 was formed under tensimetric conditions, ammonolysis was found be more extensive when ammonium chloride was removed from the reaction xture by washing it with liquid ammonia; $VCl(NH_2)_3$, $2NH_3$ was isolated in this y. Removal of ammonium chloride from the products of the ammonolysis of zir- nium(IV) chloride does not, however, effect a greater replacement of chlorine ms, and the ammonobasic zirconium(IV) chloride predicted in the tensimetric periments can be isolated in almost quantitative yield. The small amount of onium (7%) found in the soluble portion probably results from the formation of plex zirconium anions similar to those found in the titanium(IV) halide–ammonia tems[4]. Such complex formation would be small and would occur only in concen- ted solutions of ammonium chloride.

More extensive ammonolysis may sometimes be effected by heating the ammono- sic metal chlorides *in vacuo* and then re-treating with liquid ammonia[5], but this is very effective with zirconium(IV) chloride because a second zirconium–chlorine nd is only partially ammonolysed even when the product is heated to 100°. After h a treatment, however, more zirconium is found in the soluble portion, and it may that the heating helps to break down the polymeric solid so that it dissolves in the sence of ammonium chloride.

The ammonia which is attached to the ammonobasic zirconium(IV) chloride is

steadily lost when the compound is heated *in vacuo*, and at 100° the product has the composition $ZrCl_3(NH_2)$, NH_3. The thermal decomposition (*cf.* Table II) is in complete agreement with that of the mixture.

It is of interest to note that although ammonia forces the solvolysis of only one zirconium–chlorine bond, methylamine goes a stage further, which contrasts with the behaviour of titanium(IV) chloride where ammonia[6] and methylamine[7] solvolyse three and two titanium–chlorine bonds respectively. These results may be correlated with the effect of the size of the metal chloride on the relative base strengths of ammonia and methylamine[8]. Thus ammonia may be more basic than methylamine when titanium(IV) chloride is the reference acid since the four groups bonded to titanium should cause an appreciable amount of steric hindrance to the attacking ammonia or amine molecule. Since the zirconium atom is larger than the titanium atom, this steric hindrance should be less with zirconium(IV) chloride, and methylamine will be a better electron donor than ammonia.

EXPERIMENTAL

Zirconium(IV) chloride was prepared by the action of dry chlorine on heated zirconium strip (Murex), and purified by sublimation. Found: Zr, 39.3; Cl, 61.0. $ZrCl_4$ requires: Zr, 39.2; Cl, 60.8%.

Analyses for zirconium, chlorine, and nitrogen, were carried out as described previously[9].

Reaction of zirconium(IV) chloride with liquid ammonia

The white flocculent solid initially formed was filtered from the colourless solution and washed six times with 50 ml of liquid ammonia. Both soluble and insoluble products were kept *in vacuo* for 6 h before being analysed; the soluble portion, which clung tenaciously to the sides of the vessel, was hydrolysed *in situ* (*cf.* Table I, run 1). In other experiments (*cf.* Table I, runs 2, 3, and 4), the products were heated *in vacuo* for 2 h after the second and fourth washes, and kept *in vacuo* for 12 h after the final wash; the total soluble product was heated to 50° for 12 h before analysis.

TABLE I

PRODUCTS OF THE ZIRCONIUM(IV) CHLORIDE–AMMONIA REACTION

Run No.	*Temp. of pumping after 2nd and 4th washes (°C)*	*Insoluble product*				*Soluble product*	*Soluble Zr*
		%Zr	*%Cl*	*%N*	*Zr : Cl : N*	*Zr : Cl : N*	*Total Zr*
1	No pumping	30.4	34.3	28.2	1.00 : 2.90 : 6.04	1.00 : 17.1 : 17.5	0.07
2	20	32.1	35.8	26.1	1.00 : 2.87 : 5.30	1.00 : 10.9 : 11.9	0.10
3	50	31.6	34.6	27.6	1.00 : 2.82 : 5.69	1.00 : 10.1 : 10.0	0.20
4	100	34.1	33.7	26.6	1.00 : 2.54 : 5.08	1.00 : 6.74 : 7.76	0.33

mples of the insoluble products were heated *in vacuo* at 50° and then 100° for var-
us periods (*cf.* Table II).

TABLE II

INSOLUBLE PRODUCTS, THERMAL DECOMPOSITION

Temperature (°C)		50				100			
Run No.	Time (h)	%Zr	%Cl	%N	Zr : Cl : N	%Zr	%Cl	%N	Zr : Cl : N
1	12	37.3	43.0	16.6	1.00 : 2.96 : 2.90	39.6	44.9	11.9	1.00 : 2.92 : 1.96
2	24	39.2	43.5	13.9	1.00 : 2.86 : 2.31	40.1	44.1	13.3	1.00 : 2.83 : 2.16
3	6	34.6	38.7	21.7	1.00 : 2.88 : 3.24	39.6	43.3	14.0	1.00 : 2.83 : 2.30
4	12	—	—	—	— — —	41.1	40.4	14.0	1.00 : 2.53 : 2.22

We are grateful to the Esso Petroleum Company for providing a maintenance grant
.E.D.), and Messrs. Murex for a gift of pure zirconium metal.

G. W. A. Fowles and F. H. Pollard, *J. Chem. Soc.*, (1953) 4128.
G. W. A. Fowles and D. Nicholls, *J. Chem. Soc.*, (1958) 1687.
G. W. A. Fowles and D. Nicholls, unpublished observations.
G. W. A. Fowles and D. Nicholls, *J. Chem. Soc.*, (1959) 990.
H. Moureu and C. H. Hamblet, *J. Am. Chem. Soc.*, 59 (1937) 33.
G. W. A. Fowles and F. H. Pollard, *J. Chem. Soc.*, (1953) 2588.
R. T. Cowdell and G. W. A. Fowles, *J. Chem. Soc.*, (1960) 2522.
H. C. Brown, *J. Am. Chem. Soc.*, 67 (1945) 378.
J. E. Drake and G. W. A. Fowles, *J. Chem. Soc.*, (1960) 1498.

J. E. Drake
G. W. A. Fowles

ept. of Chemistry,
he University,
uthampton (Great Britain)

Received August 4th, 1960

J. Less-Common Metals, 2 (1960) 401–403

Book Reviews

Beryllium, by G. E. DARWIN AND J. H. BUDDERY, Butterworths Scientific Publications, London 1960, 392 pages, £3 10s.

The growing interest in beryllium and its development in this country in the nuclear engineering field are alone sufficient reasons for welcoming a good survey of present knowledge on this rarer metal and its oxide. This book summarises the various methods of extracting beryllium, and provides extensive information on the fabrication of the metal and on its properties. The authors remark that at this stage of development some of the available information is contradictory and in such cases they have taken pains to supply the fullest experimental details. Owing to the growing importance of beryllia a chapter is devoted to its preparation, fabrication into shapes, and fundamental and structure-sensitive properties. The uses of beryllium as a true alloying constituent and as a minor alloying addition are considered in detail, as are the applications of the metal, its alloys, and its oxide. Interest in the use of beryllium-base materials in nuclear engineering centres largely around the extremely low thermal neutron absorption cross-section of beryllium, and the authors have devoted special attention to the nuclear properties of the metal and to its uses in reactors. Not without justification, detailed consideration has been given to the health hazards arising in the handling of beryllium-containing materials and to their control.

The book is well written and the reader would have difficulty in criticising either the presentation of the extensive information contained in its twelve chapters or in suggesting how this information could be elaborated. With the additional help of the copious references included, this book should enable anyone seeking the latest knowledge on the subject it covers adequately to satisfy his requirements. As the latest monograph in the series on the metallurgy of the rarer metals the book fully maintains the high standard set by its predecessors.

J.W.C.

J. Less-Common Metals, 2 (1960) 404

3e Colloque de Métallurgie sur la Corrosion (3rd Metallurgy Symposium on Corrosion), North Holland Publishing Co., Amsterdam, 1960, 240 pages, 38.00 guilders, £ 3.12s.

This Colloquium on the corrosion of metals and alloys under dry and aqueous conditions contains eighteen authoritative papers dealing with many aspects of the fundamental and practical significance of this important subject. The first paper considers existing theories of oxidation and examines the results obtained in recent studies of oxidation phenomena. Further papers deal with the inhibition of the corrosion of magnesium heated in wet air; with the gaseous attack of magnesium and uranium; with the corrosion of stainless steels by pure water at high temperature; with the stress corrosion cracking of Inconel in high-temperature water; with the corrosion of steels by hydrogen sulphide; with the morphology of oxidation films; and with the influence of hydrogen on the corrosion of zirconium and its alloys in high-temperature water. In a short review it is impossible to refer individually to all of the papers that make up this compilation, but while some have been specifically mentioned it is not to be inferred that the remainder are of any less interest or importance. Only a few of the papers deal with metals falling exactly within the terms of reference of the Journal of the Less-Common Metals, but readers of that Journal wishing to acquaint themselves with recent work in the corrosion field would do well to refer to this publication. Much of the fundamental information it contains is, of course, applicable to common and less-common metals alike, and the fact that many of the papers do not deal directly with the latter does not detract from the value of the book as a contribution to basic knowledge on a subject with which many less-common metals are closely associated.

J.W.C.

J. Less-Common Metals, 2 (1960) 404

CONTENTS

solubility factor series for solid metals
by Y. L. YAO (Ottawa) 321

ne plutonium–zirconium phase diagram
by J. A. C. MARPLES (Harwell) 331

ne variation of unit-cell edge of uranium monocarbide in arc melted uranium–carbon alloys
by J. WILLIAMS, R. A. J. SAMBELL AND D. WILKINSON (Harwell) 352

ne melting point of osmium
by A. G. KNAPTON, J. SAVILL AND R. SIDDALL (Aldermaston, Berks.) 357

me studies on inorganic peroxy-acids.
I. Peroxymolybdic and peroxytungstic acids
by E. RICHARDSON (Whitehaven, Cumberland) 360

me observations on uranium–molybdenum–niobium alloys
by G. H. BANNISTER AND J. R. MURRAY (Harwell) 372

esearch on the alloys of noble metals with the more electropositive elements
III. Micrographic and X-ray examination of some magnesium–platinum alloys
by R. FERRO AND G. RAMBALDI (Genoa) 383

ardening of a molybdenum alloy by nitride dispersions
by A. K. MUKHERJEE AND J. W. MARTIN (Oxford) 392

ort Communications

rain boundary migration in niobium
by W. F. SHEELY (Niagara Falls, N.Y.) 399

he ammonolysis of zirconium(IV) chloride
by J. E. DRAKE AND G. W. A. FOWLES (Southampton) 401

ook Reviews 404

ll rights reserved

ELSEVIER PUBLISHING COMPANY, AMSTERDAM
Printed in The Netherlands by
NEDERLANDSE BOEKDRUK INRICHTING N.V., 'S-HERTOGENBOSCH

BOUND IN STACKS

For Students and Teachers alike:

Inorganic Chemistry

A GUIDE TO ADVANCED STUDY

by

R. B. HESLOP, M.Sc., F.R.I.C.

and

P. L. ROBINSON, D.Sc., F.R.I.C.

- An outline of current inorganic chemistry, sufficient for basic reading up to honours degree standard, is provided in one small volume.
- The approach is general and reasonably fundamental, thus, some of the material is suitable for advanced level and scholarship pupils in schools and for non-specialist students in universities and technical colleges.
- Teachers will find this book very useful when planning instruction at all levels.

6 x 9" viii + 542 pages + index 294 illustrations 136 tables
1960 45s. Dfl. 24.00

Write for additional information to:

ELSEVIER PUBLISHING COMPANY

110-112 SPUISTRAAT AMSTERDAM HOLLAND